UNIVERSITÀ DEGLI STUDI DI BRESCIA

Dipartimento di Ingegneria dell'Informazione

———————————————-

DOTTORATO DI RICERCA IN TECHNOLOGY FOR HEALTH

ING-INF-07

CICLO XXXVI

UNIVERSITÀ
DEGLI STUDI
DI BRESCIA

Electrical Stimulation and RealTime Monitoring for Cell Culture

Supervisore:
Prof. Mauro Serpelloni

Dottoranda:
Ileana Armando

2023

"Ma io sono fiero del mio sognare,
Di questo eterno mio incespicare,
E ridi in faccia a quello che cerchi
e che mai avrai"
— Francesco Guccini.

Abstract

In the field of biotechnology and *in vitro* cell culture, considerable efforts are being devoted to research and technological advancement, with a focus on improving protocols to produce large-scale tissue engineering products, suitable for obtaining scalable and safe products through the use of standardized and automated cell culture devices. The development of innovative methods within the field of regenerative medicine sees enormous application and advancement possibilities in the study of physiological and pathological models and drug testing. Furthermore, the application of biophysical stimulation that mimics physiological processes and activates the cascade of molecular pathways, to these engineered products promotes the acceleration of various bioprocesses (e.g., cell proliferation and maturation). The application of stimuli to the construct can be of different types, in addition to the use of external chemical compounds, mechanical or electromagnetic stimuli, depending on the biological tissue and as needed. Finally, the creation of *in vitro* models requires continuous monitoring and readjustment of the ongoing biological process, to obtain an automated device capable of producing large-scale engineered products. This requires the use of techniques for real-time, non-destructive monitoring of cell culture and its various parameters in order to achieve the desired final construct. The high cost and the long time required to obtain engineered, optimized and functional constructs are still the major limitations in the advancement of regenerative medicine, in addition to the limitations related to frontier research, in which tissue engineering is located. The following thesis aims, using of low-cost and non-invasive techniques, to interact with growing cell cultures and enable real-time feedback, allowing for an improvement of traditional techniques, fostering the development of automated and scalable methods, and taking advantage of technological advances in engineering and biology to promote cell growth and differentiation. This thesis will present two main applications in the field of biotechnology research that aim at improving existing methodologies in biomedical laboratories. Specifically, this thesis presents the development of technological approaches applied to biotechnology for the realization and application of biophysical stimulation for the improvement and optimization of physiological processes.

Furthermore, the fabrication of devices, by exploiting rapid prototyping techniques for real-time monitoring of cell cultures is presented. In detail, tissue engineering will be introduced and explored in the thesis, with a specific focus on the current state of the art related to biophysical stimulation and real-time monitoring of *in vitro* cell culture. Next, a brief introduction to neurophysiology will be introduced with a brief discussion of neuronal physiology and electrophysiological methods of action potential recording that will cover the real-time monitoring approach that will be developed in subsequent chapters. After that, the development of a system for electrical stimulation using an electric field to accelerate the differentiation and maturation of dopaminergic neurons derived from human induced pluripotent stem cells (hiPSC) is presented in the first application. The following work led to relevant results concerning the efficacy of the electrical stimulation device, which was found to be functional and in line with good laboratory practice, and concerning the results on induced pluripotent stem cells, the electrical stimulation protocol had significant effects on cell differentiation from a morphological point of view, achieving statistically significant results in terms of length and number of dendrites and cell soma area. Following the relevant results obtained in the work on electrical stimulation, the realization of a device capable of promoting both electrical stimulation and real-time monitoring of the differentiation process by recording action potentials generated by mature neurons (differentiation from induced pluripotents) will be proposed in order to overcome some limitations brought to light in the previous application. In particular, the fabrication of a printed microelectrode array using additive manufacturing printing techniques is described. Specifically, the design of the bioelectronic device was studied in a preliminary phase by exploiting computational modeling techniques used in order to define the optimal parameters and requirements necessary for the device realization (e.g., electrode size and electrode spacing). Accordingly to the design, the device was fabricated with a multilayer structure through the use of the Aerosol Jet Printer, and finally, the device was characterized geometrically and electrically to ensure that the imposed design requirements were met and evaluate the stability and long-term use of the device. In addition, the electrode array was also tested in terms of sterilization and biocompatibility, obtaining good results in terms of viability and adhesion of cells to the printed substrate. Finally, an early-stage realization of a low-cost analog front end for connecting the printed MEA was developed to enable real-time monitoring of neuronal culture.

Sommario

Nell'ambito delle biotecnologie e delle colture cellulari *in vitro*, notevoli sforzi vengono dedicati al progresso e all'avanzamento della ricerca e della tecnologia, con particolare attenzione al miglioramento dei protocolli per la produzione di prodotti di ingegneria tissutale su larga scala, atti all"ottenimento di prodotti scalabili e sicuri tramite l'utilizzo di dispositivi di colture cellulari standardizzati e automatizzati. Lo sviluppo di metodi innovativi che rientrano nel campo della medicina rigenerativa, vedono nello studio di modelli fisiologici e patologici e nella sperimentazione di farmaci, un'enorme possibilità applicativa e di avanzamento. Inoltre, l'applicazione di una stimolazione biofisica che riproduce i processi fisiologici e attiva la cascata di pathway molecolari, a questi prodotti ingegneristici promuove l'accelerazione di diversi bioprocessi (ad es. proliferazione e maturazione cellulare). L'applicazione di stimoli al costrutto può essere di diverso tipo, oltre all'uso di stimoli chimici esterni, meccanico o elettromagnetico in base al tessuto biologico e in base alla necessità. Infine, la realizzazione di modelli *in vitro* prevede un continuo monitoraggio e riadattamento del processo biologico in corso, anche in ottica di ottenere un dispositivo automatizzato in grado di realizzare prodotti ingegnerizzati su larga scala. Questo richiede l'utilizzo di tecniche per il monitoraggio in tempo reale e non distruttivo della coltura e dei diversi parametri che lo caratterizzano, in modo da ottenere il costrutto finale desiderato. L'elevato costo e i lunghi tempi richiesti per ottenere costrutti ingegnerizzati, ottimizzati e funzionali sono ancora un grande limite nell'avanzamento della medicina rigenerativa, oltre a tutti i limiti legati alla ricerca di frontiera, in cui l'ingegneria tissutale si pone. In quest'ottica, la seguente tesi si pone l'obbiettivo, tramite l'utilizzo di tecniche economiche e non invasive, di interagire con le colture cellulari in crescita e consentire un feedback in tempo reale, consentendo un miglioramento delle odierne tecniche, favorendo lo sviluppo di metodi automatizzati e scalabili e sfruttando i progressi tecnologici dell'ingegneria e della biologia per promuovere la crescita e il differenziamento cellulare. La tesi presenterà due applicazioni principali nel campo della ricerca biotecnologica che hanno come obiettivo il miglioramento delle metodologie esistenti nei laboratori. In particolare, questa tesi vede lo sviluppo di approcci tecnologici

applicati alla biotecnologia per la realizzazione e l'applicazione di stimoli biofisici per il miglioramento e l'ottimizzazione dei processi fisiologici e la realizzazione di dispositivi, sfruttando le tecniche di prototipazione rapida per il monitoraggio in tempo reale delle colture cellulari. In dettaglio, nella tesi verrà introdotto e approfondito il tema dell'ingegneria tissutale, con un focus specifico sull'attuale stato dell'arte relativo alla stimolazione biofisica e al monitoraggio in tempo reale della coltura cellulare *in vitro*. Successivamente, verrà introdotta una breve introduzione sulla neurofisiologia con una breve trattazione della fisiologia neuronale e sui metodi elettrofisiologici di registrazione del potenziale d'azione che riguarderà l'approccio del monitoraggio in tempo reale che verrà sviluppato nei capitoli successivi. In seguito, nel primo lavoro viene presentato lo sviluppo di un sistema per la stimolazione elettrica tramite l'utilizzo di un campo elettrico per accelerare il differenziamento e la maturazione dei neuroni dopaminergici derivati da cellule staminali pluripotenti indotte umane. Il seguente lavoro ha portato ad ottimi risultati per quanto riguarda l'efficacia del dispositivo di stimolazione elettrica che è risultato funzionale e in linea con le buone norme di laboratorio e, per quanto riguarda i risultati sulle staminali pluripotenti indotte, il protocollo di stimolazione elettrica ha avuto notevoli effetti sul differenziamento cellulari dal punto di vista morfologico, ottenendo risultati statisticamente significativi in termine di lunghezza e numero di dendriti e ampiezza del soma cellulare. A seguito dei rilevanti risultati ottenuti nel lavoro sulla stimolazione elettrica, verrà proposta la realizzazione di un dispositivo in grado di promuovere sia la stimolazione elettrica sia il monitoraggio in tempo reale del processo di differenziamento, tramite la registrazione di potenziali d'azione generati da neuroni maturi (differenziamento dalle pluripotenti indotte). Nello specifico, viene descritta la realizzazione di un array di microelettrodi stampati, utilizzando tecniche di stampa di additive manufacturing. In particolare, la progettazione del dispositivo bioelettronico si è sviluppato in una prima fase in cui tecniche di modellazione computazionali sono state utilizzate in modo da definire i parametri e i requisiti necessari alla realizzazione del disposito (ad es. dimensione degli elettrodi e distanza degli elettrodi). In seguito alla progettazione, il dispositivo è stato realizzato con una struttura multilayer tramite l'utilizzo dell'Aerosol Jet Printer e infine, il dispositivo è stato caratterizzato dal punto di vista geometrico ed elettrico, in modo da garantire, in primo luogo, il rispetto dei requisiti di progetto imposti e valutare infine la stabilità e l'utilizzo a lungo termine del dispositivo. Inoltre, l'array di elettrodi è stato testato anche in termini di sterilizzazione e biocompatibilità, ottenendo buoni risultati in termine di vitalità e adesione delle cellule al substrato stampato. Infine, è stato sviluppato un primo studio per la realizzazione di un front-end analogico a basso costo per connettere l'array di microelettrodi stampato e per consentire il monitoraggio in tempo reale della coltura cellulare neuronale.

Contents

Abstract **iv**

Sommario **vi**

List of Figures **xii**

List of Tables **xvi**

Acronyms **xvii**

1 Introduction **1**

1.1 Tissue Engineering 1

1.2 Electrical Stimulation 3

1.3 Real Time Monitoring 7

1.4 Thesis Outline and Motivation 12

2 Neurophysiology **14**

2.1 State of the art 14

2.2 Neurophyisiology fundamentals 15

2.2.1 Neurons 15

2.3 Electrophysiological Methods 18

2.3.1 Intracellular recording 19

2.3.2 Extracellular recording 20

3 Electrode for stimulation and recording for neuronal application 25

3.1 Introduction . . . 25

3.2 Electrical requirements . . . 26

3.2.1 Stimulation electrodes . . . 26

3.2.2 Recording electrodes . . . 28

3.3 Charge-injection mechanisms . . . 29

3.4 Emerging Materials . . . 30

3.5 Electrode Characterization . . . 30

3.5.1 Cyclic Voltammetry . . . 31

3.5.2 Impedance Spectroscopy . . . 31

3.5.3 Voltage Transients . . . 31

4 Electrical Stimulation of Human Induced Pluripotent Stem Cell 33

4.1 Introduction . . . 33

4.2 Aim . . . 35

4.3 Material And Methods . . . 36

4.3.1 Design Requirements . . . 36

4.3.2 Experimental Set-Up . . . 38

4.4 Results . . . 40

4.5 Conclusion . . . 41

5 A feasibility study of a printed Micro-Electrode Arrays 44

5.1 Introduction . . . 44

5.2 Aim . . . 46

5.2.1 MEA requirements . . . 48

5.3 Design and Modelling . . . 48

5.3.1 Set up for FEM and evaluation parameters . . . 48

5.3.2 Simulation results . . . 53

5.3.3 Design of Micro-Electrode Array and Material Selection . . . 59

5.4 Fabrication process 63
5.5 Result and discussion 67
5.5.1 Characterization of the preliminary printed layer 67
5.5.2 Characterization of the printed prototypes 71
5.5.3 Discussion 78
5.6 Electronic Front-End 82
5.6.1 Introduction 82
5.6.2 Design of AFE 83
5.6.3 Realization of the front end 84
5.6.4 Interface 89
5.7 Biocompatibility evaluation of the MEA 89
5.7.1 Culture Chamber and MEA Adapter 89
5.7.2 Biocompatibility test 90

6 General Conclusions and Future Outlooks **92**

Appendix A Electronic Front End **95**

Ringraziamenti **98**

Bibliography **99**

List of Figures

1.1 Different type of electromagnetic stimulation divided according to the type of electrodes and the position according the cell culture. 4

2.1 Simplified representation of a neuronal cell. Created with BioRender.com 16

2.2 Intracellular action potential waveform of a neuronal cell. Created with BioRender.com 17

2.3 Graphical representation of the intracellular recording techniques (Patch clamp) and extracellular technique (Microelectrode array). Created with BioRender.com 19

3.1 Typical current waveforms applied in neural stimulation with charge-balanced injection. The parameters vary widely depending on the application and size of the electrode 27

4.1 Rendering of the Induced Pluripotent Stem Cell with differentiated cell collected from a donor, after that the reprogramming of the somatic cell into stem cell and finally, the differentiation in a neuronal cells 34

4.2 Distribution of the electrical potential and the electric field within the bottom of petri dish according to the electrode set up of C-Dish^{TM} . . . 37

4.3 Schematic representation of the electrical stimulation system composed of the different blocks 39

4.4 Photo of the commercial patent C-DISH^{TM} lid for electrical stimulation with 6 well cell plate 39

4.5 Schematic representation of the experimental protocol with the indication of the protocol for the electrical stimulation and the morphological tests. 40

4.6 a) Photographs acquired with microscope that show the hIPSCs fixed after the electrical stimulation. b) Bar plots that show the statistical results according to the morphological evaluation according to dendrite length, dendrite number, and soma area. 42

5.1 Rendering of the geometrical domains of Comsol Multiphysics simulation of 1-2) MicroElectrode Array and 3) Neuronal Cell. 49

5.2 Equivalent electrical circuit for the Hodgkin–Huxley model of the neuronal cell action potential. V represents the voltage across, a small patch of membrane. The C_m represents the capacitance of the membrane patch, whereas the four g's represent the conductances of three types of ions. The two conductances on the left, for potassium (K) and sodium (Na), are shown with arrows to indicate that they can vary with the applied voltage, corresponding to the voltage-sensitive ion channels. 52

5.3 Single action potential signal generates as input for Comsol Multiphysics simulation according to the parameters of the imposed equivalent circuit for Hodgkin–Huxley neuron model. 54

5.4 Plot of the action potential signal in input and recorded signal by the electrode at distance between them of a) 80 µm and in b) 30 µm. 55

5.5 Detection field area of a single electrode configuration according to the cell-electrode distance and the action potential signal recording on that electrode. The electrode is localised in the *x-y* origin. 57

5.6 Detection field area of the two electrode configurations according to the cell-electrode distance and the action potential signal recording on that electrode. The 1° first electrode is localized in the *x-y* origin and the 2° electrode at 200 µm away. 58

5.7 Action potential signal from the recorded electrode with an insulating layer of 10 µm and 300 µm, respectively. 59

5.8 Rendering of the three layers of the MicroElectrode Array. Substrate, 1) 16 conductive tracks in silver ink, 2) the passivation layer deposit with NOA 81, and 3) 16 electrode patches in PEDOT:PSS. 60

5.9 Photograph and detail of the printed MicroElectrode Array, composed of the contact pad to connect to the electronic front-end. 63

5.10 Rendering of the three layers of the microelectrode array. 1) 16 silver tracks for the conduction of the signal, 2)Insulating layer in Norland Optical Adhesive (NOA) and 3) 16 electrode patches in PEDOT-PSS. . 63

5.11 Rendering of the fabrication process. In the first step, the printing of silver tracks was performed; in the second, the passivation layer was deposited and finally, the electrode patches were printed in the third step. 65

5.12 Detail of the schematic drawing of the Micro Electrode array. Two tracks of the MEA are represented to show the different layers composed of electrode patches, passivation coating and conductive tracks. 66

5.13 Optical microscope image of the different number of overlapped deposition of silver layers. 68

5.14 Profilometer images of the different overlapped deposition tracks after the filtering process and plot of the profile. 70

5.15 Profilometer view of the thickness of Norland Optical Adhesive 81. . . 71

5.16 Profilometer images of the 16 electrodes array printed with PEDOT:PSS-based ink. 72

5.17 Plot of the measurement resistance value for different overlapped deposition. 73

5.18 a) Average profile of silver tracks (solid red line) and coating made by NOA 81 tracks (solid blue line). The shadow area is the standard deviation calculated on 128 profiles acquired from the four MEAs. b) Average profile of PEDOT:PSS coating (solid green line) and underlying silver layer (solid red line). The shadow area is the standard deviation calculated on 64 profiles of the sensing electrodes acquired from the four MEAs. In the inset the rendering of the tracks that show the crosssection. 74

5.19 Plot of the measured resistance value for different conductive tracks length with mean values and standard deviation calculated on at least 8 tracks, considering all the four MEAs. 75

5.20 Experimental setup used to the Electrochemical Impedance Spectroscopy. The sensor is filled with PBS and then, the PalmSens is connected to the sensor and the measurement are performed and data send to a computer for the data analysis. 76

5.21 Impedance magnitude change over frequency (reusability test) on 14 days. Error bars show the standard deviation on two MEAs. The impedance was measured between the electrodes and the reference electrodes. 77

5.22 Impedance magnitude over 14 days in PBS for the stability of two sensor at frequency of 100 Hz and 1 kHz. Error bars show the standard deviation of two MEAs. 78

5.23 Theoretical impedance module according to frequency variations for the Randles circuit model (in the inset) for the electrode/electrolyte interface used for the fitting of the experimental results. 79

5.24 The Nyquist plot with real and imaginary part of the experimental results obtained in the stability test of the printed MEA within two weeks. . . . 80

5.25 Block Diagram of Bio-Potential Measurement System 85

5.26 Scheme of the filter amplifier 85

5.27 Scheme of First Amplifying Stage. 86

5.28 Scheme of Second Stage. 87

5.29 Photograph of the STO cell line at the following days, the cells were visualized with the Olympus IX51 microscope (Olympus Italia Srl, Milan, Italy) to monitor the vitality and growth of cells. 91

A.1 Layout with a) top view and b) bottom view for the board of the analog front end of the printed MEA recording system 95

A.2 Photo of the PCB assembled of the board of the analog front end of the printed MEA recording system 96

A.3 Block diagram of Electronic Front End for printed MEA 97

List of Tables

1.1 Classification of the sensor for *in vitro* cell culture 9

1.2 Type of monitored parameters of *in vitro* cell culture 9

4.1 Electrical parameters for the different material domains used in the simulation. 37

5.1 Electrical parameters for the different material domains used in the simulations. 50

5.2 Printing parameters used during the production process. 66

5.3 Geometrical features of the tracks with average and standard deviation values. 68

A.1 Bill of Material of the Analog Front End for MEA recording 96

Acronyms

AM Additive Manufacturing

AD Alzheimer's Disease

ADC analog-to-digital converter

AP Action Potential

AJP Aerosol Jet Printing

AFE Analog Front End

BCI Brain Computer Interface

CAD Computer-Aided Design

CC Capacitive Stimulation

CMRR Common Mode Rejection Ratio

CNS Central Nervous System

CPE Constant Phase Element

CV Cyclic Voltammetry

DA Dopaminergic

DAC Digital Analog Converter

DAQ Data Acquisition System

DBS Deep Brain Stimulation

DC Direct Current

DO Dissolved Oxygen

ECM Extracellular Matrix

EF Electrical Field

EIS Electrochemical Impedance Spectroscopy

ES Electrical Stimulation

FEM Finite Element Model

GBW Gain Bandwidth product

GLP Good Laboratory Practice

hiPSC human induced Pluripotent Stem Cell

hPSC human Pluripotent Stem Cell

HPF High Pass Filter

IA Instrumentation Amplifier

LFP Low Field Potential

LPF Low Pass Filter

MEA MicroElectrode Array

MP Membrane Potential

NOA Norland Optical Adhesive

PANI Polyaniline

PBS Phosphate-buffered saline

PCB Printed Circuit Board

PD Parkinson's Disease

PDMS polydimethylsiloxane

PEDOT:PSS Poly(3,4-ethylenedioxythiophene): polystyrene sulfonate

PEMF Pulsed Electromagnetic Field Stimulation

PPY Polypyrrole

PSRR Power Supply Rejection Ratio

SCCM Standard centimeter cube per minute

SLA Stereolithography

SNR Signal to Noise Ration

RM Regenerative Medicine

TE Tissue Engineering

VEGF Vascular Endothelial Growth Factor

WHO World Health Organization

Chapter 1

Introduction

Worldwide, tissue and organ failure due to disease, injury, and developmental defects have become a major economic and healthcare burden. Nowadays, the use of donated tissues and organs in the clinical practice to address the situation is limited due to the shortage of organ donors, the increasing number of people who need transplant waiting lists, and an ever-increasing aging population, dependence on donated tissues and organs is no longer a practical approach. Moreover, the problem of organ rejection is crucial and the use of anti-rejection drugs requires permanent use throughout life with other several related problems. For this reason, the need to promote personalized therapies that anticipate the use of cells or tissues from the patient himself and the study of personalized pathological models through biomedical research leads to the resolution of many problems in the clinical field [1, 2].

1.1 Tissue Engineering

Tissue engineering (TE) has become a promising alternative to provide the replacement and repair of tissue within the body, to address the critical medical need. TE and regenerative medicine (RM) are multidisciplinary fields that combine knowledge and technologies from several research fields such as biology, chemistry, engineering, medicine, pharmaceutical and material science to develop therapies and products for repair or replacement of damaged tissues and organs [3]. Tissue engineering refers to the combination of cells, scaffolds, and biologically active molecules and biophysical stimulation to achieve functional engineering tissues. The main goal of tissue engineering is to assemble functional constructs that restore, maintain, or improve damaged tissues

or whole organs. The process of TE is multistep and involves engineering of different components that will be combined to generate the desired neo-tissue or organ and to study physiological or pathological models to better understand several cardiovascular or neurodegenerative disorders. Nowadays this research field has advanced a lot in the development of personalized therapies for patients who have severe chronic diseases in order to promote also precision medicine. Tissue engineering, with its goal and promise of providing bioengineered functional tissues and organs for repair or replacement has the power to revolutionize the clinical in the next years. Moreover, in the biotechnology research field and industry, significant efforts are being made in terms of research and technological advancements. In particular, the aim is the realization of improved protocols and methods for large-scale production and clinical realization of tissue engineering products. Furthermore, the development of novel platforms and methodologies for drug testing and disease modeling required process monitoring to validate the results. In particular, the monitoring of biological processes and enhanced detection methods could improve treatment options. Moreover, providing biophysical stimuli that mimic the physiological system could help to improve cell culture growth or accelerate the bioprocess present *in vivo*. One of the most exciting frontiers in research areas such as tissue engineering and regenerative medicine lies in the ability to interact with growing cell cultures and their products through cost-effective, non-invasive procedures, enabling real-time feedback in order to realize automated and scalable methods, taking advantage of technological advances in both engineering and biology that make it possible to exploit new physiology-related knowledge to promote cell growth and differentiation. Recently, significant efforts have been made to develop robust protocols to cultivate neuronal networks in controlled laboratory environments in order to observe and investigate the complexity of the nervous system. The *in vitro* approach has consistently driven fundamental research in neuroscience, demonstrating that studying both physiological and pathological nervous systems through *in vitro* is relevant also according to the 3Rs principle that refers to the replacement, reduction, and refinement of animal testing used in research and industry, exploiting the scientific knowledge and the advancements in technology within the research field. In neuroscience, the pursuit of comprehending the development, arrangement, and emergent behaviors of neuronal networks is being propelled by the continuous progress of new technologies. Furthermore, the neuronal cell culture has undergone continuous refinement since its inception. The progressive enhancement of this technology has facilitated more profound investigations into the foundational cellular and molecular mechanisms governing brain functionality. The utilization of neuronal cultures as a cost-effective and easily accessible surrogate model system has been greatly propelled by these endeavors. It is contended that the scope of

scientific inquiries, and their potential resolutions, can be heavily reliant on the available methodologies at any given time. This assertion is particularly applicable when delving into the intricacies of the mammalian nervous system and, by extension, deciphering the molecular pathophysiology underlying human neurological disorders. At present, and frequently, the pursuit of answers to pertinent inquiries may find optimal realization within a reduced, *ex vivo* configuration of tissues or cells. Despite certain limitations, the benefits presented by *in vitro* models serve as compelling incentives for advancing the technology further, particularly as a complementary approach alongside other established paradigms in neurobiological investigation[4].

1.2 Electrical Stimulation

The ultimate goal of tissue engineering is the ability to generate bioproducts that are equivalent, in terms of structural and functionality, to the physiological tissue present *in vivo*. The human body is subjected to different biophysical and biochemical stimuli that maintain the homeostasis and the functionality of the human tissue. In order to create high-fidelity *in vitro* tissues, bioengineering has been employed to create physiological environments that mimic the biological tissue's survival and function. This includes the customization of appropriate extracellular matrix using scaffold, growth factors, and using biophysical stimulation i.e. mechanical and electrical. In several works present in the literature, it has been shown that electrical stimulation and mechanical stimulation of biological tissues promoted proliferation and maturation. Thus, biophysical stimulations are essential for developing and improving the quality of engineered tissue, by acting on the phenotypic maturity of tissue-engineered constructs. These stimuli are designed to be biomimetic and simulate the native environment to facilitate proper proliferation and maturation or orientating to the differentiation of a certain phenotype [5]. In particular, Electrical stimulation (ES) has been used in both *in vivo* and *in vitro*, the stimulation has been adopted in tissue engineering for cardiac and skeletal muscle and nerves. The application of an endogenous electric field (EFs) plays an essential role not only in action potential signals in electrogenic cells but also in cellular functions, e.g. proliferation, differentiation, and migration, and also in gene expression and morphology. ES can change cell behavior, such as: migration, orientation, proliferation, and maturation and regulate gene expression of extracellular matrix proteins in tissue. The most basic method of electric stimulation is an applied DC voltage. Other stimuli can be in the form of monophasic or biphasic, sinusoidal, saw tooth or square wave signals [6]. In the literature, methods to delivery the stimulation were exploited (Fig. 1.1):

- **DIRECT STIMULATION** the electrode is in direct contact with the cell culture. This can lead to problem of toxicity: insufficient biocompatibility of the electrodes and changes in pH.
- **INDIRECT STIMULATION** the electrode is not in direct contact, non-invasive:
  - **Capacitive stimulation (CC)** a homogenous electromagnetic field is created between two parallel layers of metal, placed above and below the culture medium with a small gap.
  - **Inductive stimulation** electromagnetic fields generated by coils placed around the cell culture. A subtype of this modality is known as "pulsed electromagnetic field stimulation" or "pulsed electromagnetic field stimulation" (PEMF), where the stimulus is delivered in pulses (rather than being static or continuously harmonic) to mimic, for example, the natural strain-generated potentials observed in bone.
  - **Combined stimulation,** a combination of an alternating current and a static magnetic generated using a transient electromagnetic field.

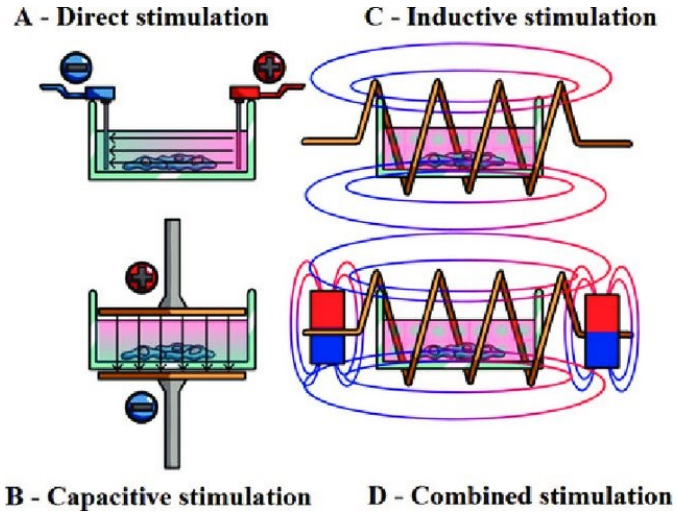

Figure 1.1 Different type of electromagnetic stimulation divided according to the type of electrodes and the position according the cell culture.

In the literature [7–10], several waveforms are demonstrated to be capable of activating the cell membrane. Rectangular, sinusoidal, triangular waveforms and symmetrical, asymmetrical, balanced, unbalanced, monophasic, biphasic pulses, constant-current or constant-voltage controlled can lead to the desired effect of stimulation according to the needed. The waveform, intensity and duration of stimuli vary according to type (*in*

vivo, *in vitro*) and main goal (cell membrane depolarization, nerve excitation, muscle contraction, cellular proliferation, maturation or migration) of the stimulation. The amplitude of the voltage applied by the electrical stimulation equipment is one of the most relevant parameters in cell culture. The outcome, especially regarding cellular migration, orientation, and gene expression has an important dependence upon the amplitude of the voltage applied. Regarding cellular proliferation and vitality, indeed, the amplitude acts as a limiting constraint, since if a certain threshold is overcome, the cells undergo apoptosis. The maximum pulse width is limited by current density: the higher the current of the stimulation is, the shorter the duration must be in order to avoid necrosis (i.e., there is a limit on the electrical energy that can be absorbed by the cell safely). Nonetheless, none of the temporal durations, from 0.025 to 380 ms, which have already been applied in cell culture experiments, have proved to be ineffective or damaging. A wide range of frequencies (7.5-60000 Hz) have been applied in previous experiments, though most of these were below 100 Hz. The choice for the low-frequency range is due to *in vivo* physiological value and therefore, the most likely to have a beneficial effect on the cells [11–14]. The effects of electrical stimulation at the cellular level are related to several theories associated with electrical fields that affect cells directly involved in mechanotransduction and chemotaxis pathways. The key component in this process is the intracellular calcium level and the electrical stimulation has an important influence on these trigger pathways. In particular, the intracellular calcium concentration was modified through stimulation and this produced a series of triggering events that led to a positive effect on differentiation and maturation [8].

At the tissue level, galvanotaxis is the phenomenon of electric gradient-guided migration, where cells migrate, according to the type, either toward the cathode or the anode of the electrodes, providing a orientation of the tissue. Thus, controlling direction and rate of cell movement, orientation, has the potential to stimulate or inhibite certain process e.g. tissue construction/reconstruction, immune responses, blood vessel, and neuron growth. *In vitro* studies have already shown the ability of EFs to influence the behavior of a variety of cell types [15, 16]. The usefulness of electrical stimulation in skin tissue engineering and wound treatment is demonstrated by its ability to induce the re-epithelialization of cutaneous and corneal wounds through promoting migration and proliferation of fibroblasts, keratinocytes and epithelial cells, enhancing angiogenesis, improving blood circulation, and blocking edema formation [17].

There are also multiple indications that electrical stimulation can promote central and peripheral nervous system regeneration. The *in vivo* stimulation is applied in numerous clinical applications, e.g cochlear implants or spinal cord injury treatment. In addition,

novel studies performed *in vitro* report the ability of electrical stimulation to increase nerve growth and blood vessel density in nerve model [18]. The positive effects of electricity in healing bone fractures has been noted as early but interest in such treatments increased considerably when Fukada and Yasuda demonstrated the piezoelectric properties of dry bone during the 1950s and 60s, providing a basis for the use of electrical stimulation as an osteoinductive tool. Such methods have been successful in treating osteoporosis, osteoarthrosis, normal, and nonunion fractures and promoting the integration of implanted biomaterials [19].

Electrical stimulation has also been suggested as a promising tool for various cardiovascular-related problems. The proven ability of electrical stimulation to induce VEGF expression both in endothelial and muscle cells both *in vitro* and *in vivo*, together with the galvanotaxis effect on the tissue, is crucial in controlling angiogenesis, consequently improving vascularization tissue and promoting endothelialization of artificial vascular implants. Furthermore, bioelectricity can greatly benefit cardiac tissue engineering by providing a tool to differentiate the engineered myocardium. This is because greater proliferation and differentiation, together with better coupling between cells and improved contractile and conductive properties, have all been attributed to the positive influence of electrical stimulation [20].

Due to the readily accessible stem cell differentiation protocols, many *in vitro* human tissues have been created to study various aspects of human diseases and drug testing responses. However, the major limitation of human pluripotent stem cell-derived(hPSCs) has been their immaturity. Since differentiation protocols produce cells that are usually associated with fetal-like maturity, it becomes difficult to model the behavior of the adult cell using hPSC. In such context, biophysical stimulation promotes proliferation and maturation providing maturity to the human stem cells [21].

Electrical stimulation and biophysical stimulation applied to cell culture have the potential to overcome some of the issues that are present in tissue engineering, cancer treatment, drug testing, and other biomedical scientific fields. Furthermore, electrical stimulation is proving to be effective in the oriented and aligned growth of cells, opening up new possibilities in tissue and organ engineering, and allowing greater complexity in the design of the tissue-engineered constructs. Electric stimulation has the potential to provide better control over the *in vitro* and *in vivo* proliferation and differentiation of cells and the properties of the resultant tissue, both spatially and temporally. Stem cell fate could be controlled, directing them to specific lineages, yielding a homogenous cell culture.

Electrical stimulation offers a cost-effective, simple, and flexible methods to promote intracellular pathways by inducing the cells themselves to proliferate, maturate, differentiate or migrate. Another advantage of electrical stimulation is due to the treatments that involve incorporated growth factors and gene therapy, its effects disappear with the stop of the treatment. This benefits for clinical usage allow better control of the treatment.

To reduce the cost and time of the whole process, together with electrical stimulation, other techniques can be used synergistically, reducing the required levels of expensive growth factor and promoting the ultimate goal of therapeutic application. Finally, to obtain an automated cell culture device able to control and monitor the bioprocess and improve standardization, a monitor system is necessary, composed of sensors in order to realize a feedback loop able to correct the parameters [6, 22].

1.3 Real Time Monitoring

The implementation of sensors within cell culture has revolutionized the biotechnology industry, providing a drive toward the monitoring and control of bioprocess. Different fields have benefited from this, both in research and industrial fields such as biological science, biomedical and clinical manufacturing. Thanks to technological advances in biosensing techniques and analytical tools, the realization of sensors for cell culture monitoring has become a cost-effective highly varied and customizable possibility. The main idea is to recreate a proper condition for cell culture, thus implementing a monitor and control system that supports the culture of the primary target cell or cell lines. The monitor involves media composition, temperature, gas level, pH, mass transfer, and agitation. In light of this, the monitoring of cell culture is pivotal for the continuous characterization of the bioprocess. It helps to understand the cell status e.g. viability, growth or maturation, and metabolism properties in order to establish and ensure the reproducibility and standardization of cell culture. Cell culture monitoring is useful to understand and predict the culture process in order to measure the magnitude and time course of response of development of the tissue and the different treatments of the culture. Therefore, an optimally regulated and controlled environment allows cells to reach the desired functionality and maturation and move on to further applications, including cell culture expansion, and metabolite study using drug screening or pathological models. Other important parameters to monitor regards the metabolic profiles control the exceeding according to defined thresholds in the cell culture environment. In this context, the nutrients and accumulation of metabolic byproducts were measured with traditional analytical tools such as the optical microscope, spectrophotometer,and other expensive

laboratory facilities. Monitoring the cell culture environment is functional in understanding the media replacement and the correct parametric profiles to reach the homeostasis. The cell culture process according to cell preparation, environment and media assessment and the critical parameters to take into account is time and cost consuming. Due to this, continuous monitoring of cellular and environment profile is fundamental to achieve and optimize such process. Several improved methods have been employed to monitor and control bioprocess, together with traditional methods, that remain the golden standard, by exploiting microfabrication, optical[12,20] and conductive materials, sensitive signaling probes, and sensorized microfluidic chips. Sensor systems are essential tools for investigation and standardization in cell culture. Electrochemical and optical sensors are predominant, which enable the marker-free, continuous, online recording of transient effects and deliver information differently from traditional techniques that regard analysis at end-point tests. A lot of effort has been made in the progress of cell culture monitoring, therefore limited is the integration and translation in standard cell culture procedures. In particular, the monitoring of the culture and tissue parameters is essential for:

- tracing of the culture process,
- elucidating the physical/biochemical mechanisms of tissue development,
- implementation of feedback-controlled strategies aimed at optimizing the culture progression,
- automation and scale-up of tissue manufacturing.

Sensors for environment monitoring can be classified into three categories according to the position of the sensing probe relative to the culture chamber:

- invasive, sensor is placed directly inside the chamber, either immersed in the culture fluid or in direct contact with the construct,
- non-invasive, sensor is not in contact with the interior of the chamber, and is capable of measuring via interrogation through the chamber wall,
- indirect, directly on the culture media, but via sampling means.

Sensors for environment monitoring can be classified in three categories as shown in Table 1.1:

	Advantages	Drawbacks
Invasive sensing	High specifity High sensitivity	Need for sterility Difficult calibration
Non-invasive sensing	No need for sterilization Ease of calibration	Low specifity Low sensitivity
Indirect sensing	High specifity High sensitiviy	Artifact Impaired feedback

Table 1.1 Classification of the sensor for *in vitro* cell culture

Monitoring the construct can be divided as illustrated in the table 1.2 in:

	Environment Parameters	Construct Parameters
Physical	Temperature, pressure and flow rate	Stiffness, strenght and permeability
Chemical	Ph, dissolved 02 and CO2, chemical compounds, metabolites/catabolites as glucose, lactate and secreted proteins	Composition of the scaffold extracellular matrix formation
Biological	Bacterial contamination (sterility)	Cell number and viability, proliferation rate, concentration of intracellular proteins

Table 1.2 Type of monitored parameters of *in vitro* cell culture

Important parameters to monitor in cell culture include temperature, concentration of O_2, CO_2, pH, and nutrient concentration e.g. glucose and lactate due to the importance of cell vitality for maintain the homeostasis of the cell culture. Cell culture monitoring was performed at different levels, intracellular or extracellular, where the measurement of certain parameters was performed directly inside or outside the cell respectively. And finally, in the environmental measurement that provides an indirect monitoring of the cell culture status such as oxygen or glucose and lactate level. Nowaday, mostly of the techniques are related to imaging monitoring, fluorescence and staining techniques that are expensive and require specific devices and are techniques mainly invasive and destructive for the cell culture.

The monitoring of cellular physiology involves assessing of various aspects regarding cellular viability, behavior, and related characteristics. This parameters includes cell morphology, cell counts, cell density, cell viability, adhesion, and migration events. The golden standard requires microscopy, common method employed for the measurement of these features, as a fundamental methodology to observe the cellular status and behavior. However, along with technological advancements, image processing algorithms, and optical and electrical sensing technologies are now utilized to enable quantified and continuous monitoring of these cellular physiology parameters.

Furthermore, the monitoring of the cellular environment parameters is crucial in cell culture. Critical factors include environmental properties such as temperature, pH, carbon dioxide, and dissolved oxygen (DO) levels. Monitoring these environmental conditions is an indirect method to evaluate the cellular status to ensure optimal cell growth and performance. Traditionally, these parameters have been monitored. Thus, highly optimized and reliable sensors are currently utilized. However, thanks to the emergence of fabrication and analytical technology, cell culture devices require miniaturized and reliable sensing techniques for integration into the culture platform. Translational approaches are the current trend and incorporate methodology and tools from both traditional and novel sensing probe technologies in order to involve large-scale, miniaturized, disposable, and non-invasive applications.

Assessing cellular metabolites is a significant parameter for evaluating cell quality and predicting yield. To achieve this goal, the quantitative monitoring of chemicals and biological metabolites, such as nutrients, byproducts, and cell-secreted products are required. Additionally, monitoring the bioproduct presence is helpful in order to maintain homeostasis and identify the optimal culture condition parameters. During the culture process, the cells produce and consume metabolites, including nutrients, waste, and other molecules. Nutrient quantification for cell consumption is a critical parameter for understanding the cell growth rate, phenotype, and metabolic behavior.[1,13,80–83] In bioreactor or other culture devices with a larger volume scale, metabolitic analysis were frequently evaluated exploiting online and inline sampling-based nutrient assessment for cell culture. Nowadays, the miniaturization of electrodes, enhanced enzyme encapsulation, and reliable sensor format to the cell culture monitoring system provide a valid alternative. Electrical sensors can detect a wide range of molecules and be embedded in microelectronic devices by applying techniques such as voltammetry, potentiometry, amperometry, and electrical impedance spectrometers. Similarly, the availability of optical sensing components driven by the sensitive optical probes (e.g., absorption, plasmonic,

luminescent, Raman) has gained momentum with the rapid developments in the field of nanotechnology.

The novel technologies approaches exploited in cell culture monitoring (e.g. optical and electrical biosensors), differ from traditional methods that involve the use of tabletop analytical instruments i.e. spectrometry and chromatography. Such traditional techniques have excellent sensitivity, accuracy, and specificity, and are the golden standard. These tools suffer from some disadvantages, limited in continuous monitoring, portability, and compatibility with bioreactors and customized culture devices. Various biosensors have been developed in order to overcome these limitations. The biosensor converts particular physical phenomena and transduces them in optical or electrical signal with quantitative and qualitative information about the detected specimen. This kind of sensor has a small footprint and perform a continuos measurement to multiple targets according to the functionalization, and can be located within the cell culture, providing customized and tailored applications. Furthermore, biosensors offer numerous advantages due to their flexibility with acceptable sensitivity, accuracy, biocompatibility, and cost-effectiveness.

Optical Biosensors are currently used in biosensor applications due to the different types of optical analysis. This class of biosensor is able to provide label-free, online and parallel detection of the target analytes and it is performed by exploiting the interaction of the optical field with a biorecognition element [23, 24]. The optical biosensors are good candidates for obtaining information in terms of sensitivity but suffer from high cost and the miniaturization is difficult due to the complexity of the measurement system and to perform wireless communication. Consequently, the integration of optical measurement in customized culture devices still remains an important issue.

Electrochemical sensor can be defined as an integrated tool capable of providing quantitative information with contact with a biochemical receptor for the recognition of particular compounds with an electrochemical transduction element. At the interface, a chemical reactions process occurs, thus generating an electrical signal that can be easily measured. In the literature, many studies have revealed that this class of biosensors presents many advantages over the previously presented ones such as detection speed, low cost, high sensitivity, and relatively simple instrumentation [24].

The biosensor realization is done through the employment of microfabrication and printed technologies for electrical and electrochemical sensors. The fabrication patterning results in a high sensitivity and accuracy on the sensing surface. However, the reproducibility and stability for long-term sensor operation are not ensured and remain a future development.

Sensorized cell cultures are expected to provide controlling and monitoring cell parameters. In addition, the possibility of a wide range of monitor parameters through optical and electrical techniques suggests several facilitation through the understanding of optimal cell culture more efficiently. Together, combining novel approaches in fabricating and printing techniques for microstructures, enhanced biocompatibility of materials, improved customized and modular techniques, and image processing, will support a substantial strides for the developing of integrated platform for monitoring and control cell cultures.

The advanced technology exploited in the cell culture monitor is a key element in various biotechnological research and industrial applications. These technologies are an important step in promoting the standardization and automation of cell culture techniques and protocols. The main advancements include online monitoring, for various cell cultures, allowing also multi parameters monitoring in order to assess production quality with high performance by sensing the parameters from physiological, environmental, and target molecules, including metabolites and contaminants. Cellular environment monitoring is traditionally controlled by the incubator. However, in the case of experiments requiring specific cell culture formats like bioreactors, electrical sensors with specific molecular recognition and precise micropatterns offer accurate and sensitive measurements. Consequently, these advancements have paved the way for more comprehensive and precise cell culture methodologies, holding significant promise for future developments in the field of biotechnology and healthcare.

Nowadays, cell culture trials and regulatory agencies require precise investigation and in-depth results, and extensive and real-time monitoring is a prerequisite for obtaining detailed process understanding. Thus, it is fundamental to establish standardization and automatization of large-scale and high-throughput cell production and clinical products.

1.4 Thesis Outline and Motivation

In biotechnology, substantial efforts are dedicated to advancing research and technology, with a focus on improving protocols for large-scale tissue engineering product production. The development of innovative methods for drug testing and disease modeling also requires biophysical stimulation to accelerate several bioprocesses (e.g. cellular proliferation and maturation) and process monitoring. One exciting research frontier involves cost-effective, non-invasive procedures to interact with growing cell cultures and enable real-time feedback, fostering the development of automated and scalable methods.

This leverages technological advances in both engineering and biology to promote cell growth and differentiation. And finally, to achieve this objective necessitates a robust collaboration across various scientific and technological research fields. Biotechnological applications are discussed in this Ph.D. thesis, in which the combination of advanced technology, biophysical stimulation, and printed electronics are exploited as suitable tools for obtaining relevant results in terms of cell culture improvements and quantitative feedback from cells, with low-costs and limiting the invasiveness for the cell culture. In addition, the development of a system for label-free and non-destructive monitoring with continuous measurement of the construct development status would allow continuous and immediate optimization of the culture protocol to the actual needs of the construct itself.

The dissertation will present two main applications in the biotechnology research field that have as their objective an improvement of existing methodologies available in biotechnology laboratories, following the introduction presented in these previous paragraphs. In detail, the thesis is organized in chapters as follows: In chapter 1 the theme of tissue engineering is introduced and deepened, with a specific focus on the current state of the art related to biophysical stimulation and real-time monitoring of *in vitro* cell culture. Subsequently, in chapter 2, an introduction about neurophysiology with a brief discussion about neuron physiology and the electrophysiological methods for action potential recording is presented and finally an overview about the properties related to the electrode used in electrical stimulation and recording in the field of neuronal application are analyzed in chapter 3. The first work presented in chapter 4 provided the initial insight into the development of an electrical field stimulation to improve differentiation and maturation of human induced pluripotent stem cells-derived dopaminergic neurons. Then, in chapter 5 the realization of a printed microelectrode array for electrical stimulation and real-time monitoring for cell culture is discussed in terms of design, development, and characterization. Finally, the dissertation will conclude with an overall conclusion underlining the results and limitations obtained and analyzing the possible future outlooks in chapter 6.

Chapter 2

Neurophysiology

Tissue engineering is crucial in many fields of research, based on the relevance exposed in recent years about the possibility of exploiting it to repair or replace tissues in the different compartments of the human body and to exploit new technologies either in basic research or industry for discovery and understanding in the biological field or for large-scale production or realization of TE products in the clinical and drug testing fields. Also in the field of neuroscience, tissue engineering opens up the possibility to bring a major contribution to the resolution of the main issues associated with various neurodegenerative disorders. In this chapter, the various insights related to neuronal applications will be addressed.

2.1 State of the art

Worldwide, neurological disorders e.g. epilepsy, Parkinson's, and Alzheimer's disease, and mental disorders (depression and schizophrenia) are the leading cause of physical and cognitive disability, currently affecting approximately 15% of the worldwide population[25, 26]. Absolute patient numbers have considerably climbed over the past 30 years. On top of that, the burden of chronic neurodegenerative conditions is expected to at least double over the next two decades. Because of this evolution, due to these data and the huge increase of population and aging people, this issue is becoming an important socio-economic problem, so it is fundamental to invest a huge deal in basic research and in the development of new techniques and devices in order to enhance research and clinical products in terms of neurological disorders[27].

Neurodegenerative diseases occur when nerve cells in the brain or peripheral nervous system lose function over time, leading to a decline in cognitive and/or motor abilities. At the moment, the clinical treatments help to relieve various physical or mental symptoms associated with neurodegenerative disorders, however currently it is not possible to stop or decelerate the disease progression, and no cures exist. In order to develop potential treatments for neurodegenerative diseases and to understand the etiological mechanisms involved, it is crucial to study the pathway occurring within the neuronal networks and the nervous system. Given the characteristics of neuronal cells, in particular, the electrogenic features of neural tissue and the propagation of the transmitted signal through the neuronal networks, studying the transmission and the features of the neuronal function represents an absolutely challenging target. Loss of electrical functionality and transmission in the networks indicates an alteration of involved neurons and it is considered as the starting point of neurodegenerative disorders. Due to this, several strategies have emerged in the last decades. Furthermore, for this scope, in the field of neuroscience, several tools are emerging to record the signal transmissions.

Neuroscience is a multidisciplinary science that study the behavior of nervous system and its functionality in order to better understand physiological and pathological performance to understand the several neurological disorders present worldwide. To this end, in order to better understand the nervous system, it is necessary to start to analyze the behaviour on *in vitro* cell culture. In modern neuroscience, electrophysiology often refers to the study or research approach implemented to investigate the electrical properties of brain cells and tissues. It is sensitive enough to measure basal voltage/potential or electrical currents from a single ion channel or a whole cell, while also possessing the ability to study electrical processing within an entire brain region.

2.2 Neurophyisiology fundamentals

2.2.1 Neurons

The nervous system is the control center of the body that control, regulate, and communicate to the all body. It mantains the stability (homeostasis) of the living biological system. The nervous system is composed by two principal neuronal classes:

1. Neuronal cells
2. Glial cells

The neuronal cell shown in Fig. 2.1 represents the functional unit of the nervous system. It is composed by three main components: Soma, dendrities and axon. The soma is the body cell of the neurons, where the action potential signal is generated, the axon is a thin cable-like structure of <1 μm that transmit the action potential from the soma to the dendrites of another neurons, often surrounded by a mieling sheath that insulates them and increases the electrical pulse speed rate, finally the dendrites are thin filaments as tree-like structure that receive the action potential. Glial cells represent the 90% of the nervous system cells and have a methabolic and structural support function to the neuronal cells.

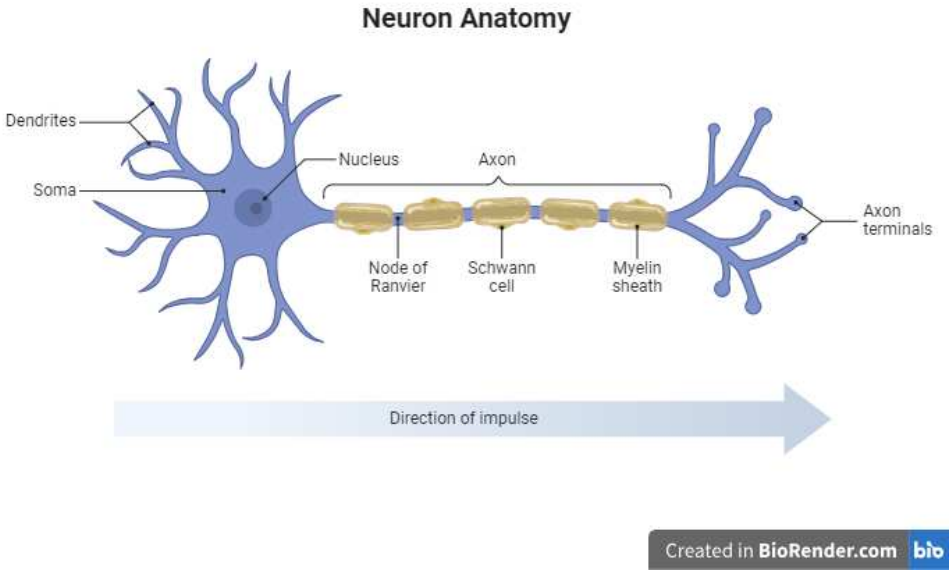

Figure 2.1 Simplified representation of a neuronal cell. Created with BioRender.com

Neurons are excitable cells that communicate throw electrical signals. Neurons produce rapid and differential electrical signals named action potential (AP). AP are rapid and wide modification of the cell membrane voltage potential between the inside and outside of the electrogenic cell. Neurons under resting conditions have an electrical potential across their cell membranes, with the inside of these cells being negatively charged with respect to the outside (extracellular spaces). This is defined as the resting membrane potential, which ranges between -40 and -90 mV in healthy neurons. These potentials exist due to an excess of negative ions inside the cells and an excess of positive ones on the outside. The distribution and the moving of the three major ions (Na^+, Cl^-, K^+) movement across the membrane produce variations of the membrane potential.

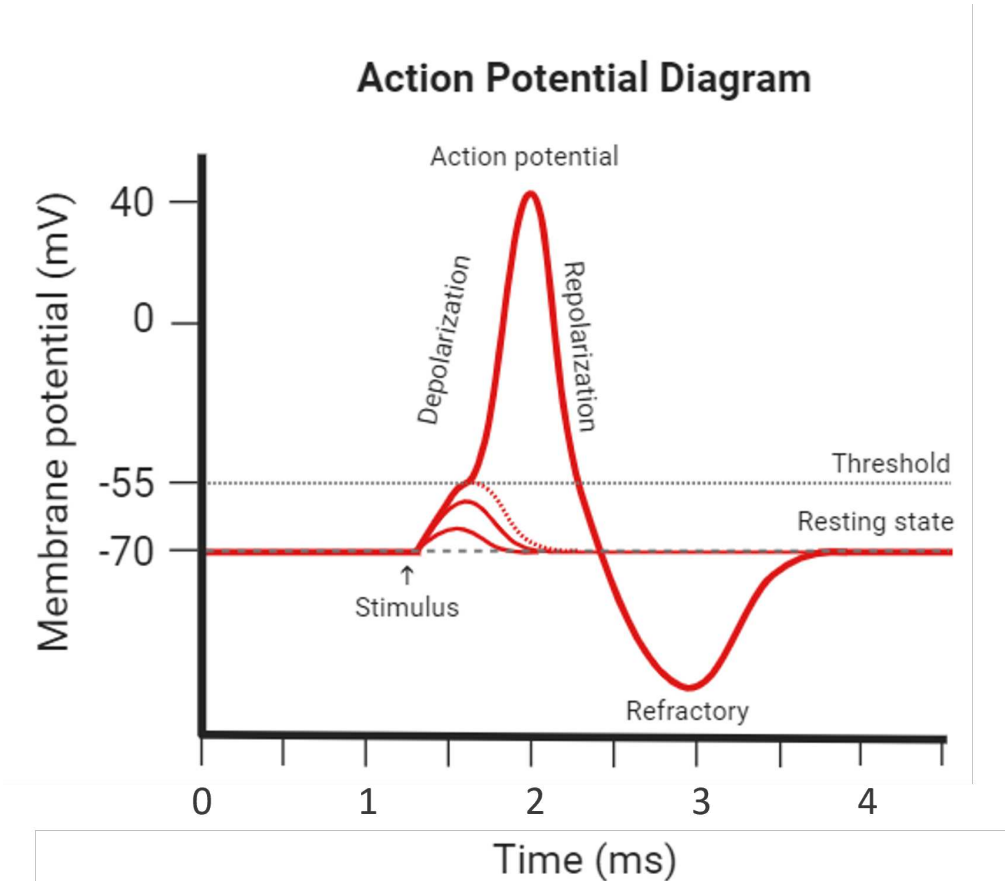

Figure 2.2 Intracellular action potential waveform of a neuronal cell. Created with BioRender.com

More specifically, the cell membrane potential is the potential difference between the internal and external cells determined by the ions' electrochemical concentration. The ion movement during excitation of the cell underlies the development of an action potential, which then propagates from the point of excitation along the surface membranes. The AP propagates along the whole axon without attenuation, due to "all-or-none" event. The action potential phases are described as follows in Fig. 2.2:

- At rest potential of generally -70mV, no signal transmitted or received, an initial local electrical depolarization (i.e., the membrane potential overcomes the threshold and reaches a voltage of +10 to +30 mV above the given resting potential), causing voltage-dependent Na channel openings and generating an action potential. The sodium permeability increases for 1–2 ms, causing the cell depolarization and driving the membrane potential toward Na equilibrium potential; then after approximately 1 ms, the channels are closed.

- After, the depolarization activates voltage-gated K channels, thus drives the membrane potential back toward the potassium equilibrium potential (-70 mV), through the repolarization phase, with a status of hyperpolarization (-90 mv) until returning to a rest potential.

Neural biopotentials are electrical signals generated by the cells of the nervous system and, thus relevant due to the possibility of recording and monitoring the network and individual behavior of neuronal cells yields information about the status of the brain and the peripheral nervous system frequently used in clinical and research settings. Several methods for recording neural biopotentials have been developed and exploited with various differences in terms of spatial and temporal resolution, and goal to achieve. The proper design of electrodes for the recording and the circuit architecture needed to amplify and process the neuronal signals are crucial in order to obtain a correctly recorded and processed signal to understand the signal characteristics. Continuous developments and technological advances in electrode materials, interface circuits, and embedded systems for neural interfaces with tailored instrumentation solutions at a range of spatial and temporal scales are driving advances toward future medical therapies and neuroscience discoveries.

In particular, the purpose of electrophysiology is to measure cellular excitability observing the ionic flow and potentials across the cell membrane. These electrical signals can be recorded with specialized instrumentation in order to assess physiological function, for neuroscience research, and even provide a communication and interface through brain-computer interfaces (BCI). Biopotentials can be recorded from different locations in the body, according to the organ or system targeted for examination. Aside from the diversity of locations and anatomical structures that can be recorded, these signals also vary significantly in their spatiotemporal properties. Spatial resolution is generally dependent on the distance between the electrodes and the target measurement source, as well as the spatial diversity of average electrical activity in the electrode's vicinity. Neuronal action potential signal can be recorded and studied both *in vivo* and *in vitro* with extracellular and intracellular electrodes and through optical methods.

2.3 Electrophysiological Methods

The different electrophysiological methods showed in Fig. 2.3 are listed and explained in detail:

- intracellular
- extracellular

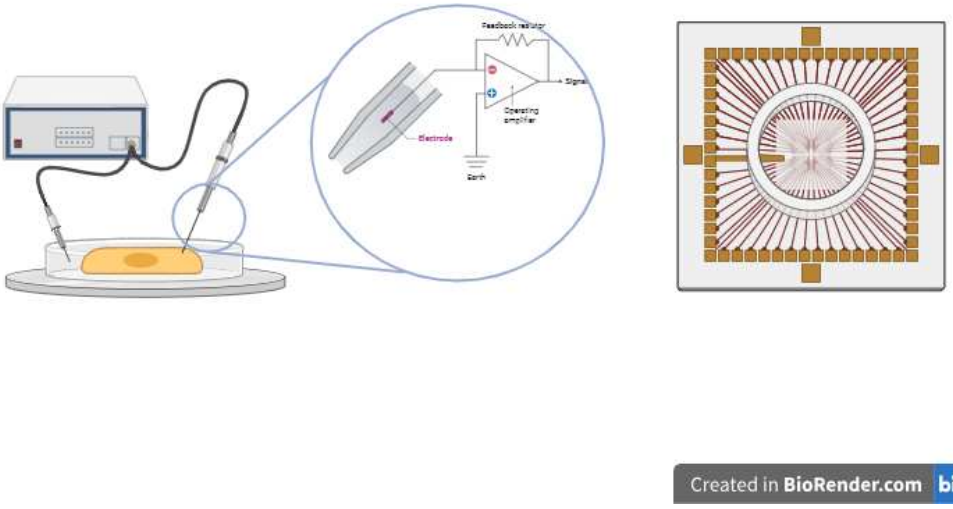

Figure 2.3 Graphical representation of the intracellular recording techniques (Patch clamp) and extracellular technique (Microelectrode array). Created with BioRender.com

2.3.1 Intracellular recording

The intracellular recording technique consists on the measurement of voltage or current across the membrane of a single cell at once, providing a better signal quality but limiting the recording number of neuronal signals [28]. It typically involves an invasive electrode (glass micropipette) inserted in the cell and a reference electrode outside the cell. The electrodes are connected to an amplifier to measure the membrane potential. The intracellular recording technique by using patch clamp (Fig. 2.3) is the gold standard for analyzing single neurons and the synaptic connectivity of some cells. This technique is limited to operator dependence skills, and due to the invasiveness and low-throughput technique, the neuron viability is altered.

2.3.2 Extracellular recording

Action potentials can be recorded with noninvasively and at high throughput by extracellular recordings, monitoring neuronal activity from outside the cell. They provide a means to measure patterns of action potentials within many areas of the peripheral and central nervous system. In addition, neuronal network activity can also be recorded [28]. Neuronal activity generates currents due to the ionic movements driven by their electrochemical gradient. This gradient is propagated in the extracellular medium and registered by the electrode. Due to the properties of the lipid bilayer of the cell membrane that acts as a capacitor, on each side of the membrane occurs an accumulation of positive and negative ions. The asymmetry of charges on each side of the membrane creates a difference of electrical potential. The quality of the recorded signal depends greatly on the proximity and the nature of the contact between the electrode and the cell: the closer is the cell or the better is the contact (the higher is the resistance), the better is the signal recorded. These voltage changes can be measured from inside the cell with intracellular electrodes, or at a distance with extracellular electrodes positioned almost in contact with the cell.

The extracellular measurement records the extracellular field potential generated by the action potentials of one or more neuronal cells. It reflects the electric field exerted on ions in a conductive medium like the extracellular compartment [29]. Recorded signals can reflect the fast spike activity of individual neurons (events in the order of 0.5-2 ms with hundreds of µV peak amplitude) or the slower superposition of action potentials and synaptic potentials resulting in waves (>10 ms duration) of high amplitude (typically from hundreds of µV to 1-2 mV) [30]. The neural activities are first amplified after sensing, then are low-pass filtered to obtain the LFP and are also high-pass filtered to identify the activity of single neurons by using spike detection and performing sorting algorithms. The LFP includes lower-frequency neural waveforms in the range of mHz to 200 Hz with an amplitude of 500 μV_{pp} to 5 mV_{pp}. High-pass filtering extracts the spikes of the nearby neurons on top of background activity. Amplitude threshold methods are used to detect these spikes. In the next step, the features of the spikes are extracted and sorted accordingly.

Microelectrode arrays (MEAs) Microelectrode arrays (MEAs) or multielectrode arrays (Fig. 2.3) are bioelectronic devices composed of an array of multiple (tens to thousands) electrodes of microdimension in which electrogenic cell (i.e. cardiomyocytes and neuronal cells) signals are recorded or electrical stimulation is provided to the cell

culture. This electrode pattern works as an interface for neural interfaces between cells and electronic circuitry [31]. MEAs are generally employed to acquire extracellular signals and to stimulate to generate evoked potential; rarely provide electrophysical stimuli able to provide physiological conditions for maturation [32, 33, 14]. Otherwise, *in vitro* measurements are related to voltage changes that can be measured with extracellular electrodes positioned almost in contact with the cell. The quality of the recorded signal depends on the cell-electrode distance and the electrode characteristics. The extracellular recording is an indirect measurement of the ionic movements in a conductive medium like the extracellular compartment. This indirect technique allows the recording of neuronal activity in both *in vitro* and *in vivo*, providing insight into patterns of action potentials in various areas of the nervous system. Recorded signals can reflect the fast spike activity of individual neurons or the slower action potentials and synaptic potentials, all this signal resulting in waves of high amplitude typically from hundreds of μV to 1-2 mV of neuronal networks [30]. Implantable MEA was positioned in the brain for deep brain stimulation (DBS) with an effective at treating movement disorders such as Parkinson's disease or cochlear implants that improve their hearing by assisting stimulation of the auditory nerve [30, 34].

The recording of the action potential, indeed, generated by the electrical potential of cells could help to identify the cell electrophysiological behavior, to better understand the communication between neuronal networks e.g., the analysis of action potential helps to understand the functionality of neuronal cells and networks. Furthermore, it is interesting to study the response of the action potentials for both pathological and physiological conditions. Multiple neuronal locations can be monitored simultaneously, providing a screening of neuronal population activity and synchronous behaviors within a neuronal network [35].

In vitro microelectrode array (MEA) technology was used as an effective methodology to study cultured neural networks. The MEA device creates a unique electrical interface with the cultured neuronal cells, in which neurons are directly seeded and grown on top of the electrode array (neuron-on-electrode configuration). Theoretical models and experimental findings indicate that the physical arrangement and biological conditions at the cell-electrode interface are critical determinants of neural recording outcomes, encompassing factors like recording yield, signal morphology, and signal-to-noise ratio. Recent interdisciplinary methodologies have demonstrated that the performance of Microelectrode Arrays (MEAs) can be significantly improved by leveraging novel materials, intricate structures, surface chemistry modifications, and advancements in biotechnology. Commonalities exist between *in vitro* and *in vivo* neural interfaces, allowing for the ex-

tension of solutions to *in vitro* neural interface challenges in addressing issues associated with brain-machine interfaces or neuromodulation techniques *in vivo*. Micro-Electrode Arrays (MEAs) are a key component for electrophysiological monitoring in several applications, from in vitro toxicity studies [36] to implantable brain-machine interfaces [37]. The multi-channel neural recordings are composed, in addition to the MEA, also by the electronics front-end that can be designed with different architectures. The most common architecture exploits one analog-to-digital converter (ADC) that is shared among all channels. Each channel has a neural amplifier and filter due to the small amplitude and bandwidth of the neuronal signals, and the neural signal of each channel is passed to the ADC. The number of electrodes is related to the improvement of the neural recording spatial resolution. The power consumption and chip area should be considered and minimized as much as possible. Generally, in the design of neural bioelectronics device, to provide the required signal quality, several factors should be considered e.g. sufficient gain, high SNR, appropriate bandwidth, high common mode (CMRR), and power supply rejection ratio (PSRR), low power consumption and low chip area. Finally, the amplified neural signals are converted to digital by an ADC before being transmitted to the data collection. Once the data are collected from the microelectrode array, it is important to extract the relevant features from the recording, to visualize and analyze the data. To address this need, the widespread availability of this user-friendly and mathematically advanced program supports the use of MEA technology in both commercial (Axion BioSystems, Atlanta, USA, Multi Channel Systems MCS GmbH, Harvard Bioscience, Inc., Massachusetts, USA) and literature papers. Finally, visualizations allow the user to prepare, validate, communicate, interpret, and verify data collected from MEA[38–40].

The traditional technique for MEA realization consists of microfabrication methods at the micron or submicron scale able to design miniaturized patterns, objects, or devices that are applicable also in biomedical fields e.g. biophysics, pharmacology, medical biology, and nanotechnology. The main technique is related to photolithography which exploits the deposition, usually a thin layer of insulating or conductive material, patterning, a sensitive photoresist layer can be deposited on top of the film and then patterned via photolithography, and finally, etching of different materials that consist in chemically remove material from the surface. The use of such techniques allows the electrode dimensions of few microns and a huge number of electrodes, together with the use of metallic layers, have imposed the need for an expensive cleanroom for the production of MEAs, imposing a high cost and time consuming as tools that researchers are pushed to reuse, compromising the reproducibility and the quality of the acquired data. A necessity exists for the innovation of fabrication methods capable of manufacturing disposable

devices that can integrate cutting-edge technologies that overcome traditional metal electrodes on rigid substrates.

Printed Electronics Printed Electronics emerges as a promising technology capable of providing efficient solutions for various biological applications. This innovative manufacturing paradigm allows the use of organic electronics and the possibility of printing biocompatible inks based on polymers and carbon materials. The primary advantages are related to cost-effectiveness compared to traditional production techniques and its ability to adapt to curved and stretchable surfaces due to its compatibility with flexible substrates. Moreover, the choice of printing methods can be tailored to specific needs, including resolution requirements, substrate, ink properties, and specific patterns, as well as economic and technical considerations. Printed electronics are particularly attractive for biotechnological applications, that require low-cost and disposable solutions for single-use devices, biocompatibility and cytocompatibility for biological cells and their products, and the possibility of direct printing on different irregular substrates and easily integrated within cell cultures, scaffolds, or bioreactors to obtain information about the cellular environment i.e. cell adhesion, growth, differentiation, and electrical activity or the products generated in biological samples. As well as the realization of bioelectronic devices e.g. microelectrode array for action potential recording.

Aerosol Jet Printing Aerosol Jet Printing (AJP) is an innovative additive manufacturing (AM) technique that allows the printing of sensors and electronic components with important advantages, such as easy accessibility for the prototyping and low-volume manufacturing, processing of varied biocompatible materials, sustainability, and device customization. In particular, the possibility to print electrodes and sensors directly on the device allows the development of easy and low-cost prototypes with good resolution, repeatability, and accuracy. It is a feasible technique that allows printing inks with different electrical (both conductive and insulating inks) and chemical properties on a wide range of substrates. AJP performance allows the printing object of micro dimension. Furthermore, AJP provides a selective deposition both on planar and 3D structures, without using masks or post-processing, except the curing of the ink to obtain the desired ink conductivity, and realizing specific surface features [41, 42]. Furthermore, Aerosol Jet Printing (AJP) is a printed electronics technique that exploits the printing of small quantities of functional materials on a substrate to deposit a specific pattern. The functional ink is deposited on the substrate by exploiting the aerodynamics focusing. It allows for the precise placement of electronic inks, enabling the creation of micro

patterns, circuits, and functional structures on various substrates. Initially, the ink is loaded into an atomizer, which generates a concentrated mist of tiny droplets containing the material, with diameters ranging from 1 to 5 microns. This mist of aerosol is subsequently directed to the deposition head. Here, a sheath gas envelops the aerosol in the form of a ring, enabling fine-tuned focusing. The aerosol mist is focused by a sheath gas, which surrounds the aerosol as an annular ring inside the deposition head, from the nozzle to the substrate. Furthermore, small droplets dimensions (1-5 μm diameter) and performance achievable allow the printing of objects of micro dimension. In an AJP system, the atomizer (viscosity ranging 1-1000 cP) creates a dense mist of material starting from the liquid ink. Printed lines range from 10 μm to millimeters. This technique provides without using pre-patterned lithographic masks, and thus allows the adaptation of different geometries in a cost- and time-efficient manner [41, 43]. The system is driven by standard computer-aided design (CAD) data which is converted to make a vector-based tool path. This tool path allows the patterning of the ink by driving a 2D or 3D motion control system. Furthermore, printing technologies have enabled the evolution of printed and flexible electronics. Another advantage is the ease of incorporating newly emerging ink materials such as PEDOT:PSS, a conductive polymeric material that has excellent properties in terms of conductivity, processability, and stability. For medical applications, it shows good biocompatibility and chemical resistance. It is used as a coating for metallic material due to low impedance for electrical sensing and stimulation of cellular activity, to improve the signal-to-noise ratio (SNR) of the recorded signals and the increase of the surface area [44–46].

Chapter 3

Electrode for stimulation and recording for neuronal application

3.1 Introduction

An electrode is the primary component of an electrical circuit for a biopotential recording or stimulation instrument that interfaces with non-metallic media and is in contact with the biological environment. In electrical stimulation, the electrode sources current through ionic transport to affect the local electric fields; in a recording application, the electrode couples galvanically to capture the local field potential. Given their roles, the dimensions, geometry, and composition are of utmost importance to design requirements. This chapter presents the main theoretical concepts for understanding how neuronal stimulation and recording electrode works and how biopotentials are registered. At the end of the chapter, it will be possible to understand how the transduction of a biopotential occurs, that is, how the events which begin with the exchange of ions across the cell membrane can be represented by an electrical signal captured with electrodes inserted into the biological tissue [35, 47].

Current and emerging neural prostheses and therapies that involve neuronal stimulation and recording imply the integration of electrodes. *In vivo* these applications regard the development of upper and lower limb prostheses for spinal cord injury and stroke, prostheses for the bladder, auditory prostheses targeting the cochlear and brain-stem, visual prostheses for the retinal and cortical regions, cortical recording methods aimed at facilitating cognitive control of assistive devices, vagus nerve stimulation to address conditions such as epilepsy and depression, and deep brain stimulation (DBS) for the

treatment of essential tremor, Parkinson's disease, epilepsy, dystonia, and depression. In all instances, the electrodes used must exhibit characteristics such as low impedance for recording purposes or the ability to safely deliver reversible charge injections for stimulation and this is also valid for *in vitro* application. The present chapter reviews the properties required for electrodes used in the stimulation and recording of neural tissue *in vitro* with an emphasis on microelectrodes and their electrochemical characterization.

3.2 Electrical requirements

The main difference between stimulation electrodes and biopotential recording electrodes regards the magnitude order of the current through the electrode/electrolyte interface. On the other hand, the electrode material and the techniques involved can be the same. The ideal stimulation electrodes are those that do not modify the environment where they are applied, neither their own characteristics during stimulation. If the electrode is degraded or corroded by the electrical stimulation, there will be an increase of ionic concentration at the site of the electrode application, affecting the biological tissue pH, or promoting chemical reactions that will bring to cell death [35].

3.2.1 Stimulation electrodes

Electrical stimulation promotes a functional response through the depolarization of excitable cell membranes. This depolarization occurs as a result of the movement of ionic currents between two or more electrodes, with at least one electrode being positioned in close proximity to the intended target tissue. In the context of most neural applications, electrical stimulation is provided in the form of a sequence of biphasic current pulses. Fig. 3.1 shows representative pulse waveforms along with their associated pulse parameters.

The pulse is composed of a cathodal and anodal phase, with current amplitudes and durations that result in an overall zero net charge for the pulse, called charge balance mode. A cathodal current is reduced at the stimulation electrode, with the direction of electron flow being from the electrode to the tissue. while the anodal indicates an oxidizing current with flow in the opposite direction respect cathodal. The charge delivered by the electrodes is calculated as the time integral of the current. Due to physiological observation, the leading phase is usually cathodal. Another option is the imbalance charge between the cathodal and anodal, different amplitude between

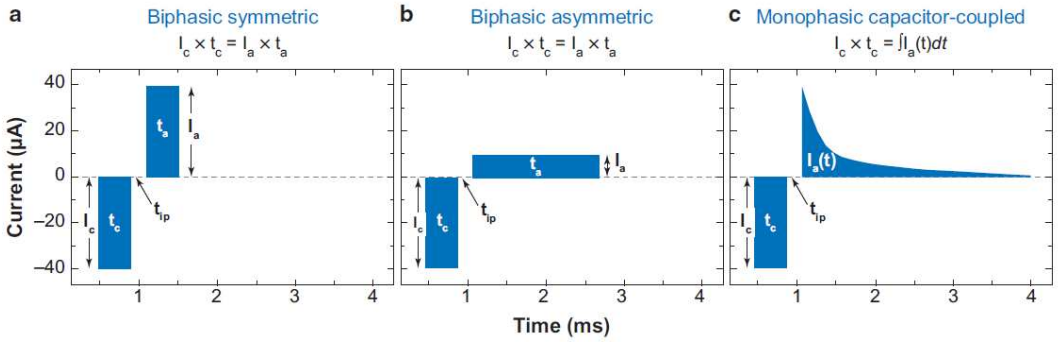

Figure 3.1 Typical current waveforms applied in neural stimulation with charge-balanced injection. The parameters vary widely depending on the application and size of the electrode

positive and negative waveform in the same pulse, has also been proposed as a way of compensating for irreversibility in charge-injection processes. In the majority of application, the charge-balanced waveform is used in order to avoid damage to electrodes and surrounding tissue. Although the charge-balance approach is an ideal practice, it was not always achieved. The importance of charge-balance is due to the necessity to maintain the electrode potential within a range that avoids the irreversible reduction and oxidation reactions. It could degrade the electrode, damage tissue, or limit the charge injection delivered in a stimulation pulse. Another important parameter regards the amplitude of stimulus waveforms that must be limited to current and charge densities to promote charge injection by reversible processes.

In vitro application due to the aqueous environment, the common irreversible process provoked by electrical stimulation is the electrolysis of water, with consequent pH changes and gas formation causing alteration of homeostasis, dangerous for cell culture. Oxidation of organic compounds, such as glucose and tyrosine, or the reduction of oxygen is also possible in case of electrical stimulation.

In general, electrodes used in neural stimulation can be divided into two categories:

- Macroelectrodes exhibit high-charge/phase thresholds and low-charge density thresholds; they are typically placed on the surface of the target tissue and have a surface area larger than approximately 100000 μm^2. Due to low charge-injection densities, typically do not have corrosion or degradation problems. But the high-charge/phase levels, however, may induce tissue damage.

- Microelectrodes have the opposite behavior, exhibiting low-charge/phase thresholds and high-charge density thresholds. Microelectrodes typically penetrate the

target and have surface areas that are smaller than approximately 10000 μm^2. The charge densities are relevant and this causes degradation and corrosion as well as tissue damage are encountered. Also the high charge/phase level could damage tissue.

In vitro application, the microelectrode is preferable for stimulation, due to the small volume and with a sufficient number of electrodes, it is possible to improve the selectivity and spatial resolution of functional responses. Several studies are performed in order to define a safe and effective stimulation range [14, 11].

3.2.2 Recording electrodes

The neuronal activity is recorded as an extracellular potential, or action potential, as reported in the chapter 1; in particular, the extracellular recording identifies the neuronal spike of a single unit. In the case of use of microelectrodes, the action potentials are recorded with microelectrodes in the proximity of neurons, and, for single-unit recording, the microelectrode geometrical surface area should be approximately 2000–4000 μm^2. The goal of a neuronal recording is to measure the action potentials with a useful signal-to-noise ratio (SNR), about 5:1 or greater. In the CNS, the amplitude of action potential spike can be more than 500 μV, typically on the order of 100 μV. In general, the action potential recording is mainly composed of the multitude of undifferentiated background action potentials (neural noise). Although, the electrode impedance is a main contribution to noise level, and higher impedance electrodes is preferable in this application due to the lower signal-to-noise ratio. In the recording application, a wide range of materials has been exploited, including metals and alloys e.g. stainless steel, tungsten, platinum, and more recently conductive polymer e.g. poly(ethylenedioxythiophene) (PEDOT). Recording electrodes are typically characterized by their impedance at 1 kHz, which is quite variable according to the material electrode, for the metallic electrode the impedance is lower with respect to the conductive polymer. The quality of the recording signal is critically affected by the proximity and the distance between neuron and electrode, and the respective sizes of each. However, the impedance value of the electrode and the composition of the neuronal tissue or biomolecular and cellular interactions that increase the impedance, affect the quality of the signal.

3.3 Charge-injection mechanisms

The electrode-electrolyte interface serves as an intermediary between the electronic charge transport in conductors and the ionic charge transport in the aqueous medium of the electrolyte. A double layer of ions is generated at the interface due to the electrical potential applied. This interface is crucial to mediating the transition from electron flow in the electrode to ion flow in the tissue. These reactions can be:

- Capacitive, it involves a charge and discharge of the electrode-electrolyte double layer. Capacitive charging can be either electrostatic, involving purely double-layer ion-electron charge separation and electrolyte dipole orientation, or electrolytic, involving charge stored across a thin, high-dielectric-constant oxide at the electrode-electrolyte interface.
- Faradaic, surface-confined species are oxidized and reduced. Faradaic reactions involve the electron transfer across the electrode-electrolyte interface and require that some species, on the surface of the electrode or in solution, undergo a change in valence, i.e. oxidized or reduced.

For noble metal electrodes, primarily Pt and PtIr alloys, the faradaic reactions are confined to a surface monolayer, and these reactions are often described as pseudocapacitive, although electron transfer across the interface still occurs. The three-dimensional structure of the coatings provides more charge for stimulation, but access to this charge is limited by the rate of electron and ion transport within the coating. The charge-injection mechanism are described in more detail in the following list:

- Capacitive charge-injection is preferred than faradaic charge-injection due to the no creation or consumption of chemical species during the stimulation phase. Because the double-layer charge per unit area at an electrode-electrolyte interface is small, high charge-injection capacity is only possible with capacitor electrodes that are porous or employ high dielectric constant coatings.
- Faradaic Charge-Injection Materials cause the reduction and oxidation of the reactions providing high levels of charge for stimulation. However, due to the oxidation and reduction of the species, changes in the electrolyte composition adjacent to the electrode and the finite rate occur and lead to irreversible processes that cause electrode or tissue damage. This event must be carefully considered to avoid these damaging reactions, also acting on the waveform set for electrical stimulation.

3.4 Emerging Materials

Recently, conducting polymers and carbon nanotubes have emerged as materials for chronic stimulation and recording as alternatives to gold, platinum and platinum alloys, and iridium oxide. This conductive polymer has some advantages e.g. the possibility of chemical surface modification with physiologically active species to enhance the biocompatibility and the functionality of the electrodes, and the mechanical properties, similar to the physiological environment.

Poly(ethylenedioxythiophene)(PEDOT) Poly(ethylenedioxythiophene) is a conducting polymer that exhibits both electronic and ionic conductivity. PEDOT is the most promising conductive polymer both for electrical stimulation and recording. Such material exhibits high electronic conductivity required for low-impedance recording or for charge-injection. In most studies, PEDOT is doped with poly(styrene sulfonate)(PSS), by electropolymerization process is incorporated into the polymer. This doping provides a material with higher electronic conductivity. PEDOT-PSS was also used as a coating for neural recordings of microelectrodes in order to decrease the impedance of metal electrodes.

Carbon Nanotubes Another interesting conductive material is carbon nanotubes as electrodes for neuronal applications due to their high conductive area compared to the surface area thanks to the 3D nanotube structure, which increases the double-layer charge capacity. Moreover, carbon nanotubes may also be chemically modified to enhance biocompatibility or change their functional properties.

3.5 Electrode Characterization

The common techniques to study the electrochemical process and electrode characterization applied for neuronal stimulation and recording are cyclic voltammetry (CV), electrical impedance spectroscopy (EIS), and potential transient measurements[47]. The *in vitro* electrode characterization and long-term characterization are carried out in an inorganic physiological saline with a buffer present, and with physiological temperature, thus mimicking the physiological environment present *in vivo* [11].

3.5.1 Cyclic Voltammetry

CV is an electrochemical measurement with a 3-electrode configuration in which the potential of a test electrode, with respect to a reference electrode, is swept cyclically at a constant rate between two potential limits while allowing current to flow between the test electrode and a counter electrode. CV identifies the presence of electrochemical reactions and provides information about reaction reversibility, the quantity of electroactive material on the electrode, and the electrode stability. The CV response according to electrode material appears different depending on the sweep rate, the geometric area and the roughness of electrode.

3.5.2 Impedance Spectroscopy

Electrochemical impedance spectroscopy (EIS) involves measuring the electrical impedance and phase angle according to a frequency range, applying sinusoidal voltage or current excitation of the electrode with a root-mean-square magnitude of the excitation source typically of 10 mV. EIS spectra are performed to assess the recording capabilities of microelectrodes. Furthermore, it can be applied to evaluate both tissue and electrode properties. Moreover, applied to evaluate the evolution of many electrochemical processes e.g. degradation and corrosion of electrodes for the evaluation of long-term stability [47]. Finally, the impedance spectroscopic approach measures the impedance to evaluate different conditions in the system. The total impedance of the cell can be modeled with an equivalent circuit in which each component can be related to a particular electrochemical process. Usually, the results of those measurements are reported in a Nyquist plot from which many different parameters can be extracted related to the electrode and the process. Observing the behavior of an electrode with EIS measurement and representing its electrochemical function as an ensemble of classical lumped circuit elements are conceptually helpful in order to better understand the occurring process. Through this equivalent model, it is possible to determine what are the components of the electrochemical process that are more relevant.

3.5.3 Voltage Transients

Voltage transient measurements are a common practice for estimating the maximal amount of the injection charge released in a current-controlled stimulation mode. *In vitro* measurements, the voltage transient is usually measured with a 3-electrode set-up with

a larger reference electrode. The voltage transients are subject to detailed analysis to determine the maximum polarization levels, including the most negative (E_{mc}) and most positive (E_{ma}) potentials observed at the electrode-electrolyte interface. These extreme potentials are subsequently compared to established maximum thresholds, which serve as safety limits beyond which electrode polarization is deemed unsafe.

Chapter 4

Electrical Stimulation of Human Induced Pluripotent Stem Cell

4.1 Introduction

Worldwide, since the introduction of human induced pluripotent stem cells (hiPSC)(Fig. 4.1) by Yamanaka and Takahashi in 2007, a powerful human stem cell technology has gained great interest as a novel and powerful tool in the research paradigm for the better understanding of human disorders and novel therapies [48]. The iPSCs are pluripotent stem cells derived from differentiated cells (e.g. skin or blood human cells) that have been reprogrammed back into an embryonic-like pluripotent state. Human iPSCs have been employed in several physiological and pathological models [49, 50], have been generated from patients with several neurological and psychiatric disorders such as Parkinson's Disease (PD), Alzheimer's Disease (AD), Schizophrenia and Bipolar Disorders [51]. IPSC provides several advantages: easy accessibility, expandability, and capacity to differentiate to any type of cell; in particular, they can differentiated in neuronal or glial cells. The main relevant properties regard the genetic background of donor contained in hIPSC, therefore they offer precious tools for pharmacological treatments and to develop precision medicine approaches. Using standardized differentiation protocols, iPSC can be differentiated into neurons whose phenotype reminds the one observed *in vivo* [52]. Recently, in the literature, Fedele et al. [53] showed the possibility of standardizing procedures to differentiate human iPSC into dopaminergic (DA) neurons. In particular, the dopaminergic neurons, which are a particular neuronal type, are the primary source of dopamine in the nervous system. Their loss or damage in the human nervous system is associated with different neurological disorders, e.g. Parkinson's

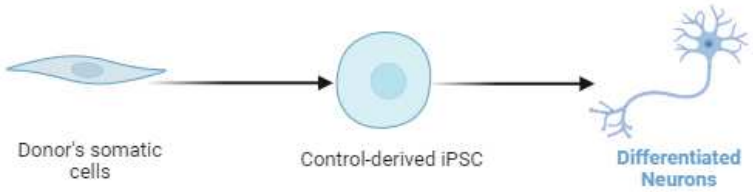

Figure 4.1 Rendering of the Induced Pluripotent Stem Cell with differentiated cell collected from a donor, after that the reprogramming of the somatic cell into stem cell and finally, the differentiation in a neuronal cells

disease and Schizophrenia. The dopamine release in the body is associated with well functioning of the human body: behavior, sleep, and voluntary movement.

The standard protocols presently available for the differentiation of dopaminergic neurons require up to 90-120 days [51, 52]; however, potentially, even with long and complex protocols differentiated neurons may result in immature features. Moreover, such differentiation protocols are time and cost expensive. Therefore, it is necessary to identify and implement novel techniques and protocols that accelerate the process of differentiation and maturation. The traditional techniques for differentiation and maturation of *in vitro* biological cells regard the use of pharmacological compounds e.g. growth factor, but recently, the use of biophysical stimulation is a relevant research field developed in tissue engineering. In particular, the provided stimuli regard mechanical and electromagnetic techniques that are developed to accelerate the maturation process. For what concern the electrical stimulation, several cell types i.e. cardiac tissue, bone tissue, and neuronal cells are subject to the electric field with relevant results concerning differentiation and maturation [20, 22, 54–57]. In the literature, several papers [58–60] demonstrate the electrical stimulation effect on the neuronal cell differentiation, in particular, on the

growing axons both *in vivo* and *in vitro*. Furthermore, recently, some works presented in the literature [61, 62] suggested that proper electrical stimulation (ES) can significantly promote neuronal differentiation and neurite growth of various cell types in vitro. The materials chosen must therefore maintain biocompatibility during all the experiments, avoiding faradic corrosion effects. According to the selected material, an inherent limit to the charge injection, beyond which the electrolysis of the water occurs, leads to damage to the cells and a change in pH.

The material chosen, in addition to having a proper limit of discharge, must have a low impedance and good resistance to long-term corrosion, these characteristics are varied, from polymers such as PPY, PANI and polythiophene which all require a great deal of effort in order to achieve a good load bearing capacity charge. On the other hand, metals such as platinum, gold, titanium and tungsten allow good *in vitro* stimulation [57, 22, 14, 11]. The carbon electrode was chosen for this specific application, due to the proper charging injection available for electrical stimulation experiments for neural and cardiac cells which combined proper impedance levels and low costs compared to metal electrodes and biocompatible properties. The main problem with carbon electrodes are related to their mode of operation -mechanical strength and high protein adsorption due to the rugosity.

4.2 Aim

This Ph.D. activity, described in this chapter, presented the preliminary results related to the application of an electric field stimulation with imposed parameters to enhance differentiation and maturation on stem cells. The study of imposed electrical stimulation with a customized electrical stimulation system to improve the maturation of human induced pluripotent stem cells (hIPSC)-derived dopaminergic neurons to optimize and enhance the differentiation protocol and *in vitro* pharmacological screening for novel drug treatment discovery in sight of a novel technique in regenerative medicine for the substitution of damaged tissue and following the innovative approach to tailoring disease prevention and treatment in precision and personalized medicine. In the literature, the majority of the works exploit a voltage-control system for *in vitro* stimulation; on the contrary, in this thesis work, a current-control was applied, which was estimated and scaled according to the enviromnental culture impedance obtaining the desired electrical field within the culture dish. Furthermore, the novelty regards this Ph.D. activity is related to the application of a current-controlled electrical stimulation on human induced pluripotent stem cells (hIPSC)-derived dopaminergic neurons to accelerate the standard

differentiation protocol. In particular, several experiments were performed to establish the suitable electrical parameters (e.g. current amplitude, stimulation frequency, impulse duration) by using a developed current generator and a commercial lid for electrical stimulation as a means to accelerate the protocols previously established [53] for the maturation of hIPSC. The relevant finding by using morphometric measurements and morphological indicators of structural plasticity (i.e. maximal dendrite length, the number of primary dendrites, and the soma area) suggests the possibility of reducing the maturation time for hIPSC-derived dopaminergic neurons.

4.3 Material And Methods

4.3.1 Design Requirements

The following design specifications have driven the development of the electrical stimulator and the customized chamber including the electrode choice in order to:

- provide *in vitro* electrical stimuli in the range of the physiological electric field experienced by neuronal cells in the literature (electric field in the range of 50 mV/mm to 200 mV/mm) [14, 11, 20, 57, 22],
- supply current-controlled stimulation to direct the ion flux within the cell culture medium,
- overall set up must be compact and easy to use in a cell culture laboratory following conventional Good Laboratory Practices (GLP),
- tunable set up in order to provide different electrical parameters,
- biocompatibility of the electrodes and electrical properties adequate to provide enough current.

Computational modeling Electric field simulations were performed to assess the uniformity of the electrical field generated by two parallel electrodes within a petri dish (standard biological equipment) in which a monolayer of hIPSC is seeded. In detail, a 3D steady-state simulation was carried out adopting a finite element-based commercial software (COMSOL Multiphysics 5.3, COMSOL Inc., Sweden) for investigating the distribution of electrical potential and electric field within a petri dish when placed between the two parallel electrodes of the electrical stimulator. The geometrical domains

are divided into four main components. Each component was modeled according to its electrical properties as shown in the table 4.1:

Table 4.1 Electrical parameters for the different material domains used in the simulation.

Domain	Material	Electrical Conductivity [S/m]	Relative Permittivity
Petri Dish	Polystirene	$6.10 \cdot e^{-12}$	2.55
Lid	Policarbonate	$1 \cdot e^{-14}$	2.50
Electrodes	Carbon	106	1.3
Culture Medium	Water	1.5	80.1

Gauss and Ohm's Laws were solved in their discretized form imposing a range of electrical potential of 0.5 V to 2.5 V with a step of 0.5 V. The geometry was discretized using $18{\cdot}10^5$ triangular and tetrahedral elements. The simulation results confirmed the homogeneity and uniformity of the electric field within the petri dish and in particular, where the cells are seeded according to the electrode position and the imposed electrical parameters. Additionally, the simulations showed in Fig. 4.2 that the contour plots, representing the electrical field intensity, on the horizontal sections of the culture chamber resulting in the region occupied by the cell monolayer is uniform, in accordance with the requirements for the electrical stimulation.

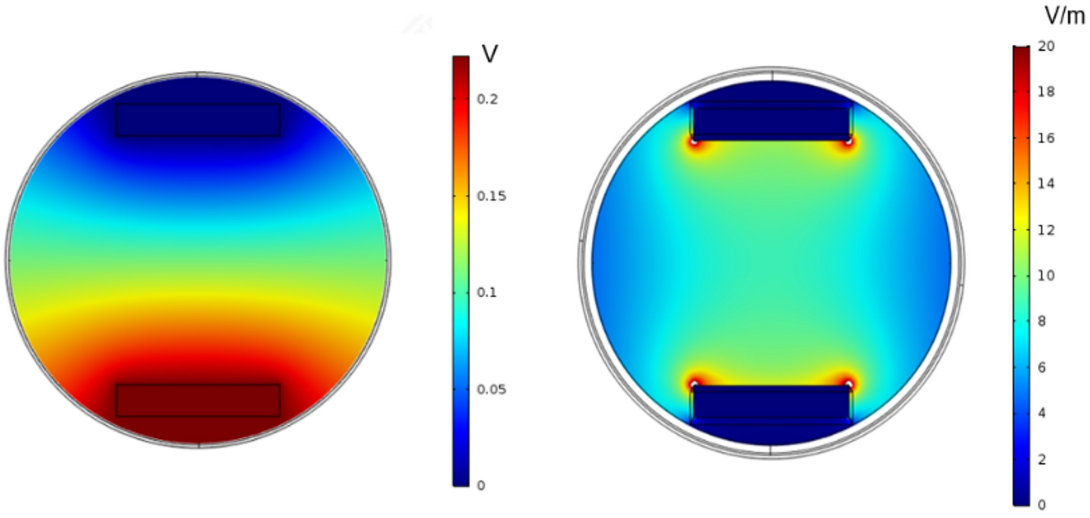

Figure 4.2 Distribution of the electrical potential and the electric field within the bottom of petri dish according to the electrode set up of C-Dish^{TM}

.

4.3.2 Experimental Set-Up

The experimental set-up and methodology exploited to perform the electrical stimulation were described in this section. In particular, the set-up is composed of a customized system, properly designed and developed to stimulate the hIPSC by using electrical stimuli to provide time and cost reduction of the maturation protocol previously existing. The stimulation system in Fig. 4.3 consists of several parts:

1. a patented C-Dish^{TM}(IonOptix, Milton, MA) in Fig. 4.4. The lid is suitable for a 6-well culture dish and consists of six lids, compliant with commercial plates, each one equipped with a pair of carbon electrodes to stimulate cell monolayers with an external electrical field. The electrodes are placed in order to have two parallel electrodes for each well. The carbon electrodes have been demonstrated to be suitable for biomedical applications [20, 54] and they have been used in several works to stimulate the cells *in vitro*. A ribbon cable connector provides access to the field-stimulating electrodes,

2. a custom circuit board, properly designed for this specific application. The circuit board is connected to the C-Dish^{TM} and it injects a controlled current through the electrodes of the wells. The current profile is defined via software by the user,

3. a commercial data acquisition system (DAQ) connected to a laptop. It provides power supply, monitors the voltage output, and defines the current value for the electrical stimulation,

4. a user interface programmed in the Labview environment to communicate with the DAQ and the custom circuit board. Furthermore, the interface allows the user to display and store the measurements acquired by the DAQ.

The current values imposed to the culture system generate an electrical field within the chamber with respectively 25-50-100 mV/mm, by a current control stimulation with specific electrical parameters of stimulation waveform, frequency, and period of stimulation, and delay between the previous and the next stimulation waveform. The electrical field parameters are chosen according to several works present in the literature, proven to be effective for the differentiation and maturation of biological cells. The current injection produces electrical charges that are transported by ions through the cell medium and by electrons in the electrodes and electrical circuits, so there is charge transport at the interface from electrons to ions, and this electrical charge transport activates the cascade of molecular pathways related to differentiation. The stimuli

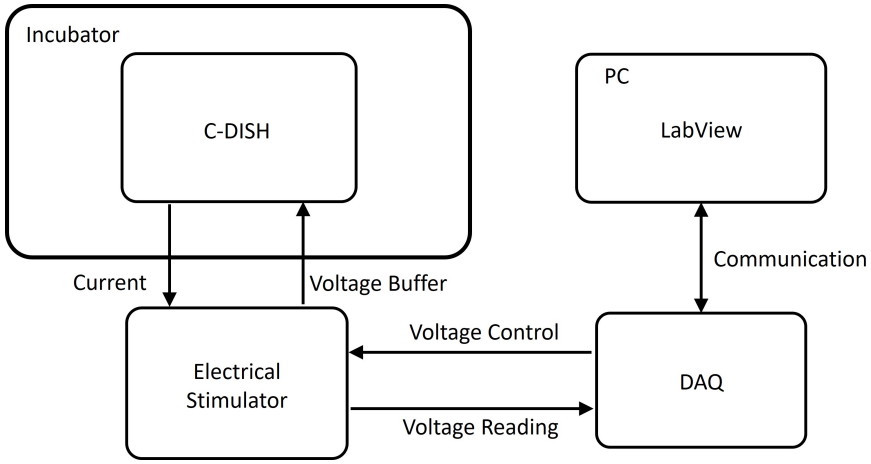

Figure 4.3 Schematic representation of the electrical stimulation system composed of the different blocks

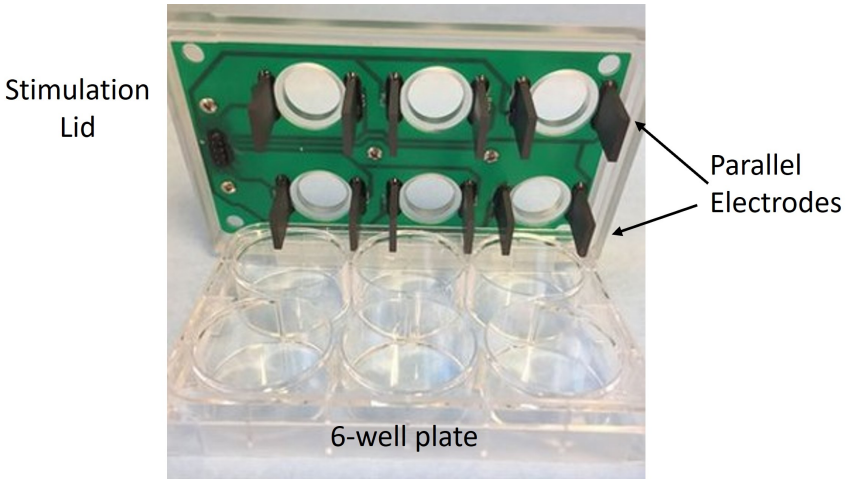

Figure 4.4 Photo of the commercial patent C-DISH^{TM} lid for electrical stimulation with 6 well cell plate

generated by a customized stimulator can generate a waveform with arbitrary parameters (peak value, frequency, pulse duration) to verify the cell behavior under different types of electrical stimulation and thus to provide optimal parameters for cell differentiation and maturation. The proper protocol will be developed for accelerating the hIPSC differentiation cells after different experimental parameters set-up before the evaluation of cell differentiation and maturation. Parallel and control wells, without stimulation, will be included in each experiment. The effect of the electrical stimulation on differentiation and maturation will be studied by morphological analysis (i.e., changes in neurite length, neurite number and soma size) and evaluation of intracellular molecular pathways.

The experimental protocol, proposed in this thesis shown in Fig. 4.5, consists in a single electrical stimulation of the hiPSCs at 30 day. In particular, all the wells are electrically stimulated with the same current injection and compared with a control (vehicle with a maturation induced with chemical compounds, Ropinirole, dopamine receptor with a positive effect on the structural plasticity of the neuron, typical of the standard differentiation protocol). After three days, the neuronal cells (both control and stimulated) were fixed and staining to characterize in terms of morphological analysis.

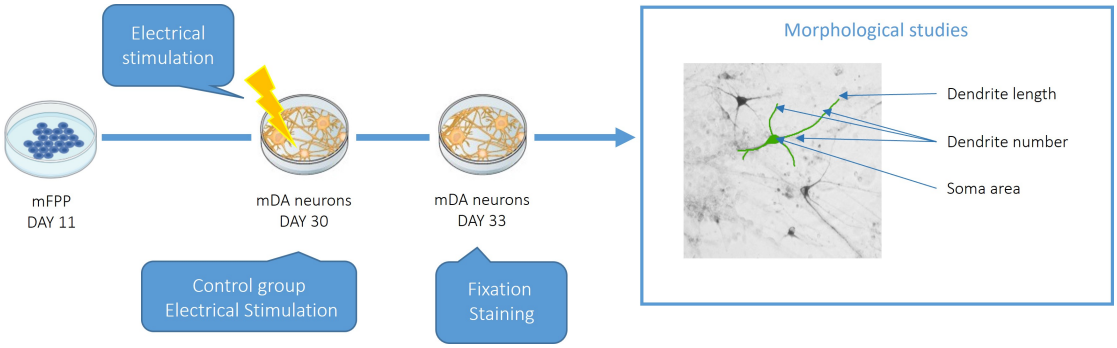

Figure 4.5 Schematic representation of the experimental protocol with the indication of the protocol for the electrical stimulation and the morphological tests.

4.4 Results

The electrical stimulator was characterized and tested to evaluate the proper working in terms of current injection and electrical circuit behavior according to impedance values of the culture medium taking into account the repeatability of the generated impulse and stimulation for several hours. After the promising results obtained in the preliminary tests, several trials were performed stimulating the hiPSC to evaluate the performance of the entire system and identify the suitable stimulation parameters.

After the stimulation, the neuronal cells were fixed and immunocytochemistry was performed on both cellular samples exposed to the electrical stimulation and control. Digital images of stained DA neurons were acquired with an optical microscope, Olympus IX51 connected to an Olympus digital camera and a PC, in order to perform the morphometric measurements on digitalized images through the software ImageJ.

The following morphological indicators of structural plasticity [63] were considered:

- the maximal dendrite length, defined as the distance from the soma to the longest dendrite of each cell,

- the number of primary dendrites, defined as the number of the dendrite attached to the soma,
- the soma area, measured in μm^2.

Data were expressed as mean $\pm$ standard error of the mean (S.E.M.). The data analysis of the morphological indicators were performed using one-way analysis of variance (ANOVA) followed by a posteriori Bonferroni's test for multiple comparisons provided by GraphPad Prism (GraphPad Software version 9.0 package, San Diego, CA). ANOVA test was performed on the stimulated wells according to the vehicle.

The results highlighted that the electrical stimulation produced a significant effect on the differentiation and maturation of the hIPSC. The stimulation influenced all three predetermined morphological indicators. In each well, a single electrical stimulation produced structural plasticity of human dopaminergic neurons derived from iPSCs three days after exposure. In particular, in each well according to Fig. 4.6, the electrical stimulation promotes an increased trend of dendrite length and dendrite number of human DA neurons showing statistically significant results ($P<0.001$). Poor statistical significance resulted on the soma area compared to the control with Ropinirole.

4.5 Conclusion

In this preliminary work, developed through the Ph.D. activity, to assess the stimulation effect on the hiPSCs, a customized electrostimulation system was realized and tested to accelerate the differentiation protocol of hiPSC-derived neuronal cells. The system includes the ease of use and sterilization of the instrumentation, only the C-dish needs to be sterilized, while the rest of the equipment remains outside the incubator. Moreover, the system is easy to install and easy to use on the laptop and the possibility to monitor the function and the circuit status at various points, both in terms of waveform and current measurement and with the size and depth of the wells, elements of considerable interest have been proven. The experiments confirm the positive effects produced by electrical stimulation on the growth of hiPSC, obtaining plasticity results similar to those obtained with pharmacological stimulation. The use of electrical stimulation in place of the use of pharmacological compounds reduces the cost and the time compared to standard protocols. Moreover, this stimulation methodology has proved to be safe and biocompatible, and highly repeatable for *in vitro* experiments. These results achieved with morphological analysis are preliminary in terms of structural plasticity, future

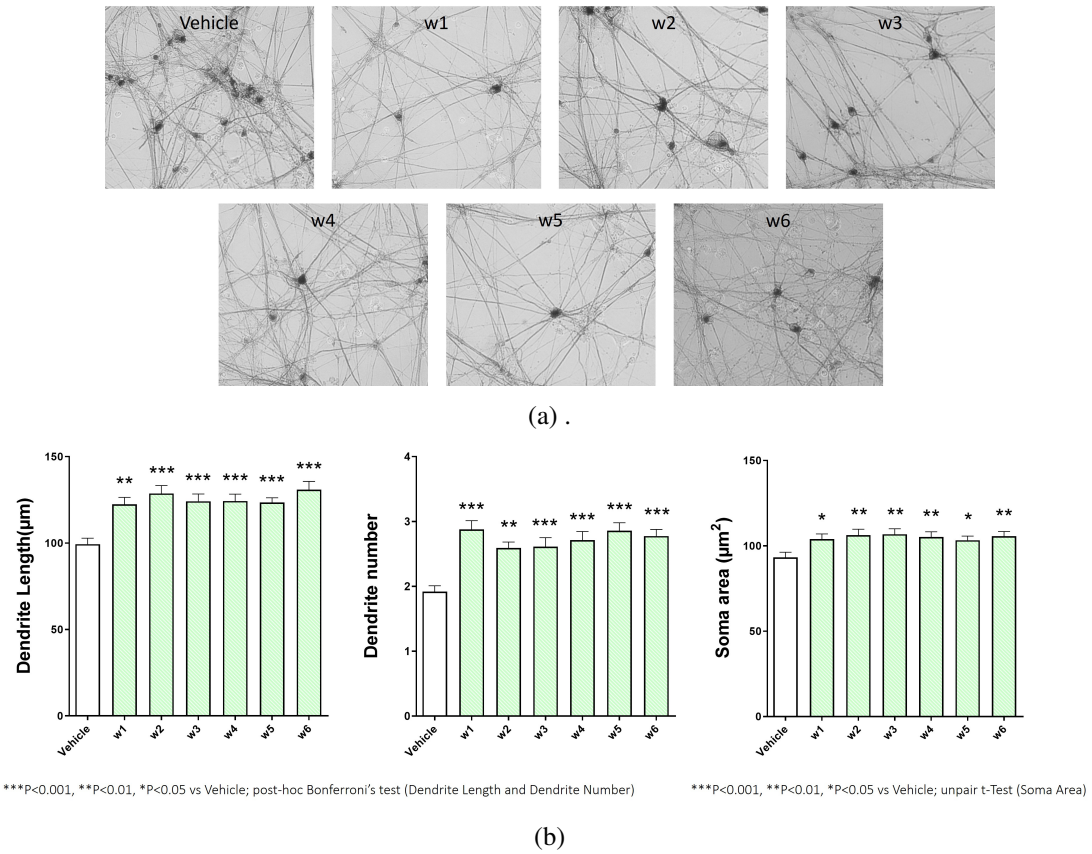

Figure 4.6 a) Photographs acquired with microscope that show the hIPSCs fixed after the electrical stimulation. b) Bar plots that show the statistical results according to the morphological evaluation according to dendrite length, dendrite number, and soma area.

investigations related to assessing the phenotype of the hiPSCs, the examination of gene expression, and alkaline phosphate activity should be performed (e.g. quantitative real-time PCR (qPCR)). Finally, the electrophysiological measurements, to study the electrical activity of neurons, and in particular the action potential activity, that led to the conceptualization of the next Ph.D. activity reported in the chapter 5.

Critical Aspects The realization of this experimental setup led to a critical analysis of the works, in particular, the large amount of cell culture medium and grow factor needed for the 6-well C-dish, and the related increasing cost. Furthermore, the possibility of real-time monitoring of the differentiation process arises as a necessity for large-scale production and clinical applications.

This first work reported in the Ph.D. activity gives the possibility to critically analyze the problems related and the improvement needed:

- a system for both stimulation and real-time monitoring in order to obtain and verify the results of the stimulation on the functionality of the neuronal cells,
- a system with reducing the overall dimension of the well, in order to reduce the total amount of grow factor and cell culture medium concerning the commercial set-up,
- paralyzing the system to perform several experimental,
- customize the electrical stimulation electrodes both in terms of position and materials.

Futhermore, due to the relevant finding in this section related to the possibility of accelerating the proliferation and the maturation process of human Induced Pluripotent Stem Cells (hIPSC) in neuronal cells in order to reduce the time and cost according to traditional differentiation protocol; in the next section will be analyzed the realization of a printed MEA, designed in order to give the possibility to supply electrical stimulation with an appropriate stimulation system. In particular, the design will be developed in order to provide appropriate electrical stimulation and a homogeneous electrical field. The fundamental relevance of the next work lies in the use of human induced pluripotent stem cell (iPSC)-derived neurons in drug development and disease modeling. Since iPSC-neurons were first generated, their characterization has become a major focus of research. Micro-electrode array (MEA) systems can provide a non-invasive user-friendly platform for detailed electrophysiological analysis of iPSC neurons including drug testing to identify potential targets and the assessment of risk.

Chapter 5

A feasibility study of a printed Micro-Electrode Arrays

The research works reported in this section were published in [64–66].

5.1 Introduction

In vitro electrophysiological recordings are an important step in the study of physiological and pathological models of neuronal cells and electrogenic cells in general, which generate these signals [4], besides being a significant tool for the realization of functional tissue and engineering products [67]. Recorded signals can reflect the fast spike activity of individual neurons or the slower action potentials and synaptic potentials, all this signal resulting in waves of high amplitude typically from hundreds of μV to 1-2 mV of a neuronal network [30, 35]. Traditional intracellular recording techniques used to measure the electrophysiological signal such as patch clamp, involve the use of an invasive electrode to perform the biopotential measurement on a single cell at once with an invasive method, providing a better signal quality but limiting the recording number of neuronal signal [28]. Otherwise, these voltage changes can be measured with extracellular electrodes positioned almost in contact with the cell. This indirect technique allows the recording of neuronal activity in both *in vitro* and *in vivo*, providing insight into patterns of action potentials in various areas of the nervous system. Micro-Electrode Array (MEAs) are a key component for electrophysiological monitoring in several applications, from in vitro toxicity studies [36] to implantable brain-machine interfaces [37]. Such bioelectronic devices are composed of a grid of tightly spaced

electrodes to record the electrogenic cells (i.e. cardiomyocytes and neruonal cells). MEAs are generally employed to acquire extracellular signals [31] and to stimulate in order to generate evoked potential; rarely provide electrophysical stimuli able to provide physiological conditions for maturation [32, 33, 14]. Nowadays, microfabrication techniques are the most common methods for the fabrication of MEAs due to the possibility of electrode dimensions of 10-100 µm with thousands of microelectrodes but they are expensive concerning time and cost production [44, 68–71]. This leads to the reuse and extending the lifetime of the MEA with a decrease in the quality of the recorded signals. Furthermore, another major disadvantage of a standard MEA is the fixed position of the electrodes and the lack of a customized MEA design for the adaptability to different architectures of a specific neuronal network [72–74]. Driven by the recent progress in the understanding of neuronal physiology, the development of MEAs with customization properties and low cost and time consumption has gained considerable importance. Therefore, alternative production techniques to overcome these limitations are exploited for the development of MEA [36, 32, 75]. Innovative fabrication techniques, e.g. AM and printed sensors, are becoming crucial, due to important advantages such as easy accessibility, processing of varied biocompatible materials, sustainability, and device customization. Furthermore, the printed electronics give the possibility to print the circuit and the sensors directly on flexible substrate and on the medical device allowing the development of prototypes with high resolution, repeatability, and accuracy [76, 77]. In this work, Aerosol Jet Printing (AJP) was exploited allowing the printing of sensors and electronic components with important advantages, such as easy accessibility for prototyping and low-volume manufacturing, processing of varied biocompatible materials, sustainability, and device customization. In particular, the possibility to print electrodes and sensors directly on the device allows the development of easy and low-cost prototypes with good resolution, repeatability, and accuracy, providing a selective deposition both on planar and 3D structures, without using masks or post-processing, except the curing of the ink in order to obtain the desired ink conductivity, and realizing specific surface features [41]. Such technique is also used for biomedical applications [41, 42]. In particular, Aerosol jet printing (AJP), like other printing technologies, has enabled the use of conductive biocompatible materials, such as PEDOT:PSS, a polymeric material that has excellent properties in terms of conductivity, processability, and stability. Its biocompatibility and conductivity ensure that the PEDOT:PSS can be used safely in biomedical applications as a coating layer for the metallic material [46], to improve the signal-to-noise ratio (SNR) of the recorded action potential signal, due to its higher surface area [69, 44, 45]. AJP technique has already been adopted for in vitro tissue engineering applications, e.g. the realization of MEA for biocomponent detection of

dopamine and other biological components [44] to develop an array of electrodes with dimensions not suitable for action potential recording. In addition, the feasibility related to AJP technique gives the possibility to print biological components, e.g., proteins and ligands. And, in specific MEA applications, this gives the possibility to selectively print the ligands to create a tailored architecture with a selective coating to promote cell adhesion [78, 79]. Likewise, AJP has also been employed in combination with 3D printing techniques such as stereolithography to develop MEA for the recording of action potential signals or bioelectronic devices [68, 80].

Finally, the employment of computational modeling methods for the design and analysis of bioelectronic devices enables efficient exploration of large parameter sets, e.g., geometrical setup and electrical and multiphysics parameters, where preclinical and clinical studies would not be feasible. The 3D finite element method (FEM) simulation can connect the model with the measurement environment, allowing the analysis of the recorded data regarding the geometry setup. Proper electrical characteristics of the MEA, cell environment, and cells, need to be employed to achieve proper conclusions to assess a realistic model of the device. To this end, FEM has been used to analyze cell–electrode connections affecting the electrical stimulation and recording of cells, cell growth, and cell–electrode interfaces in general. Such simulations provide predictions of measurement values and to study various measurement arrangements about the biological matter but lead to some limitations due to the simplified model. The FEM simulation enables the analysis of different design setups to find the ideal result. In this context, *in silico* models are a valid tool to predict the behaviour of neuronal cell activity [81–83].

5.2 Aim

This thesis work proposes the use of AJP technology as a means of customized and low-cost fabrication of MEAs for both recording action potential signals and stimulating electrically the biological cells using suitable ink and customized design to improve the MEA performance. Furthermore, in this application, the AJP technique gives the possibility to easily realize different geometry according to CAD design and to allow rapid design changes with scalable fabrication according to the need regarding the purpose of the study to develop tailored MEA according to biological cell architecture. The novelty of this Ph.D. work is the fully AJP printed technique developed for the fabrication of microelectrode array for stimulation and recording of the action potential of neuronal cells, able to reach the microscopic electrode dimension suitable for such biomedical applications and the customized design suitable by using printing techniques.

Due to important advantages, e.g. easy accessibility, processing of varied biocompatible materials, sustainability, and device customization, including the possibility of realizing complex geometries quickly and easily, the AJP employment is fundamental for the realization of the printed MEA. Besides, concerning the printed sensor and electronics techniques, the possibility of printing the circuit and the sensors directly on cell culture device allows the development of prototypes with high resolution, repeatability, and accuracy. In particular, the focus of this chapter is the design, fabrication and characterization of a fully AJP-printed Micro Electrode Array. The design of the MEA electrodes is fundamental for the realization of a bioelectronic device in agreement with the principal requirements needed for the action potential recording. In addition, the customization of electrode position is promoted by the employment of AJP compared to traditional MEA fabrication. The fully AJP-printed MEA can achieve the microscopic size of electrodes suitable for such biomedical applications due to the resolution of additive manufacturing techniques compared to other printing techniques. Thus, preliminary design and material selection studies were performed in order to evaluate the feasibility of the printed MEA. Furthermore, the opportunity to use conductive polymer opens up the handle of proper material for applications with biological materials (e.g., cells, tissue, biological molecules). Finally, the employment of the two conductive inks, the organic polymer PEDOT:PSS and the silver ink selected due to the high conductivity properties and the coating of the PEDOT:PSS in order to promote and enhance the biointerface between the neuronal cells, and the use of AJP, ensure a better signal quality and spatial resolution, and alignment of the different printed layers compared to other additive manufacturing techniques [69, 84]. Furthermore, the application of computational simulation methodology in terms of distribution of electrical potential analysis of action potential of neuronal cells leads to an optimization of the design of printed microelectrode array that is intended to be fabricated with AJP technique. The study includes the realization of a model to predict the microelectrode array performance through the evaluation of electrode detection area and ideal insulated layer thickness to obtain appropriate insulation and limit signal crosstalk of recording signals. In addition, the definition and characterization of the parameters for the single fabrication layers of MEA and the process parameters of AJP technique were exploited. Finally, the multilayer structure was printed with the optimized design and characterized both in terms of geometrical and electrical performance.

5.2.1 MEA requirements

The MEA requirements must be clearly defined according to the transduced biopotential signal characteristics of neuronal cells and the intended acquisition system for data transmission and analysis. The following design requirements have driven the development of the printed MicroElectrode Array considering the intended use and the chosen fabrication technique. In particular, the design will follow the requirements for delivering electrical stimulation to the cell monolayer to enhance differentiation and maturation, and recording of action potential signal for monitoring the differentiation of hIPSC into functional neuronal cells.

The main requirements that must be implemented according to the destination use and the fabrication techniques in order to realize a printed Microelectrode Array for action potential recording and electrical stimulation signals are the following:

- Number of electrodes 16-32-64 in case of passive MEA,
- Patch dimension and conductive tracks 30-100 μm $\sim$ biological cell dimension,
- Distance between electrodes 100-400 μm $\sim$ biological cell dimension,
- Overall sensitive area 1-15 mm^2,
- Biocompatible and conductive material,
- Appropriate electrical stimulation and homogeneous electrical field, also taking into account the choice of material suitable for the current release of few mA and electrode position,
- Insulated layer to separate the conductive tracks.

5.3 Design and Modelling

5.3.1 Set up for FEM and evaluation parameters

Once the MEA requirements have been defined, to verify the feasibility of the proposed printed MEA, it is necessary to carry out several simulations aimed at evaluating several specifications that need to be improved and promote an improved design phase. In particular, the simulation aims at defining the following design parameters:

- distance between electrodes,
- attenuation of the recording signal,
- optimal thickness of insulation layer for limit signal crosstalk,

to obtain an enhanced fabrication process and an optimized design in terms of electrode geometry and position. The finite element method (FEM) models of AJP microelectrodes, cells, and culture medium are developed and implemented in COMSOL Multiphysics (COMSOL, Inc., Burlington, MA, USA). The computational tool was used to compute the evaluation of the ideal insulated layer thickness to avoid crosstalk of recording signals and the design enhancement of MEA according to the Aerosol Jet Printed requirements to assess the detection area of the electrodes. We constructed a 3D model with planar square electrodes on the surface of the insulating substrate, as in the commercial MEAs, with a cell immersed in culture medium in Fig. 5.1.

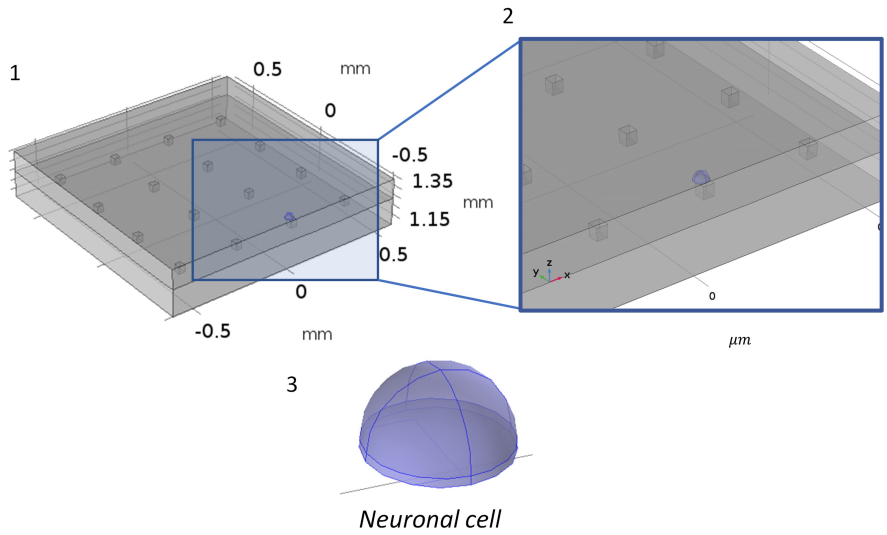

Figure 5.1 Rendering of the geometrical domains of Comsol Multiphysics simulation of 1-2) MicroElectrode Array and 3) Neuronal Cell.

The position of the cell was changed in various positions of the detection area in the proximity of the electrodes to assess different simulation parameters. Furthermore, to compute the crosstalk evaluation, in addition to the electrodes and the insulating substrate, the conductive silver tracks were added to the domains, in order to take into account the different layers of the MEA. Regarding the single domain representation, the neuronal cell was modeled as an adherent cell to MEA substrate surrounded by culture medium. The typical radius of the soma of a human neuron is between 7 to 20 μm. Here, we assumed a neuronal cell of 15 μm radius. In addition, the cell was assumed without

Table 5.1 Electrical parameters for the different material domains used in the simulations.

Geometrical Domain	Material Domain	Relative Permittivity	Electrical Conductivity
Medium	Ionic Water	80	3
Cell Membrane	[83]	11.3	$1*10^{-24}$
Conductive Electrode	Silver	1000	$5.99*10^{7}$
Passivation Layer	NOA 81	3.2	$9.09*10^{-9}$
Sensing Electrode	PEDOT:PSS	100	$5*10^{4}$

axons and dendrites and thus propagation signals to reduce computational cost and complexity. The electric properties of the various domains used in the Comsol simulation are reported in Table 5.1. Comsol material database provided the electrical properties of silver material, in terms of relative permittivity and electrical conductivity. The specific electric properties of the other domains were set according to the electrical parameters reported in the literature [83]. Considering the insulating layer, the Norland Optical Adhesive properties had a crucial importance in simulations and MEA realization due to its function in the passivation layer, and electrical conductivity was set to $9.09 \cdot 10^{-9} S/m$.

The electric current module was imposed as physics in COMSOL Multiphysics to calculate the electric fields and the electric potential distributions in the entire volume of the model and across the insulating layer associated with the analyzed electrode configurations. In particular, for numerical modeling of the coupling between the cell and the MEA, Maxwell's equations were used. These equations are represented in the differential form of Gauss's law to model electric current flow in conductive and capacitive medium and solve a current conservation problem. The stationary equation of continuity must be considered for stationary electric currents in conductive media. The Ohm's Law 5.4 is:

$$J = \sigma \cdot E + Je \tag{5.1}$$

Where

- J: total current flux
- Je: externally generated current density
- σ: electrical conductivity of the material

The utilized physics solves the equations based on Ohm's law using the electrical potential as a dependent variable. Gauss's law for electric charge distribution to handle current

sources, the static form of the equation of continuity can be generalized:

$$\nabla \cdot J = Q_{j,v} \tag{5.2}$$

- Q: total charge enclosed within the V

Dielectric model for macroscopic properties of the model:

$$D = \varepsilon_r \varepsilon_0 E \tag{5.3}$$

Where

- D: is the electric displacement
- ε_0: is the vacuum permittivity
- ε_r: is the relative permittivity
- E: is the electric field

Based on Gauss's law for electrical field and Ohm's law, electrical potential distribution in each domain of the system was calculated by the COMSOL software. The electrical insulation boundary condition is defined as

$$n \cdot J = 0 \tag{5.4}$$

The boundary conditions concern the current conservation on all the domains and the electric insulation on all boundaries. A potential difference according to action potential signal was fed in the surface via terminal at the entire cell surface, while all the external domain boundaries were set to ground. The array of microelectrode was used to record the propagation of action potential signal around the cell, specifically the distribution of electrical potential in the electrode domain. The simulation was set with a time-dependent step between 0 to 0.02 s, the duration of a single spike of the action potential, and the consequence refractory period. The input signal was fed as a terminal for the generation of the electrical potential and consequently, the signal recorded by the microelectrode array for neuronal cells is the action potential signal, a potential difference between the outside and inside of the membrane. The difference in the concentration of ions between the inside and outside through the membrane of the cell leads to membrane potential. Such potential difference changes over time, starting from a resting potential

of -70 mV to a rapid depolarization, positive membrane potential with a peak of 50 mV and subsequently, repolarization of the membrane. Finally, a refractory period leads to resting potential. For the generation of the action potential of the neuron provided as an electrical potential input to the cell membrane presented in this work, the model of Hodgkin–Huxley was chosen. The mathematical model of the neural electrical is based on their electrophysiological experiments in the giant axon of the squid [85]. The neuron was represented as a single compartment, ignoring any spatial propagation in electrical activity. The neural membrane is described in Fig. 5.2 by a capacitance C_m in parallel with three conductance (g_{Na}, g_K, g_L).

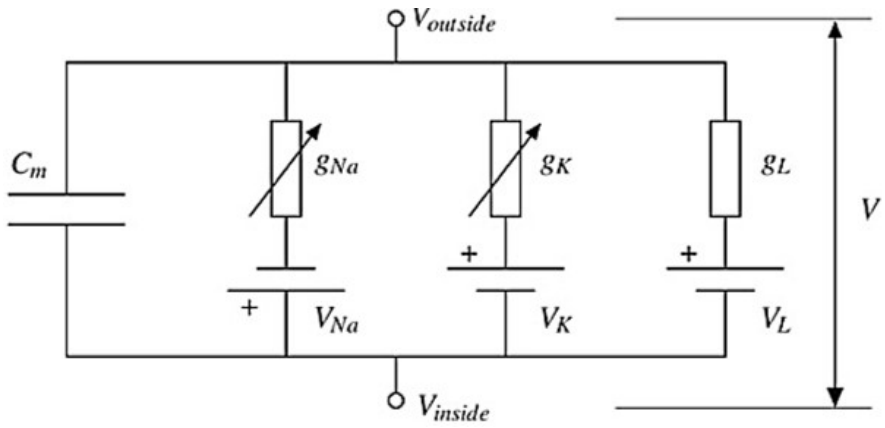

Figure 5.2 Equivalent electrical circuit for the Hodgkin–Huxley model of the neuronal cell action potential. V represents the voltage across, a small patch of membrane. The C_m represents the capacitance of the membrane patch, whereas the four g's represent the conductances of three types of ions. The two conductances on the left, for potassium (K) and sodium (Na), are shown with arrows to indicate that they can vary with the applied voltage, corresponding to the voltage-sensitive ion channels.

$$i_N a = g_{Na}(V - V_{Na}) \tag{5.5}$$

$$i_K = g_K(V - V_K) \tag{5.6}$$

$$i_L = g_L(V - V_L) \tag{5.7}$$

$$C_m \cdot \frac{dV}{dt} = -(i_{Na} + i_K + i_L) \tag{5.8}$$

- C_m: membrane capacitance
- i_{Na}: Na^+ ionic current
- i_K: KC ionic current

- i_L: non specific leakage current
- g_{Na}: Na^+ ionic conductance [S]
- g_K: K^+ ionic conductance [S]
- g_L: non-specific leakage conductance [S]
- V: transmembrane potential
- V_Na: reversal potential for Na+ membrane current
- V_K: reversal potential for K+ membrane current
- V_L: reversal potential for non-specific leakage membrane current.

Hodgkin–Huxley neuron model [85] responds to a brief stimulus, shown in the membrane potential V against time. Using a square-wave profile, this stimulus current is given by

$$i_{stim} = \begin{cases} i_0, & t_{on} \leq t < t_{on} + t_{dur} \\ 0, & otherwise \end{cases} \tag{5.9}$$

In the specific case of the simulation reported in this work, the values assigned are:

- i_s= 600 A/m^2
- t_{on} = 0.001 s
- t_{dur}= 0.001 s

The resulting action potential on the cell membrane according to the values assigned is shown in Fig. 5.3 with a peak with an amplitude of 50 mV after 0.002 s, the duration of a single impulse is about 0.02 s. Finally, the mesh allows the discretization of the model, using the finite element method that divides the model into elements with a simple geometrical shape. An extra fine mesh is imposed to improve the computation accuracy, but this leads to increased memory usage and a reduced speed.

5.3.2 Simulation results

Evaluation of the simplified model The results of Comsol simulations in Fig. 5.4 show the electrical potential distribution of the geometry composed of a microelectrode

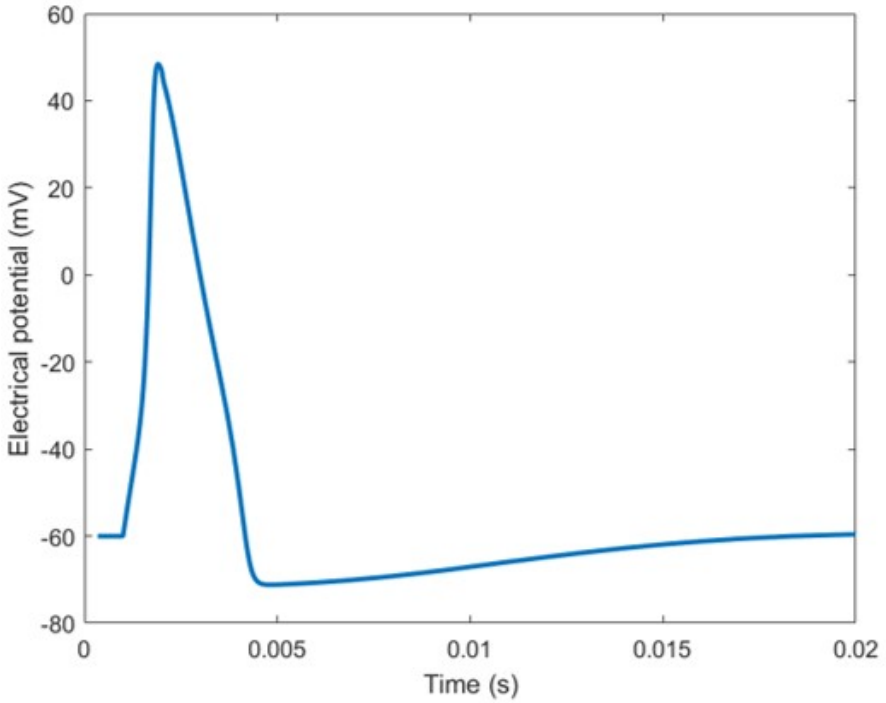

Figure 5.3 Single action potential signal generates as input for Comsol Multiphysics simulation according to the parameters of the imposed equivalent circuit for Hodgkin–Huxley neuron model.

array (electrode, insulating layer, and conductive tracks), cell and medium. The orange signal is the action potential input of the cell membrane, peaks at 50 mV while the blue waveform is the signal recording of electrical potential by the electrode when the cell is located at 80 µm (Fig. 5.4b) and at 30 µm (Fig. 5.4a) along *x*-axis. The figure shows how the action potential profile is recorded by the electrode; meanwhile, the field intensity of the signal decreases with the distance from the electrogenic cell according to the inverse square law of electricity [86]. Compared to Appali [87], which uses a model with a higher level of complexity in terms of geometry domains and the physics that use a ramification cell model and propagation of the action potential, we modelled the action potential with a simplified physics, a single imposed stimulus and a cell geometry composed of a single cell with hemispherical shape. In spite of the simplification of the model presented in this work, our simulation reported a proper rendering in terms of profile recording and signal decrease according to the distance.

Assessment of the detection area of MEA Comsol Multiphysics was applied to compute the detection area for the electrode array. We estimated the distribution of the electrical potential delivered according to the position of the cell according to the electrode array. It allows assessing the correlation between cell and electrode distance.

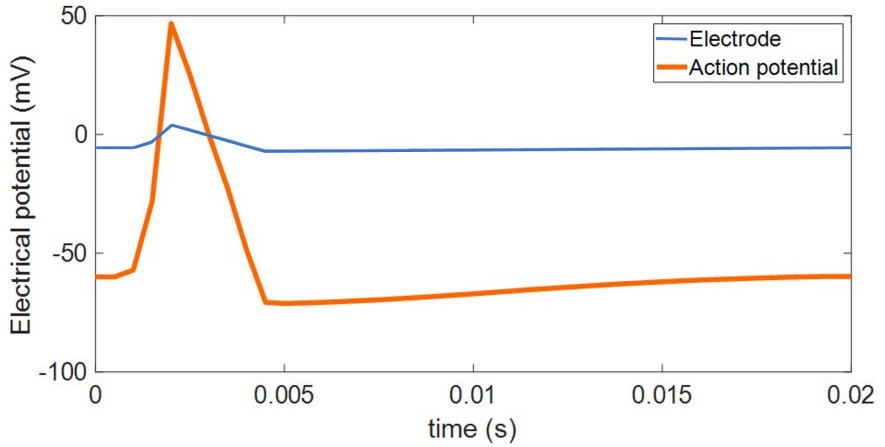

(a)

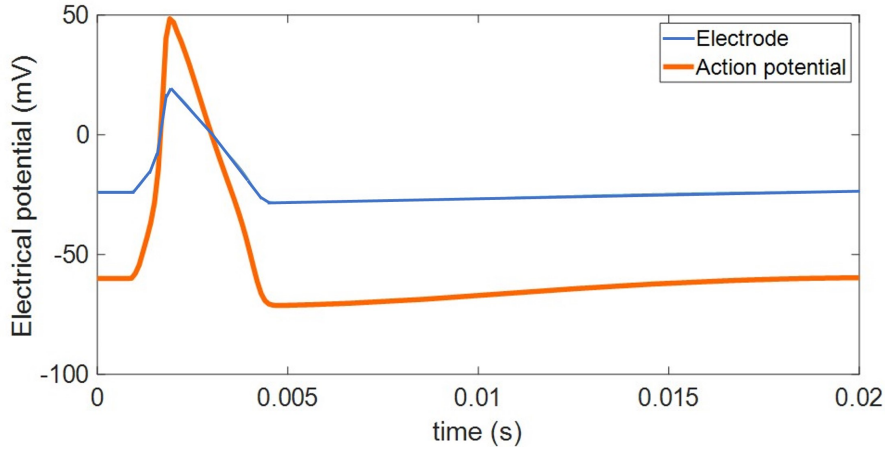

(b)

Figure 5.4 Plot of the action potential signal in input and recorded signal by the electrode at distance between them of a) 80 µm and in b) 30 µm.

The plot in Fig. 5.5 shows on the$y$-axis the amplitude peak of the cell action potential recording from the electrode, assuming the diameter of 50 µm, while the position of the electrode is plotted on x-axis. For the evaluation of the detection area of the electrode, the spike of the action potential was taken into account, i.e. the electrical potential peak at which the maximum potential difference is reached during a single 50 mV peak stimulus. The plot in Fig. 5.5 shows how the distance between electrode and cell influences the action potential recording. The plot was obtained from several simulations carried out by moving the neuronal cell along the x-axis. The electrode is in the origin position. The detection field results the highest in the area close to the center of the electrode at $x = 0$, as expected. Due to the size of the cell (of 30 µm diameter), the area of major sensitivity is extended. Moving away from the electrode, the sensitivity rapidly decreased as can be seen in the Fig. 5.5. The presence of the cell near the electrode of 10 µm provides a decrease of the signal of 20 mV. At distances $x > 20$ µm from electrode in the$x$-direction, sensitivity drops below 40%, and down to 10% at $x = 30$ µm. The detection area decreases very fast as shown in the image, and the recording signal is about 2 mV with a cell-electrode distance of 100 µm. The signal is equal to 0 for a distance more than 150 µm, it means that the action potential is no longer detectable for distances larger than 150 µm. As seen from Fig. 5.5, the measurement sensitivity of an electrode setup is positive in the entire analyzed area, and maximum at the center of the electrodes where the electrical potential is the highest due to the position of the cell on the top of the electrode. According to Fig. 5.5, a cell in a vicinity of a microelectrode caused an increase of the potential, leading to an increase of the recording signal. The electrical potential and the recording signal from the electrode increase depending on the location of the cell.

The definition of a single electrode detection area leads to an analyze of the cross-sensitivity of two electrode configuration to investigate the interelectrode distance to achieve the optimal MEA design. Concerning the design requirements of the microelectrode array, the ideal distance between two consecutive electrodes is greater than the neuronal cell diameter, and concurrently the gap should not exceed in order to avoid areas where the action potential signal is not recorded by the sensors. Due to the intrinsic limitation of the printed MEA, the minimum interelectrode distance achievable is 200 µm. We estimated the electrical potential distribution with two-electrode configuration at the chosen distance, based on the Comsol Multiphysics simulation carried out. Fig. 5.6 shows the cross-detection area of two electrodes, and the behaviour is the same of the configuration of the single electrode. It is interesting to observe what happens in the cross- detection area, the minimum recorded signal that can be detected from the sensor is 2 mV, due to the interelectrode Fig. 5.4. Plot of the action potential signal and

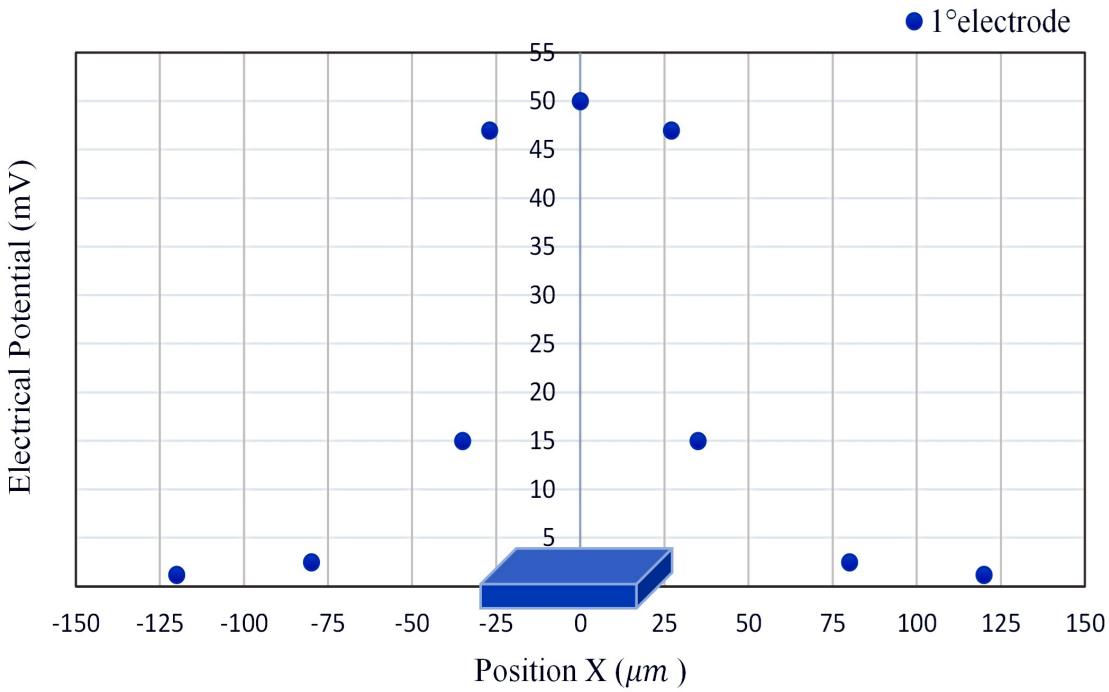

Figure 5.5 Detection field area of a single electrode configuration according to the cell-electrode distance and the action potential signal recording on that electrode. The electrode is localised in the *x*-*y* origin.

recorded signal by the electrode at distance between them of a) 80 µm and in b) 30 µm. The first electrode is localized in the*x*-y origin and the second electrode at 200 µm away. An increase of the inter-electrode distance more than 200 µm would result in a detection area in which the signal is no more recordable.

Evaluation of the Insulated layer thickness The extracellular electrode can record the field potential generated by the action potential of more neurons *in vitro*. The recorded signal reflects the spike of individual neurons and low field potential and synaptic potentials. Therefore, it is necessary to reduce the possible additional noise, such as the interference crosstalk signal between the several action potentials and the conductive tracks in silver that can be generated by a non-adequate insulated layer thickness. For such reason, the width of the insulating layer must be studied to avoid crosstalk between the signal recording by the electrode and the interference between external action potential signals and conductive path. Several simulations are performed to evaluate the optimal compromise between layer thickness from AJP requisite and crosstalk limitations. The thickness values are chosen as follow: for the inferior limit, 10 µm was chosen because it is the minimum layer thickness that can be printed with

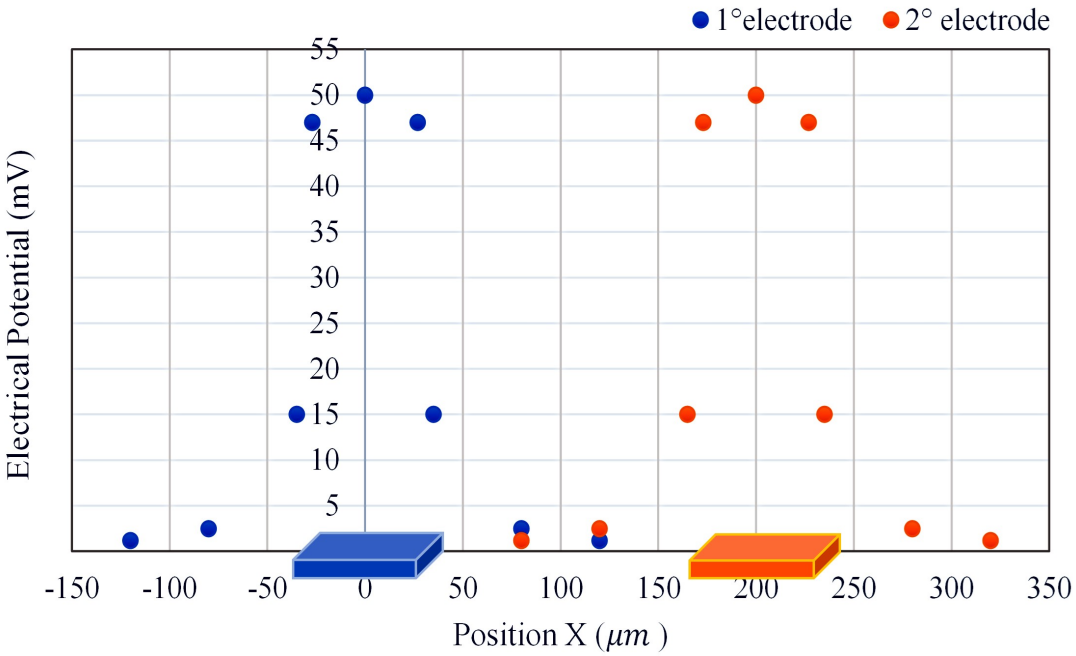

Figure 5.6 Detection field area of the two electrode configurations according to the cell-electrode distance and the action potential signal recording on that electrode. The 1° first electrode is localized in the *x*-*y* origin and the 2° electrode at 200 µm away.

AJP with the NOA and for the superior, we tested 300 µm. The results obtained for the different layer thickness regard the entire action potential signal. The Fig. 5.7 shows how the variations of the electric potential for 10 µm of thickness differ by 1% from 300 µm. Therefore, the variation of the potential is not relevant to interfere with the signal of the recording electrode.

Conclusion In this work, the importance of FEM model for the optimization of the design for the realization of microelectrode array is underlined, in particular for a novel fabrication technique that involves the use of Aerosol Jet Printing. The detection area analysis of the electrode array for the recording of action potential of neuronal cells led to the definition of an interelectrode distance of 200 µm. Furthermore, according to the intrinsic requirements of AJP and the results obtained from Comsol simulation, the evaluation of insulating layer thickness led to an optimal thickness of Norland Optical Adhesive used as passivation layer of 10 µm, because such value do not lead to an undue noise concerning the electrical potential signal recording by the electrode. In conclusion, the system used in the simulation is necessarily ideal, including the assumed geometry, e.g. neuronal network is assumed as a single neuron with hemispherical shape and the propagation of the action potential is negligible. Nevertheless, a well-defined

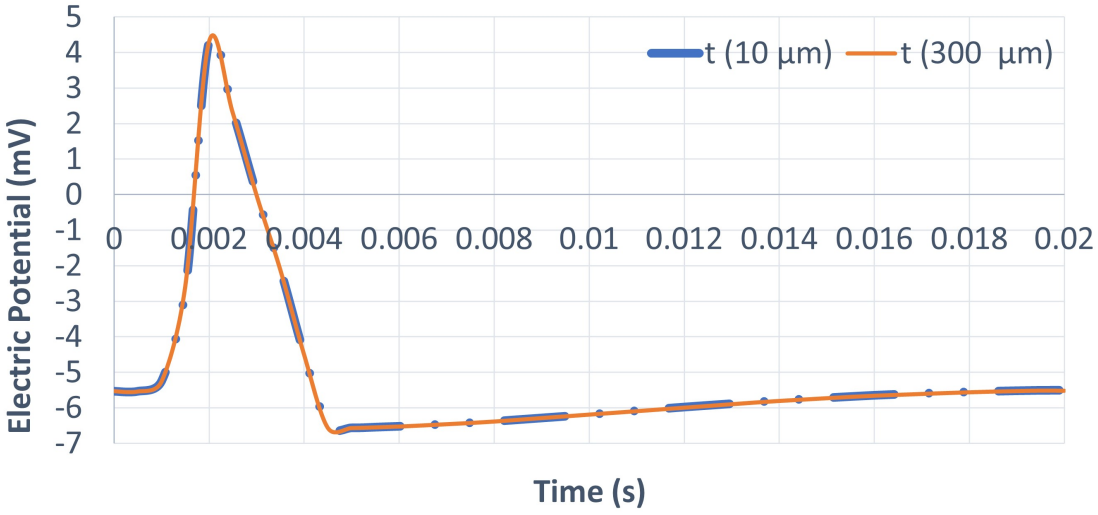

Figure 5.7 Action potential signal from the recorded electrode with an insulating layer of 10 µm and 300 µm, respectively.

and simplified geometry in MEA system is necessary to achieve a basic understanding of action potential measurement and bioelectronic device. Although concepts and results obtained from the simulation will assess the design optimization considering the geometry set-up and electrode dimensions for microelectrode array. The model is a good compromise of computational power and model predictability. Based on the results achieved by the computational model, it is possible to proceed with the realization of the printed microelectrode array by Aerosol Jet Printing.

5.3.3 Design of Micro-Electrode Array and Material Selection

Design of the printed MEA The design and the accurate selection of the printed materials are fundamental for the proper realization of the MEA by AJP and the requirements listed in the chapter above were followed. The schematic drawing of the micro-electrode array (MEA) is shown in Fig. 5.8. The MEA electrode layout was an array 4x4 sensing electrodes of 50 µm diameter with a total distribution of the recording sensitive area of 1 mm^2. This sensitive area is considered an optimal choice according to the literature [30, 37] for what concerns the spatio-temporal resolution and overall dimension of the printed chip. Regarding the number of electrodes, 16 were considered enough to exploit the action potential study generated by electrogenic cells and validate the proposed solution as a proof of concept. The layout was defined according to the ability of AJP technology to realize close and thin geometric elements. The sensing electrode diameter must be comparable to the cell size (4-100 µm in diameter), in order

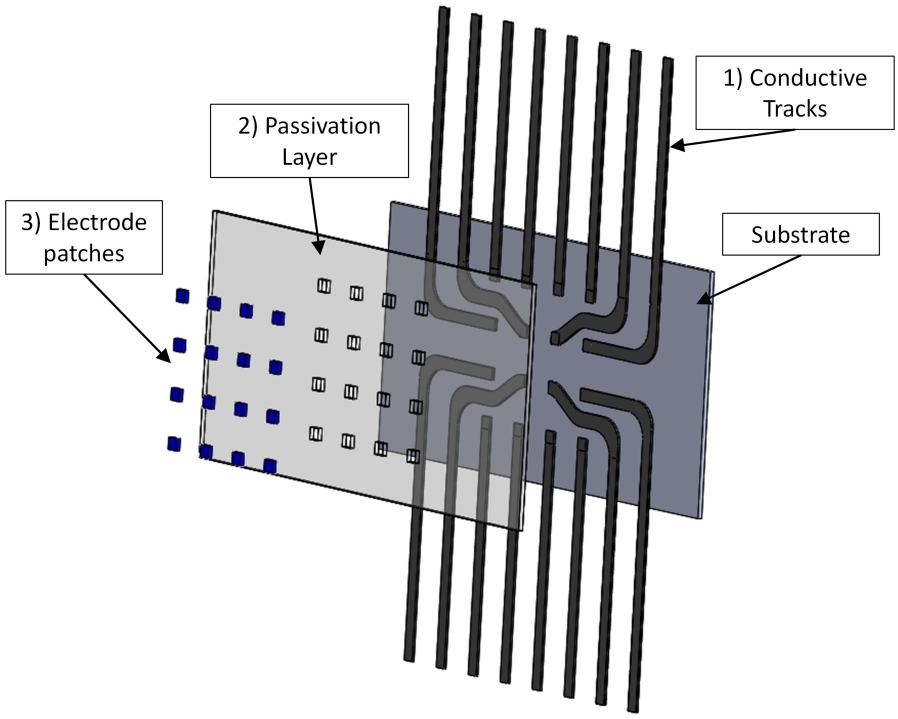

Figure 5.8 Rendering of the three layers of the MicroElectrode Array. Substrate, 1) 16 conductive tracks in silver ink, 2) the passivation layer deposit with NOA 81, and 3) 16 electrode patches in PEDOT:PSS.

to obtain an improved response of singular neuronal cell, while the distance between the electrodes must be greater than the cell size, according to the literature [31]. Therefore, the dimension of a single electrodes was designed with a diameter of 50 µm according to the requirements for MEA fabrication. The interelectrode distance was defined as 250 µm, according to intrinsic AJP specifications and electrode geometry range. Finally, the overall dimension of the printed MEA complies with the biologists' request to optimize the volume and consequently, the costs of biological compounds (i.e. cell culture medium and grow factors for promoting cell maturation). The image of the micro-electrode array (MEA) in Fig. 5.9 shows the two shared reference electrodes designed on both sides with larger dimensions compared to the electrode array (400 µm x 700 µm). In case of electrical stimulation, the two electrodes are necessary to provide the current stimulus with a homogeneous field without damaging the electrode properties, while reference electrodes are fundamental for action potential recording. Then, 18 conductive tracks and their corresponding contact pads (4 mm x 1.2 mm) were designed to connect the MEA electrodes with the electronic front-end. The distance between contact pads was designed with pitch of 2.54 mm to connect with specific standard connector.

The proposed design of the MEA is a multilayer structure composed of three different layers. The pattern of each layer was realized by using a computer-aided design software to create precise 2D drawings, AutoCAD. The output file was then converted into a file with customized software for AJP printer movements, that allow the manufacturing process. The possibility to generate personalized 2D drawings brings a customization of the geometry of electrodes and the dimensions in order to realize a customized device for recording action potentials. Biocompatibility and no corrosion of the selected materials are important for MEA realization. In the next paragraph, due to the novelty of the AJP technique adopted in the MEA fabrication and to provide a customized design able to detect neuronal action potential signals, several computational simulations were performed to investigate the optimal design of the printed electrode array and to satisfy the MEA requirements by using Comsol Multhyphisics, a finite element method (FEM) [68]. In particular, *in silico* models were exploited in order to provide satisfactory results about the dimensions of sensing electrode and interelectrode distance, proving a proper measurement of the action potential signal. Another crucial part was the definition of a sufficient thickness of passivation layer for a correct isolation and limit signal crosstalk. Several in silico studies [64, 88, 89] were performed to explore the crosstalk in polymer MEA and to predict interference in signal recording. According to [14], a single insulation layer is enough to reduce significantly the crosstalk and measure correctly the action potential signals produced by neuronal cells. Furthermore, in order to minimize the crosstalk in the printed MEA, two reference electrodes with large overall dimensions were added in the layout proposed in [89]. The preliminary design of printed was designed with three steps: first, the 16 conductive tracks were printed onto a substrate. Second, the passivation layer was printed surrounding and on top of the conductive traces, leaving openings at the end of the Ag traces that correspond to the 16 electrodes. All conductive tracks were designed with a width of 50 μm, while the openings in the dielectric layer had a width and a length of 50 μm as the nominal area of electrode patches in the MEA design.

Material selection Kapton was preliminarily selected as a substrate for the MEA for adhesion properties and ease of handling and adopted as a substrate in order to glue a 3D printed ring to create the culture chamber. Though the final goal will be the direct printing on cell culture chamber, after the optimization of the design and the fabrication processes.

The first layer of conductive tracks was printed with Smart Aerosol Conductive Ink (S-CS61308, Genesink, France) - an ink based on silver nanoparticles - suitable for appli-

cations requiring high conductivity and high resolution at very low curing temperatures. The silver ink selection is necessary due to the need of an high conductive material able to bring the signal to the hardware for the signal recording of the action potential of neuronal cells. However, such ink has cytotoxic effects on biological cells, and it is not corrosion resistant in aqueous environments, in fact undergoes corrosion effect. In fact, a passivation layer with insulating and biocompatible material is added to avoid the corrosion of the silver in the electrolyte solution and the crosstalk between the several recording signals.

The second layer for the passivation, as a coating to the silver track, and for the realization of a multilayer structure was obtained with an insulating ink, Norland Optical Adhesive, NOA 81 (Norland Products Inc., Cranbury, New Jersey, USA), a UV-curable polymer. It results to be hard, resilient bond with good adhesion on the glass. Besides having low conductivity, it is a transparent and biocompatible material, in order to create a surface coating for silver conductive tracks. This ink is characterized by a viscosity of 300 cP at 25° C. The NOA 81 was selectively printed in order to leave 16 openings on the silver track ends in the center of MEA that correspond to the 16 sensing electrodes.

The selectively opening for the electrode array was coated with biocompatible and conductive properties materials, that is needed at thevinterface between the silver and the cell culture, to prevent also a cytotoxic effect on the cells. The use of metal conductive material to realize sensing electrodes is largely exploited both in commercial and in the literature, but with some limitations. Recently, conductive polymers have been used as biocompatible materials in bioelectronic device, e.g. with poly 3,4-ethylenedioxythiophene (PEDOT), polypyrrole (PPy), and polyaniline (PANI). Furthermore, they have more suitable and physiological-like mechanical properties. The Young's modulus of polymers is usually only a few GPa—much lower than metallic materials and this allows a better cell adhesion and maturation as the environment more closely to the physiological characteristics [1]. Another main aspect to consider in recording action potential signals is low electrical impedance; due to smaller electrode size in neural cell application, which increases the spatial resolution of the neural signal (signal selectivity). However, a reduced electrode size is associated with a larger electrode impedance, which increases the noise of the signal (signal sensitivity) [37]. Due to the necessity of SNR improvement, the conductive silver tracks were selectively coated with conductive polymers. Poly(3,4-ethylenedioxythiophene)-poly(styrenesulfonate) (PEDOT:PSS) (Orgacon IJ-1005, Sigma-Aldrich, USA) was chosen as a surface coating (third layer) for the 18 leaving opening at the end of the silver lines of the first layer. In this way, the printed PEDOT:PSS-based contact pads are in direct contact with the cells and the electrolyte

solution of the cell culture,to obtain an increased SNR and better biocompatibility and more surface area incrementation. The last procedure ensure that only PEDOT:PSS and NOA 81 inks were exposed to the electrolyte solution.

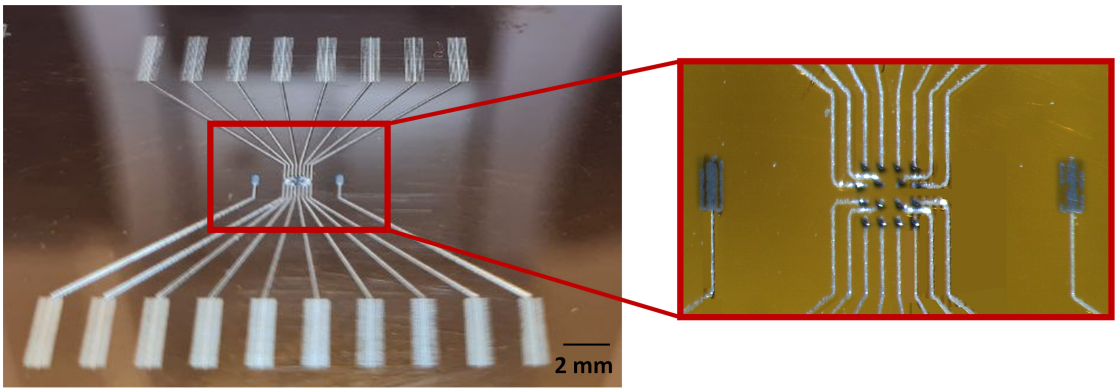

Figure 5.9 Photograph and detail of the printed MicroElectrode Array, composed of the contact pad to connect to the electronic front-end.

5.4 Fabrication process

In the preliminary fabrication phase, the printing process of MEA was composed of three steps as shown in Fig. 5.10 to realize the different layers geometries of the electrode array.

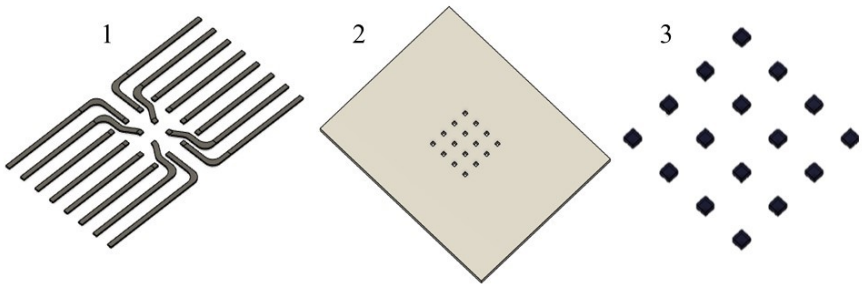

Figure 5.10 Rendering of the three layers of the microelectrode array. 1) 16 silver tracks for the conduction of the signal, 2)Insulating layer in Norland Optical Adhesive (NOA) and 3) 16 electrode patches in PEDOT-PSS.

In the first stage, the three different layers were printed separately in order to define and optimize both the process parameters and the MEA design. For the preliminary evaluation of silver ink, conductive tracks samples based on CAD drawings were printed with several overlapped depositions of ink in order to define the optimal combination of

electrical properties and geometrical design to comply with design requirements. For each number of depositions, two samples were reproduced. While for the PEDOT:PSS patches, several deposition of the array were performed to evaluate the feasibility of printing.

Finally, the fabrication process was realized in order to print the multi-layer structure and the contact pad with the electronic front-end, following the results obtained from the preliminary deposition steps of the three separated layers, A schematic representation of the proposed fabrication process is shown in Fig. 5.11 and a detail of the schematic drawing is presented in Fig. 5.12.

The fabrication process consists of three separate depositions:

1. the 18 silver tracks and contact pads, composed of the 16 conductive tracks for the electrode array and the two reference electrodes onto a substrate;

2. the passivation layer printed on the top of conductive tracks, in order to coat them to avoid corrosion and cytotoxic effect. The printing pathway was designed leaving uncovered the ends of the conductive tracks in order to obtain the 18 electrodes (16 sensing and two reference electrodes) in the center of the device and the contact pads to allow electrical connections with electronic front-end for stimulation and recording of AP signals;

3. the conductive polymer coating for the silver tracks over the 16 sensing and the two reference electrodes.

Each deposition step includes deposition and a dedicated curing phase in order to reach the required electrical parameters. In this work, the Aerosol Jet printer, AJ300 printer (Optomec, Albuquerque, New Mexico, USA) was employed to fabricate the multilayer structure MEA. The pneumatic atomizer mode, available in the AJP technique, was used for the deposition of silver-based ink and passivation layer (viscosity of 300 cP at 25°C), while the ultrasonic atomizer mode was employed for the deposition of PEDOT:PSS electrodes, due to the viscosity of the conductive polymer (7-12 cP at 22°C). The printhead nozzle was selected with 200 µm of diameter. The AJP platen, that allows the movement of the substrate in the X-Y direction, was heated at 60°C to dry the ink during the printing, and the printed speed was fixed at 2 mm/s. For the PEDOT:PSS, the temperature plate was set at 40°C and the printed speed at 1.5 mm/s.The parameters for the fabrication of MEA using AJP are listed in Table 5.2. Process flows are expressed in the unit standard centimeter cube per minute (SCCM). Once the process parameters were

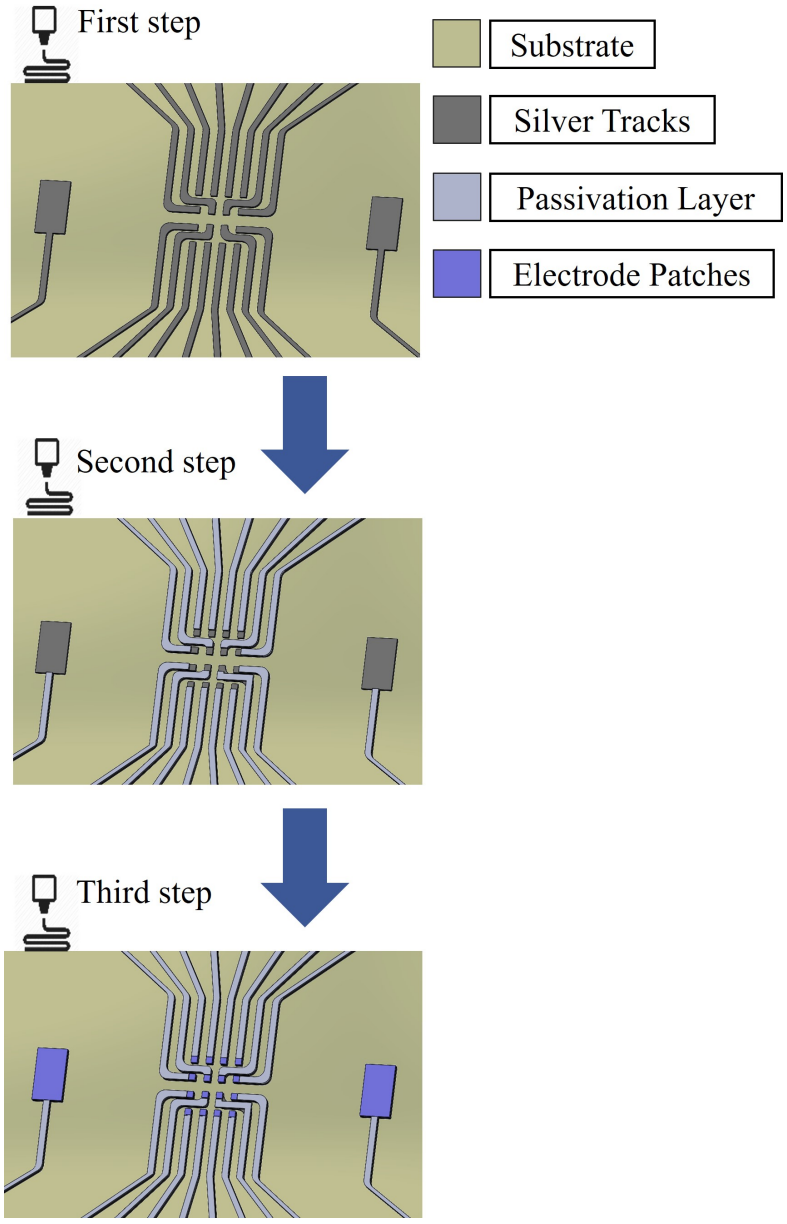

Figure 5.11 Rendering of the fabrication process. In the first step, the printing of silver tracks was performed; in the second, the passivation layer was deposited and finally, the electrode patches were printed in the third step.

optimized in the preliminary printing of each separated layer, parameters were imposed for the printing of the multilayer structure.

In the preliminary phase, for each type of deposition, the printing process was repeated several times to increase the thickness of the printed feature also accordingly to the design requirements. For the coating of the sensing electrodes with PEDOT:PSS, AJP software script was modified in order to keep the machine shutter opened for imposed

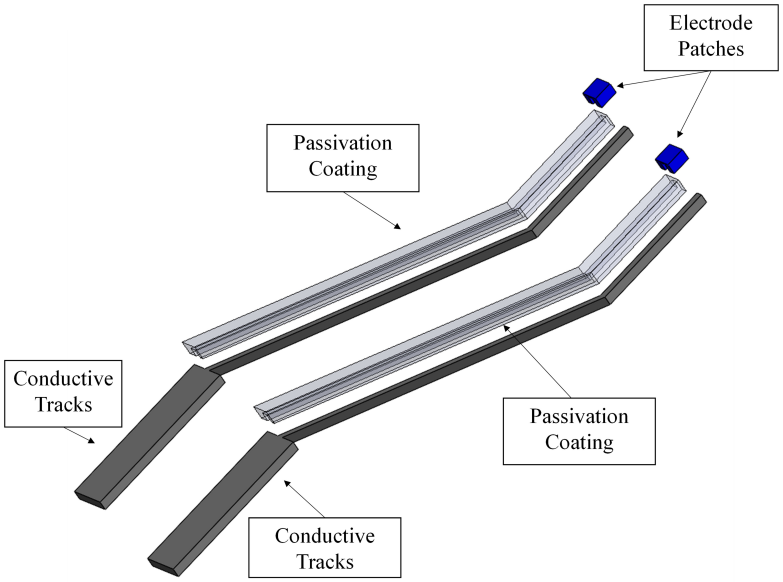

Figure 5.12 Detail of the schematic drawing of the Micro Electrode array. Two tracks of the MEA are represented to show the different layers composed of electrode patches, passivation coating and conductive tracks.

Table 5.2 Printing parameters used during the production process.

	Conductive tracks	Passivation Layer	Conductive Coating
Printed Ink	Ag	NOA 81	PEDOT:PSS
Sheat flow (SCCM)	100	40	30
Atm flow (SCCM)	635	1395	30
Exhaust flow (SCCM)	620	1365	/
Atm current (mA)	/	/	605
Substrate temperature (°C)	60	20	40
Process speed (mm/s)	2	1.5	1.5

seconds over each silver electrode, building a micropillar over each silver track opening, to realize the sensing electrode array. The silver tracks were sintered at 150 °C for 1 h in ThermoScientific VACUTherm Oven (Thermo Electron LED GmbH, Langenselbold, Germany) to reach the required conductivity, as recommended by the manufacturer. NOA81 was cured during the printing procedure using UV light by LED Spot type Panasonic (Panasonic, Osaka,Japan), 5% of the maximum peak intensity as selected power. Finally, the PEDOT:PSS-based patches were thermally cured at 130 °C for 6 min in oven, as recommended by the manufacturer.

5.5 Result and discussion

5.5.1 Characterization of the preliminary printed layer

The characterization of the printed MEA was performed in order to experimentally validate the proposed sensor's design and its fabrication method.

Preliminary tests were performed to determine the geometrical characteristics of printed layers and the resistivity of the printed tracks to decide the number of deposition needed and in accordance with the requirements imposed. The size of the features, i.e. thickness and width of the printed tracks, was measured by using the optical microscope and the Profilm3D (Filmetrics Inc.,10655 Roselle St., San Diego, CA, USA). The measurements of the resistance were performed by means of a multimeter (HP34401A, Agilent). The optimization of the printed microelectrode array requires some preliminary tests to estimate:

1. the thickness and the width of the silver tracks, the passivation layer and the conductive polymer electrode array
2. the resistivity of the silver tracks.

Geometrical characterization The morphological characterization of the fabricated MEA by means of optical microscopy and profilometer measurements was performed to evaluate the geometrical features of the microelectrode array. The optical microscope images are shown in Fig. 5.13. From a preliminary analysis acquired with the optical microscope, for the overlapped depositions of 1, 2, and 3 layers, there is no contact between the silver tracks, avoiding unwanted electrical contacts. While increasing the overlapped depositions to 4 and 5 layers, the silver tracks come into electrical contact and produce shortcuts between the tracks and an inadequate outcome as shown in the red box in the Fig. 5.13. As a result of these preliminary optical evaluation, four and five depositions were discarded.

Subsequently, the profilometer images show the profile of the depositions according to width and thickness. The images carried out with the profilometer, after the acquisition, were optimized with specific filtering techniques to enhance profile quality, and then, the geometrical features were measured. The profiles of features acquired with the profilometer were elaborated with specific filters to increase the quality of the printed profile, and then the geometrical parameters (width and maximum thickness) were measured. Three filters provided by the software Profilm3D were used to reduce the

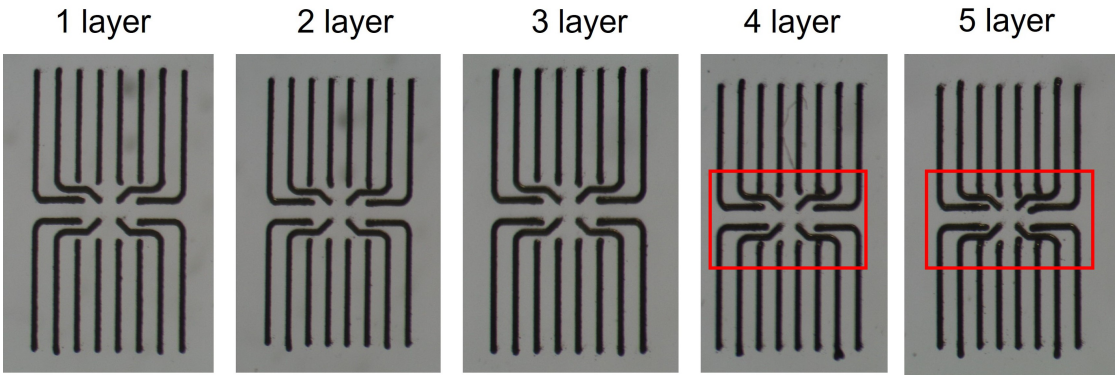

Figure 5.13 Optical microscope image of the different number of overlapped deposition of silver layers.

Table 5.3 Geometrical features of the tracks with average and standard deviation values.

Number of Layers	Geometrical Features			
	Width (μm)	Standard deviation (μm)	Thickness (μm)	Standard deviation (μm)
1	67.72	± 1.33	1.44	± 0.13
2	64.57	± 0.57	3.83	± 0.57
3	68.35	± 1.83	6.26	± 0.47
4	65.24	± 1.35	8.18	± 0.46
5	67.21	± 2.60	10.76	± 0.21

acquisition noise, such as outliers and artifacts produced by the profilometer. One filter removes outlying data points from the surface by comparing them against the nearest neighboring points. The second filter based on a 3-Point leveling method performs a better-quality acquisition of the planar substrate. The last filter was used in order to fill the invalid pixels using values interpolated/extrapolated from surrounding data. Table 5.3 shows the mean and standard deviation of width and thickness of conductive tracks for different overlapped depositions.

The width of the tracks remains approximately the same for the different layers of depositions in a range of 65-68 µm. The thickness increases with the number of depositions, as we can expect, from (1.44 $\pm$ 0.13) µm for one deposition to (10.76 $\pm$ 0.21) µm for 5 overlapped depositions. In detail, in Fig. 5.14 the characteristics of the different profiles of silver tracks obtained by varying the number of overlapped depositions are shown. For the five profiles, the filtered image taken with the profilometer is shown in insets and the mean and standard deviation of the silver track thickness (y-axis) with respect to the width (x-axis) are shown. For the mean and standard deviation values, five equidistant lines were traced on the silver profiles.

Concerning the passivation layer deposition, the NOA 81 was printed on the conductive track with a single deposition. In Fig. 5.15 the profilometer acquisitions show a uniform distribution of the NOA 81 deposition with a mean thickness of 15 µm about eight measurements of an equidistant slice taken from the profilometer image, the profile changes with ± 2 µm from the nominal value, in the x-axis is reported the width, while in the y-axis the thickness of the NOA 81 layer.

In the feasibility study of the PEDOT:PSS-based ink, it was printed according to the CAD design. In particular, the deposition of 16 spots was realized in order to obtain biocompatible interface between cells and silver and for surface coating of silver ink, avoiding the corrosion environmental for conductive tracks. After setting the optimal parameters, several depositions were performed with different setting times. The time corresponds to the open shutter time (2-4-6 seconds of open shutter) and consequently, the quantity of extruded material for the single electrode. In Fig. 5.16 the deposition of the 16 spots of PEDOT:PSS-based ink is shown through the profilometer acquisition, in 3D view the electrode array shows the results obtained from the depositions, in particular how the spots have no shortcuts between them and the formation of micropillar with height of 0.8 µm.

Electrical characterization The electrical characterization of the different layer of MEA by means of a bench multimeter was performed to evaluate the electrical resistance of the printed Ag tracks of the microelectrode array, taking into account the geometrical features of the tracks. For the measurement, five lines with different overlapped depositions as samples are printed with an imposed length to measure the resistance of the silver tracks. Fig. 5.17 shows the mean value of the resistance and the standard deviation according to the number of overlapped depositions silver layers in the x-axis (1-5). The resistance, as expected, changed considering the number of depositions. In particular, the resistance decreases proportionally with the increase in the number of layers. The 5.11 to extract the resistivity ρ from the measured resistance R is:

$$\rho = R \cdot \frac{S}{l} \tag{5.10}$$

where

- w is the average width of the tracks,
- t is the average thickness,
- l is the length of the measured silver track resistivity of the silver tracks.

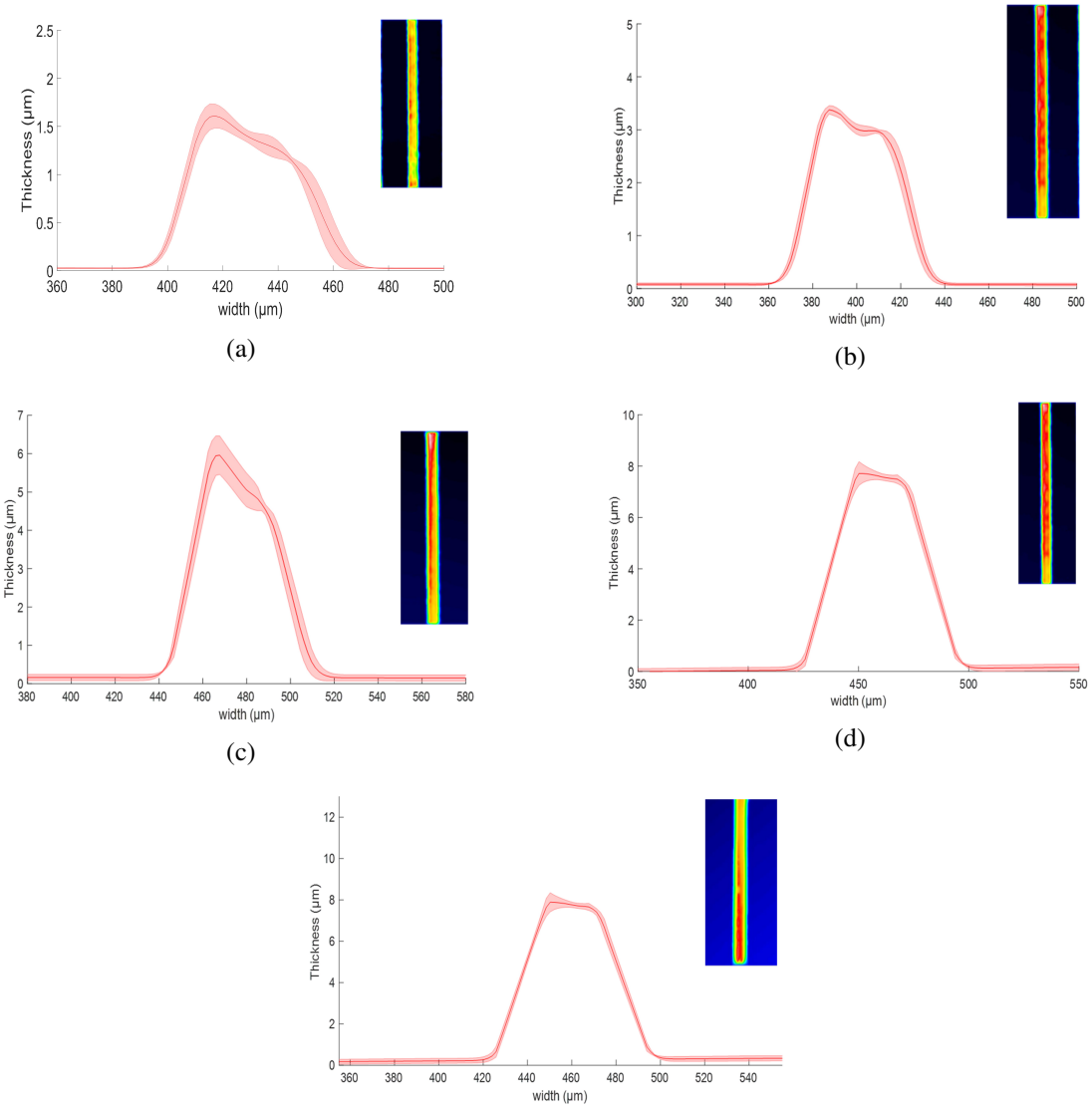

Figure 5.14 Profilometer images of the different overlapped deposition tracks after the filtering process and plot of the profile.

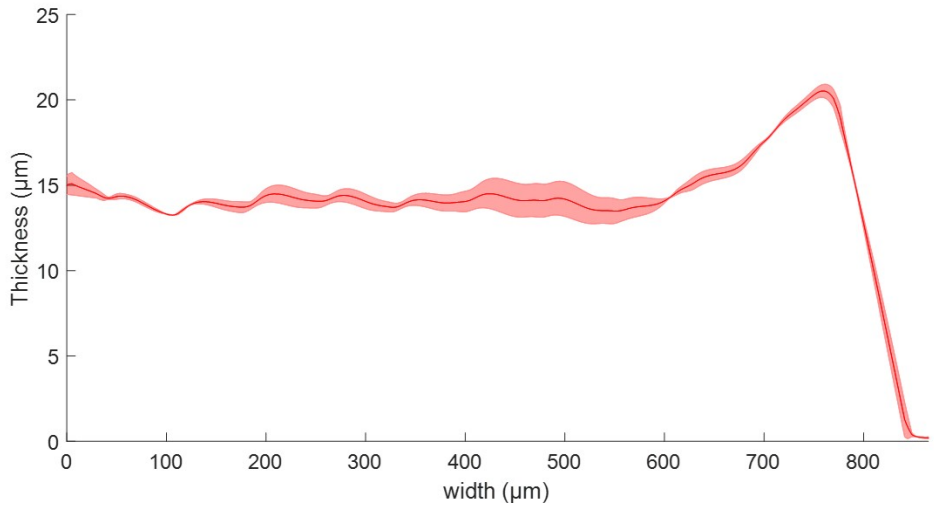

Figure 5.15 Profilometer view of the thickness of Norland Optical Adhesive 81.

The mean value derived from the 5.11 for the S-CS61308 Genesink is 5.7 $\mu\Omega \cdot cm^2$ and agrees with the manufacturer datasheet, with a slightly higher value.

In conclusion, the results obtained by the separated deposition of the three layers, specifically the conductive tracks, the passivation layer, and the sensing electrode array, confirmed the possibility of achieving the suitable designed geometrical features once the optimization of the AJP process. In particular, the three overlapped depositions of silver ink result to be a proper compromise between average width and thickness of the tracks that avoid unwanted electrical contact and the resistance obtained from the measurement. A single layer of NOA 81 is sufficient to create an insulating layer able to shield the recording signals and avoid the corrosion of silver paths. Finally, the PEDOT:PSS showed an adequate feasibility in the production of the recording electrode array for the action potential signals.

5.5.2 Characterization of the printed prototypes

Geometrical Characterization Following the characterization of the single layer of the MEA, in-house tests were carried out to assess the geometrical features and the electrical properties of the printed tracks that composed the multi-structure MEA. The geometrical characterization was performed on four MEAs. In particular, the geometrical size features of printed layers, i.e., thickness and width, were measured by using an optical profilometer, Filmetrics Profilm 3D. The profiles of features acquired with the profilometer were processed with the same specific filters used in the previous paragraph,

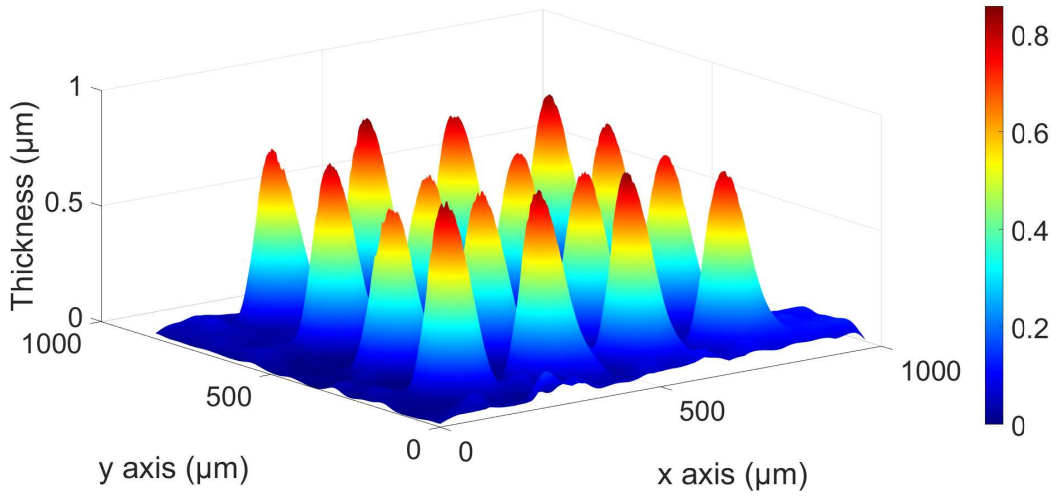

Figure 5.16 Profilometer images of the 16 electrodes array printed with PEDOT:PSS-based ink.

to increase the quality of the printed profile, and then the geometrical parameters (width and maximum thickness) were measured. Fig. 4a shows the profile analysis of silver (in red) and NOA 81 (in blue) tracks. For each track, four cross-sections equidistant from each other were considered for the profile analysis (the overall number is 128, considering all the printed tracks and tested MEAs). The red line is the mean cross-section of silver tracks, while the shadow red area is the standard deviation. The thickness of silver tracks measures (5.5 ± 0.6) µm and the width measures (68 ± 1.4) µm. These tests demonstrate the optimal overlapped silver layer deposition according to geometrical features. The correct overlap is important to ensure uniformity of the thickness of printed track and therefore of the resistivity as well, and to avoid shortcuts between the silver paths of the entire design. Finally, Fig. 5.18a shows a complete coating of silver tracks with NOA81, whose overall thickness is (33.4 ±1.4) µm. This thickness value does not involve citotoxic effect on the cells or reorientation due to substrate morphology according to the literature [90–92]. In Fig. 5.18b, the profile analysis of sensing electrodes is shown. The thickness of PEDOT:PSS micropillars is (0.8 ± 0.2) µm. The PEDOT:PSS coating over silver ink results in a micrometer layer and covers all the silver area. The several measurements and acquisitions with profilometer demonstrated that the silver ink was completely coated by PEDOT:PSS, both on sensing electrodes and reference electrodes.

Electrical Characterization The evaluation of the electrical properties of the silver tracks was performed employing a test bench multimeter (HP34401A, Agilent). The mean value (dots) and the standard deviation (error bars) of the resistance were reported in the *y*-axis of Fig. 5.19, according to the different lengths of the tracks in the *x*-axis.

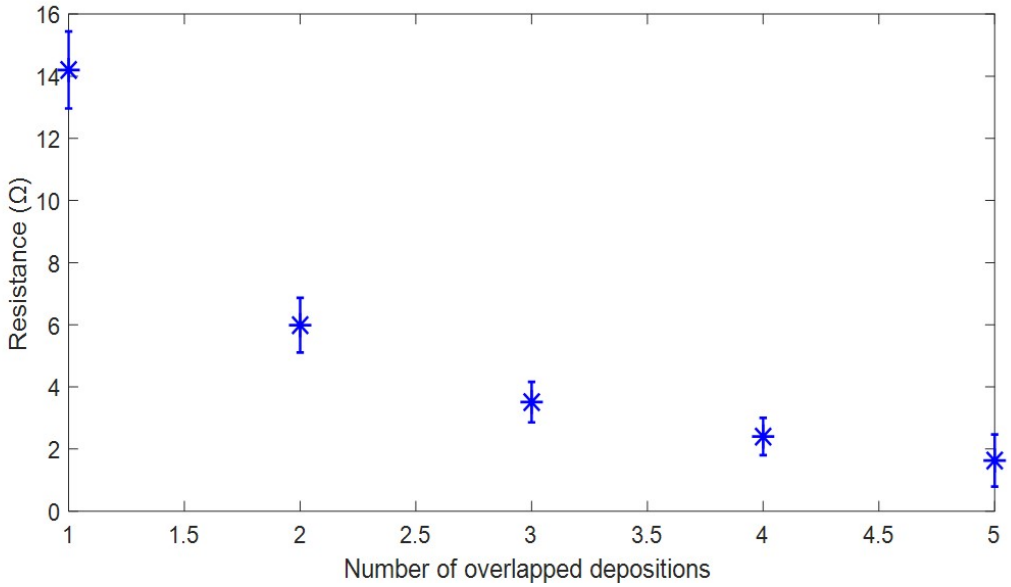

Figure 5.17 Plot of the measurement resistance value for different overlapped deposition.

In each MEAs, 17.4 mm is the length of the two tracks for reference electrodes, while the other values are the four tracks with the same length, due to the symmetrical layout choice. The resistance, as expected, increases proportionally with the length of the conductive tracks.

The resistivity ρ was calculated considering the several resistance R measurements by using equation 5.11:

$$\rho = R \cdot \frac{S}{l} \tag{5.11}$$

- w is the average width of the tracks,
- t is the average thickness,
- l is the length of the measured conductive track resistivity.

The mean value for the silver ink calculated from equation 5.11 was 5.7 $\mu\Omega$·cm and it agrees with the manufacturer datasheet of 5.75 $\mu\Omega$·cm [93].

Electrochemical Impedance Spectroscopy Characterization The long-term stability and the reusability of MEAs prototypes were evaluated using electrochemical impedance spectroscopy (EIS); in particular, the electrochemical characterization was performed on PEDOT:PSS coating to assess the electrode coating behavior for up to two weeks

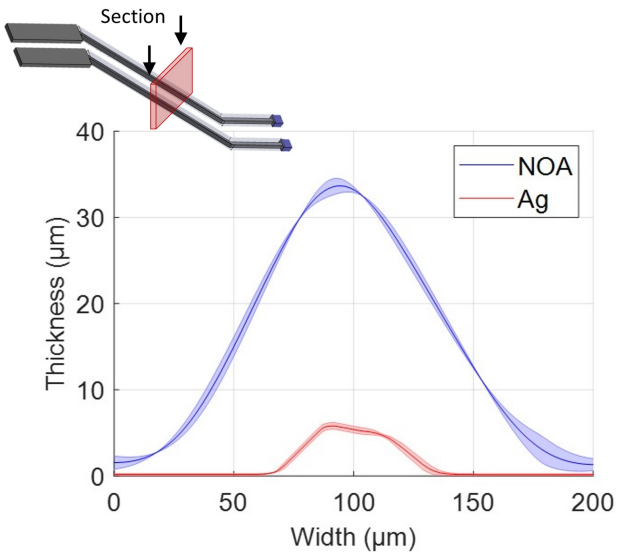

(a)

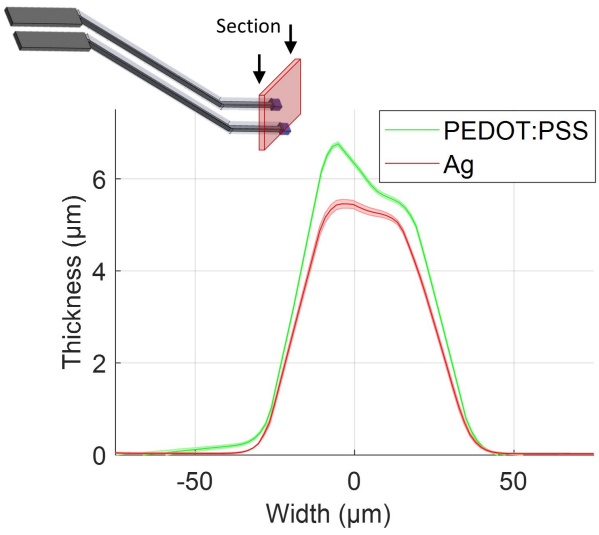

(b)

Figure 5.18 a) Average profile of silver tracks (solid red line) and coating made by NOA 81 tracks (solid blue line). The shadow area is the standard deviation calculated on 128 profiles acquired from the four MEAs. b) Average profile of PEDOT:PSS coating (solid green line) and underlying silver layer (solid red line). The shadow area is the standard deviation calculated on 64 profiles of the sensing electrodes acquired from the four MEAs. In the inset the rendering of the tracks that show the crosssection.

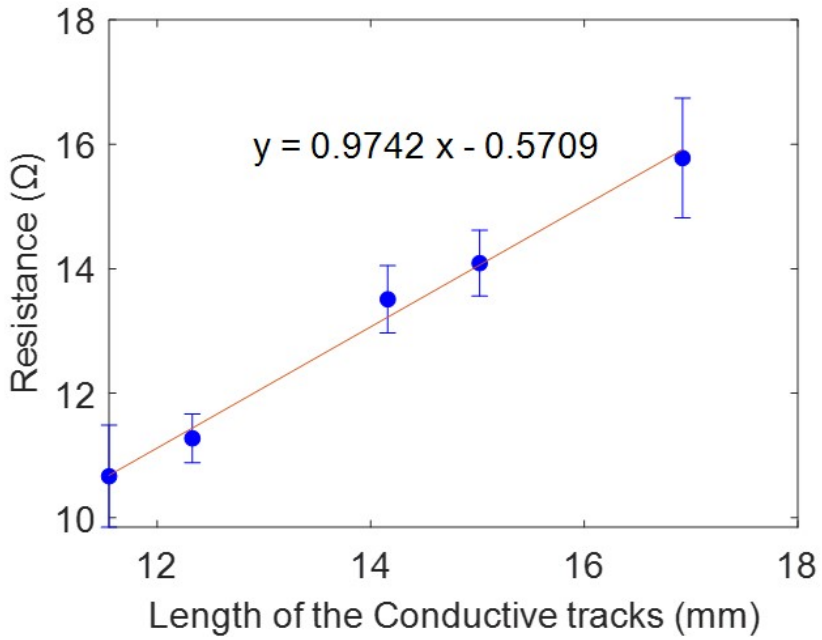

Figure 5.19 Plot of the measured resistance value for different conductive tracks length with mean values and standard deviation calculated on at least 8 tracks, considering all the four MEAs.

in aqueous environment. The setup is shown in Fig. 5.20. An o-ring was glued on the Kapton substrate to surround the printed MEA and build the chamber wall for containing Phosphate-Buffered Saline (PBS), which simulates the aqueous and ionic environment of cell culture medium [69]. EIS was performed with a commercial portable potentiostat (Palmsens 3 PS Trace, PalmSens BV, Netherlands), controlled using dedicated software (PS Trace 5.3). The EIS measurements were performed in the frequency range of 0.01 Hz – 10 kHz, with AC-amplitude of 50 mV_{rms} and DC bias of 0 V, in accordance with the typical range relevant for detecting local field potentials (1 - 300 Hz) and extracellular action potentials (300 Hz – 10 kHz) [28]. The impedance was always measured between each MEA sensing electrode and the closer reference electrode. Each measurement consisted of 10 repetitive scans, one time a day for two weeks. In order to obtain the equivalent model fitting, the tool, PS Trace included in the Palmsens 3 was used. The phase of the impedance is not reported, as suggested in previously works [69, 84, 94], where only the real part of the impedance was analyzed regarding the evaluation of reusability and stability in long-term analysis, while the impedance phase does not provide significant information about those features.

Regarding the reusability test, the chamber MEA was covered with 40 µL of PBS and ten measurements were repeated before removing the PBS. Several washes were performed to clean the sensor with distilled water, to remove the ionic solution. This procedure was

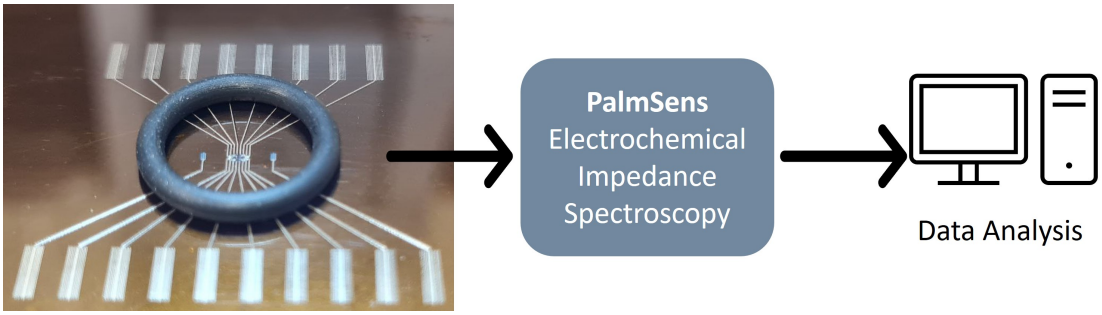

Figure 5.20 Experimental setup used to the Electrochemical Impedance Spectroscopy. The sensor is filled with PBS and then, the PalmSens is connected to the sensor and the measurement are performed and data send to a computer for the data analysis.

repeated every day for two weeks on two MEAs. The plot in Fig. 5.21 shows the mean impedance magnitude (solid line) and its standard deviation (shadow area) calculated on all performed measurements on 14 days over the frequency sweep. The impedance at 1 kHz has a value of (1370 ± 30) Ω , which is significantly below the value of 160 $k\Omega$ measured on the simplest commercially- available MEAs with gold electrodes [95]. At 100 Hz, the impedance slightly increases to (1500 ± 104) Ω but is still lower than commercially available MEAs. The impedance evaluation was performed at two fixed frequencies 100 Hz and 1 kHz, in order to provide a comparison to the literature, and this confirms that PEDOT:PSS improves the electrode-solution interface. The lower impedance values with respect to commercial MEAs ensure the printed MEA electrical compatibility with the commercial front-end for stimulation and recording.

For stability evaluation, 60 µL of PBS was used to fill the chamber without removing the solution, until the end of the test. All the measurements were performed at room temperature and in humidity-controlled conditions to limit the evaporation of liquid solution and keep stable testing conditions, in according with [94]. Fig. 5.22 shows the change of impedance magnitude during the 14 days at frequencies of 100 Hz and 1 kHz. The impedance at 1 kHz was observed due to the extensive use in the characterization of neuronal electrodes [14]. The impedance range is in line with the literature. After two weeks in PBS, the impedance magnitude is (2680 ± 654) Ω at 1 kHz, which is well below the value observed in the reported article [69] after two weeks in the medium. Furthermore, the impedance magnitude decreases over time in both 100 Hz and 1 kHz, due to evaporation of solution. The devices exhibited a small decrease in impedance values, which ensures low degradation of PEDOT:PSS coating as confirmed in the literature [94]. This ensures optimal recording signals for future applications.

The impedance measurement can be modeled as an equivalent circuit in which each component can be related to a particular electrochemical process. The impedance

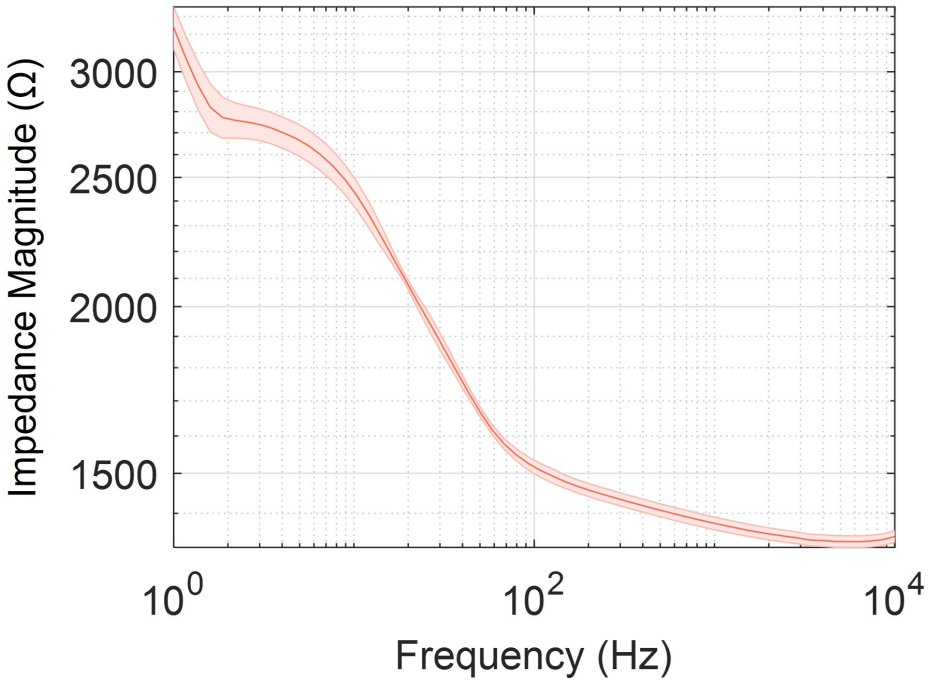

Figure 5.21 Impedance magnitude change over frequency (reusability test) on 14 days. Error bars show the standard deviation on two MEAs. The impedance was measured between the electrodes and the reference electrodes.

magnitude presented a behavior in agreement with the theory (shown in Fig. 5.23) concerning the electrochemical impedance spectroscopy of ionic liquid measurement [47]. At high frequencies, the solution characteristics dominate on impedance plot with an RC effect that depends on the concentration of ions in PBS solution. While the double-layer capacitance was modeled as a capacitor C_{dl} in series to R_s, the surface nonidealities were modeled by constant phase element (CPE). A charge transfer resistance R_{ct} is defined according to the charge transfer process that allows transferring electrons from electrode to solution (or vice-versa). Finally, at low frequencies, the predominant component regarding the diffusion of the ions was modeled by the Warburg impedance Z_W, which corresponds to a line at a phase angle of 45° in the complex plane plots [96]. Comparing the theory module of impedance shown in Fig. 5.23 with the results presented in this work in Fig. 5.21, at low frequency, before frequency of 1-2 Hz we have a phase angle higher than 45°, apparently inconsistent with the theory. Such difference was due to the thickness of PEDOT:PSS layer, as described in [97], which was shown for different depositions times (and thus thickness), a variation of the slope at low frequency, with a variation of the value of Warburg element. Finally, the equivalent model evaluation was useful for monitoring the behavior of the electrochemical system for long-term analysis. The change in the value of the electronic elements indicated modifications

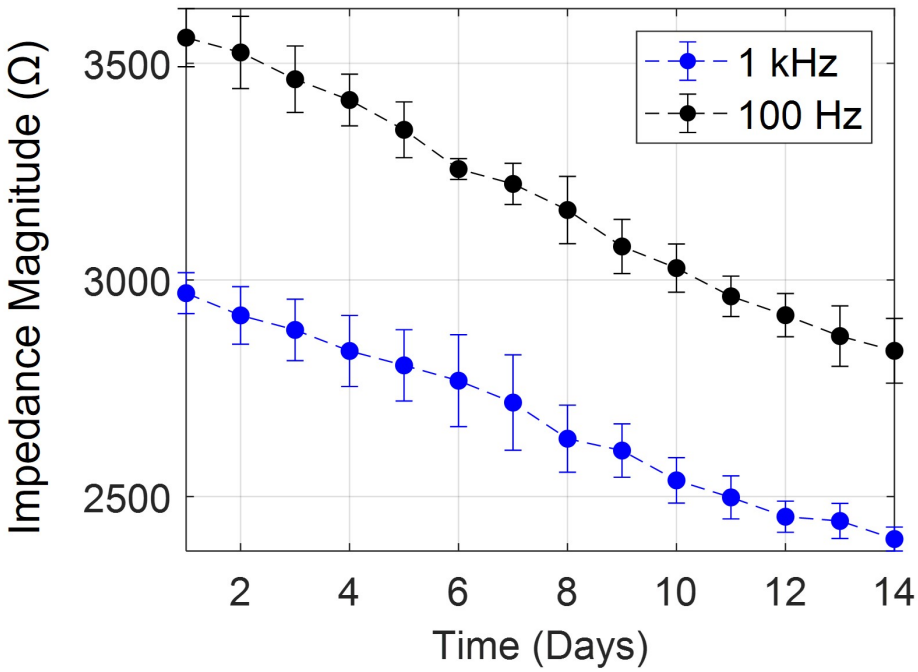

Figure 5.22 Impedance magnitude over 14 days in PBS for the stability of two sensor at frequency of 100 Hz and 1 kHz. Error bars show the standard deviation of two MEAs.

of the electrochemical properties of the cell, particularly interesting for the long-term stability analysis.

The Nyquist plots of EIS measurements obtained from the stability test shown in the Fig. 5.24 show a decrease in solution resistance over time due to the decrease of solution resistance induced by evaporation of the water. Such variation explains the behavior of the curve within the 14 days in Fig. 5.22, where the value of the impedance decreases according to the days as a result of water evaporation. While the shape of curve remained the same with no variation in the electrochemical elements of the equivalent model.

5.5.3 Discussion

This section reported the design, development, and characterization of a printed Micro Electrode Array by using AJP as an enabling additive manufacturing technology for the fabrication of a bioelectronic device for electrical stimulation and real-time monitoring of action potential signals. The realization of a low-cost and multilayer device by using suitable and biocompatible inks to improve the sensor performance is described. The possibility of depositing directly on the substrate a micropattern of sensors ensures

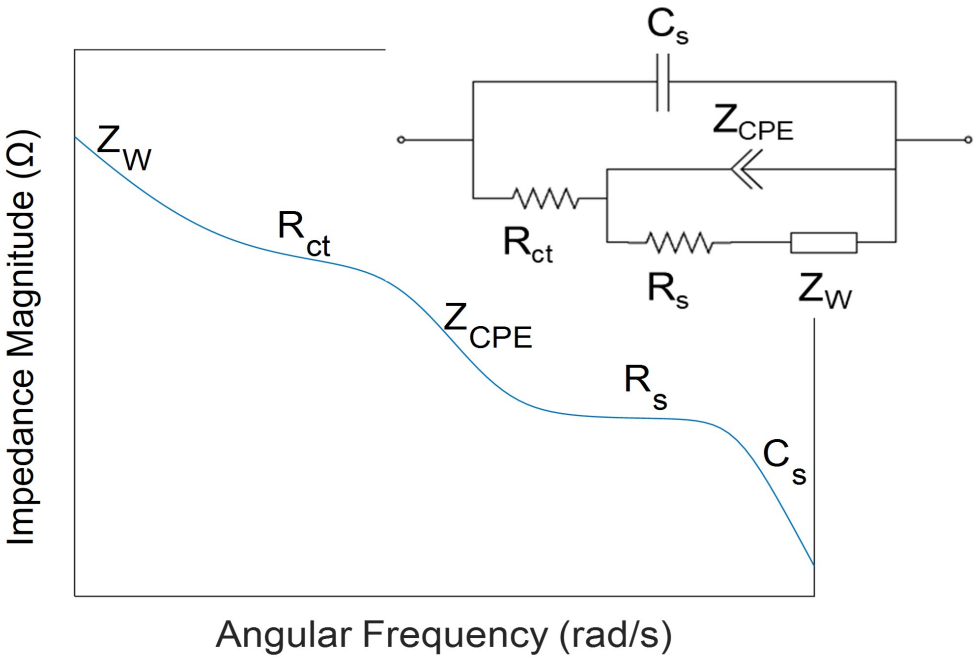

Figure 5.23 Theoretical impedance module according to frequency variations for the Randles circuit model (in the inset) for the electrode/electrolyte interface used for the fitting of the experimental results.

device customization and, low cost and quick fabrication. In particular, the work proposes itself as an alternative to the traditional microfabrication techniques that easily allow the customization of the electrode design according to the desired neuronal network architecture. The achieved printed MEAs, in this current design and fabrication process, are the result of an improvement and an optimization of the design, where a preliminary study of the design of the printed MEA and the selection of suitable materials for the biomedical application was developed.

Furthermore, it is fundamental that the optimization and customization of the micro-electrode array design to produce bioelectronic devices lead to an improvement of the knowledge in the neuronal tissue engineering and neuroscience field by exploiting the employment of new printed manufacturing techniques. In the specific, before proceeding with the realization of an electrode array device, it is necessary to design the set-up and the electrical parameters to obtain the achieved result, and this is possible due to the use of computational techniques.

Once the simulation results are obtained and analyzed, the first stage of the MEA fabrication and the optimization of the parameters of AJP machine led to the realization of the three main layers of the printed MEA. In particular, the overlapped depositions of

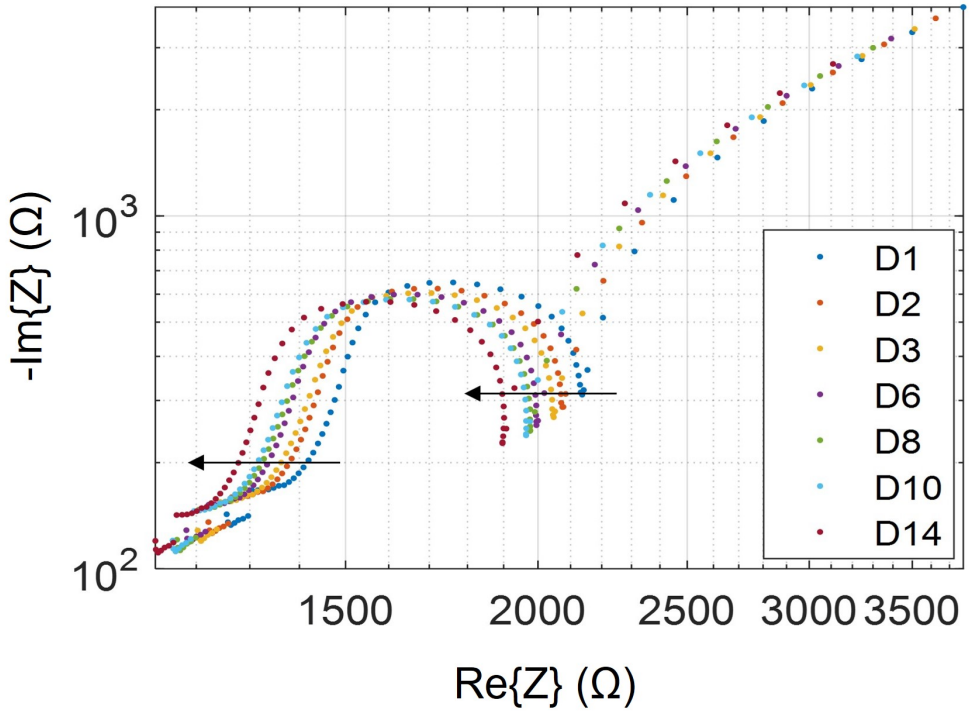

Figure 5.24 The Nyquist plot with real and imaginary part of the experimental results obtained in the stability test of the printed MEA within two weeks.

silver tracks for the conductive lines, the NOA 81 as the passivation and coating layer, and finally, the PEDOT:PSS-based ink for the biological interface and the sensing electrode array. After the design and the fabrication by using additive manufacturing techniques, the printed devices were then characterized both in terms of geometrical and electrical properties. Stability and reusability were both tested to evaluate the performance of sensor for long-term analysis. The results are promising in terms of customization of electrode design and the feasibility of a low-cost 3D printing technique with advanced flexibility and reproducibility. Furthermore, the possibility to improve the electrical stimulation with suitable electrode design and position, to enhance the cells maturation protocol, and, at the same time, to provide a device to real-time monitor for maturation of neuronal activity during cell culture. This printed MEA is an important starting point for the realization of a customized and sensorized system to improve *in vitro* cell culture. The advanced deposition and curing methods of electrodes, passivation layer, and tracks allow direct integration into the cell culture device in future applications. Furthermore, the customization offered by AJP technique suggests different opportunities, such as the possibility of selectively depositing cell adhesion protein to create a specific architecture for neuronal networks. And finally, in the following section, the Analog Front End design

was discussed in order to realize the recording system to monitor in real-time the action potential signals.

5.6 Electronic Front-End

5.6.1 Introduction

This Ph.D. thesis introduces an early-stage realization phase of a low-cost electronic analog front end (AFE) for connecting printed MEA to enable real-time monitoring of neuronal culture. In particular, this section presents the design and realization of a system for acquiring signals from bio-potential sensors. The requirements for the system will be outlined and justified according to the neuronal recording environment and translated into specifications for the system design [98]. A suitable interface to readout recording signals acquired is needed for the printed MEA, in order to make it available and usable to the end users. To this end, an acquisition system is realized with a customized electronic front end. Several commercial readout devices are suitable on the market for different applications, but the possibility to realize a customized and specific AFE is additionally beneficial for power consumption, compatibility with printed MEA and experimental conditions with an improvements in terms of cost-effectiveness and adaptability to the MEA [99].

In the neuroscience field and in particular *in vitro* extracellular recording, the microelectrode requires for the neuronal recording interface, a read-out electronic circuit, including low-noise and low-power requirements, and a data acquisition and transmission. In particular, Analog Front End (AFE) involves the need of a multi-channel systems, in order to amplify and transmit the signal of every single microelectrode to the visualization system. The role of the AFE is to amplify the very small biopotential signals with low noise generation, while filtering out interference and other irrelevant signals. Generally, a neural amplifier needs to have a high input impedance, which is significantly higher than the electrode impedance obtained in the printed MEA, to ensure signal integrity. Therefore, gain and dynamic range requirements can be quite demanding and should be adjustable, such as to cover applications with maximal amplitudes of a few hundred microvolts. This is also relevant for the flexibility in the recording bandwidth according to the relevant type of biopotential signals that one wants to analyze. In this case, the action potential signals generated by the neuronal cells have usually an amplitude at the micro-scale, thus the signal has to be properly filtered and amplified. The temporal resolution of neuronal biopotential signals varies extensively across different applications. In particular applications, the AFE must be adapted or configured with proper bandwidth to highlight target components of biopotential signals, avoiding aliasing and distortion degrading the signal. In the neuronal action potential signal, the bandwidth has a range

between a few hertz to a few tens of kilohertz, in particular at the low frequencies the low field potential (LFP) components are present, representing the excitatory and inhibitory signal of dendritic potentials recorded of the neighbouring neurons from the recording site. The action potential spike is a fast event that occurs every time the membrane potential overcomes the threshold. Due to noise and interference from the electrode and outside sources that can decrease the signal-to-noise ratio (SNR), amplifier systems are generally designed to limit undesirable content outside the frequency band of interest. The excessive bandwidth in the AFE can include more total integrated noise to the final digitized signal and needlessly consume more power.

The AFE has to be placed in proximity to the printed MEA in order to reduce the noise signal and enhance the SNR. MEA systems also include digital-to-analog conversion (DAC) and can be equipped of additional circuitry to provide electrical stimulation. MEA systems need to include an interface to transmit the data and receive commands for controlling the system's operation. *In vitro* MEA systems can be directly wired to the data-receiving device.

Another crucial choice regarding design and suitable electronic components is limiting the power consumption of the system. A consequence of high power consumption is excessive heat generation which can cause problem to the operator and to the biopotential recording equipment. The objective is minimizing power conflicts with other design requirements. The choice of low-power consumption components used in the instrumentation, particularly in the AFE, directly affects available bandwidth and signal-to-noise ratio, which are also important in the design considerations to acquire a sufficient signal quality. Therefore, the consumption management of power is of critical importance among all the blocks of a neural recording system.

5.6.2 Design of AFE

Design specification The section presents the general requirements to acquire action potential signals. The signal processing block needed to realize the analogic frontend and the requirements of each block were analyzed. The amplitudes of neuronal biopotentials are typically very small compared with sources of interference in the cell culture environment, thus an amplifier is needed which rejects the interference and amplifies the differential signal. In particular, instrumentation amplifiers (IA) are used to measure small differential signals while rejecting common mode levels. The IA requires a high input impedance, to avoid attenuating signals from sensors with high output impedance, fundamental in biopotential recording for electrodes with large impedance

due to their small size or contact. Due to the sampling frequency of neuronal action potential [28, 100], the sampling frequency of 24 kHz was imposed to accurately represent the shape and to rebuild the spike waveform. The typical electrical features of extracellular action potential signals recorded by a standard MEA are the following:

- amplitude peak-to-peak of neuronal spikes are comprised between 30 μV- 1 mV. In particular, in the literature [69] PEDOT:PSS electrodes in MEA recording with a spike amplitude of 100-400 μV;
- bandwidth of the signal is between 1 Hz to 10 kHz (comprising the LFP and spike components)
- potential offset of the microelectrode in the range of few hundred mV

According to the parameters listed above, the following requirements have been established:

- gain at center bandwidth of ~1000, amplification is needed for analyzing signals;
- bandwidth define to limit the aliasing effect;
- sampling frequency of 24 kHz to avoid aliasing [99, 101] of the signal according to the DAC device used for MEA signals;
- cutoff frequency at 1 Hz and 10 kHz according to the signal bandwidth of the action potential signals (the main components of the action potential signal of our interest are mostly present at low frequencies, and in this case, it was decided according to the Nyquist criterion the value of the sampling rate, which is sufficient for the reconstruction of the signal);
- low noise and stability of power supply;
- minimization of components number in order to reduce the footprint;
- modularity and customization

5.6.3 Realization of the front end

The following section presents the design and realization of the bio-potential amplification system. The Sistem Block Diagram is presented in Fig. 5.25, showing the system elements and their connections to each other. The design of each block will be presented

separately, including design requirements, electronic components selection, and circuit design. System construction is presented including the design of PCBs and an enclosure for the system. The block diagram integrates the printed microelectrode array sensors, the first and second amplifier filtering stages, and finally, the data acquisition device.

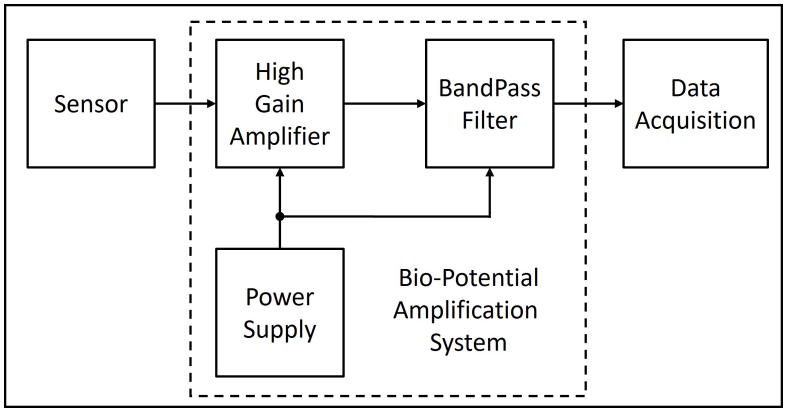

Figure 5.25 Block Diagram of Bio-Potential Measurement System

The complete schematic circuit is presented in Fig. 5.26 of the high-gain amplifier and filtering stage. The gain and bandwidth required are specified based on the amplitude and frequency range of the bio-potential signals to be measured. Two main blocks connected from the MicroElectrode Array to the Analog-to-digital converter:

- First amplification stage to amplify the action potential signal
- Second filter stage with a cutoff of 1 Hz and 10 kHz
- Data acquisition system, Analog to Digital converter (ADC) with a sampling frequency of 24 kHz integrated in PC

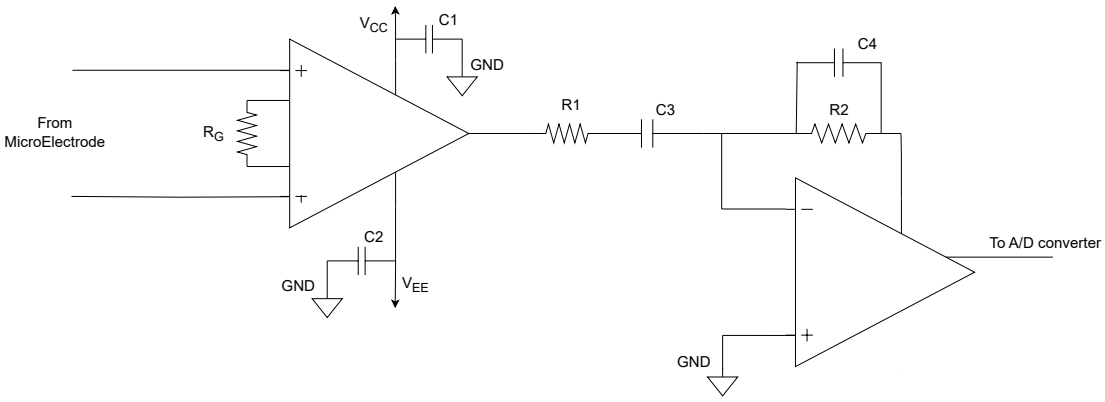

Figure 5.26 Scheme of the filter amplifier

First Amplifying Stage The first stage of the AFE is composed of an amplifier in order to amplify the recorded signal from the microelectrode array. The INA128 (Texas Instruments, USA) was selected due to the low noise and power characteristics. Furthermore, the Instrumentation amplifier is selected due to the gain bandwidth product (GBW) in agreement with the project requirements described for the action potential recording. Bypass capacitors (shown in Fig. 5.27) are applied from both positive and negative supply lines to the ground in the first stage of the front end. These capacitors provide supply voltage stability and filter high-frequency interference on the power supply lines. The capacitor value was set to 220 nF.

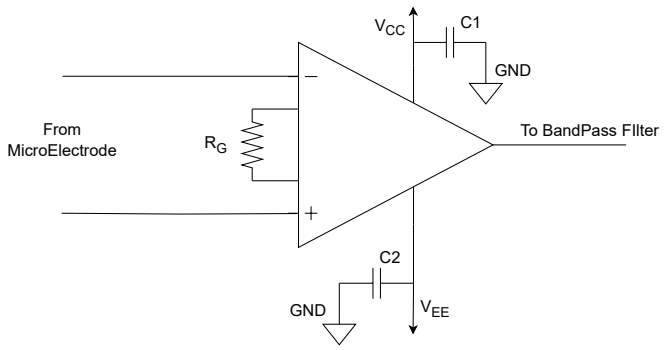

Figure 5.27 Scheme of First Amplifying Stage.

The gain of the INA128 is set by the single resistor R_G= 47 Ω as shown in Fig. 5.27 according to the datasheet. The gain is calculated by the following equation:

$$G = 1 + \frac{50000}{R_G} \tag{5.12}$$

A gain of 1000 can be set in order to solve the R_G with a resistor value of 50.05 Ω. Due to commercial readily unavailable value, a 47 Ω with a 0:1% tolerance was inserted.

The amplifier exploits a double-ended topology, one to the single microelectrode array and the other ended to the reference electrode, since MEA signals are typically acquired with respect to the reference, and in this case, to the two bigger electrodes immersed in the culture medium and tied to the ground of the system. The noise reported in the datasheet of the INA128 at the parameters exploited for the experimental characterization of the noise reported a value of e_n= 8 $nV/\sqrt{Hz}$ with G=1000, f= 1 kHz.

Bandpass Filtering Stage The second stage is an active inverting band-pass filter in order to obtain the bandwidth of the signal composed of an operational amplifier, TLV2254 (Texas Instruments, USA), and two first-order filters. The TLV2254 was

selected due to the low power characteristics, and the value of gain bandwidth product (GBW) that meets the design requirements. Bypass capacitors (not shown in Fig. 5.28) are applied from both the positive and negative supply lines to the ground in the first of the front end. These capacitors provide supply voltage stability and filter high-frequency interference on the power supply lines. The capacitor value was set to 220 nF.

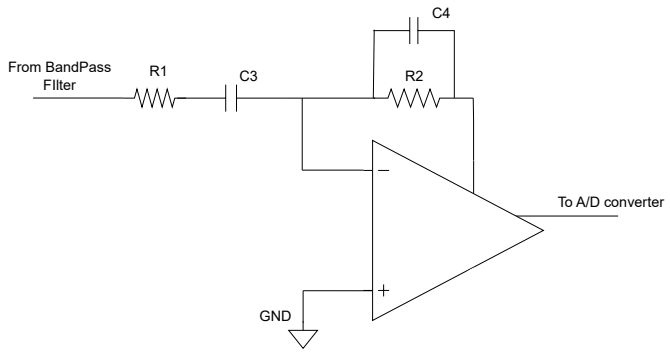

Figure 5.28 Scheme of Second Stage.

The equations relate the 1st order active band-pass filter of the circuit transfer function, lower and upper frequency and is provided by 5.13, 5.14, and 5.15, respectively:

$$\frac{V_0}{V_i} = -\frac{sC_4R_2}{(1+s\cdot C_3\cdot R_1)(1+sC_4R_2)} \tag{5.13}$$

$$F_l = \frac{1}{2\cdot\pi\cdot R_1\cdot C_3} \tag{5.14}$$

$$F_h = \frac{1}{2\cdot\pi\cdot R_2\cdot C_4} \tag{5.15}$$

$$G = -\frac{R_2}{R_1} \tag{5.16}$$

F_l is the cutoff frequency for the low pass filter while F_h is the cutoff frequency for the high pass filter. Concerning the action potential signal bandwidth, the cutoff frequency was selected with values of F_l=1 Hz and F_h=10 kHz. The values obtained are the following:

- R_1= 330 kΩ;
- R_2= 330 kΩ;

- C_3= 470 nF;
- C_4= 47 pF.

Power Supply A bench power supply, laboratory DC power supply (IPS 2303DD, ISO-TECH, USA) was chosen to supply energy to the boards, with a DC potential of Val=$\pm$5 V. Both positive and negative voltage are required to supply the PCB due to the INA128 and TLV2254 that require a dual power supply. The current generator choice is due to the stability and low noise of the device with respect to the DC/DC converter to supply the power supply required.

Printed Circuit Boards and Assembly The AFE is based on 50 mm x 50 mm Printed Circuit Board (PCB). The printed circuit boards were manufactured using standard PCB technology designed by using a software of electronic circuit and PCB design, KiCad (KiCad 7.0). In a single PCB, four channels for action potential recording are present due to the quadruple low-voltage operational amplifiers TLV2254. Pin 2. Male Female SIL Header Socket Single Row Strip PCB Connector (RS Components S.r.l.) is used to connect the Microelectrode array and to the DAQ National Instruments. Finally, the connector is present for the dual power supply and the ground in order to supply the power to the PCB.

Digital to Analog Converter The Front End is interfaced with a DAQ (PCI-6024E, National Instruments (NI), Texas, USA). The ADC is integrated into a PC. The ADC acquires and converts to digital the output signal with a sampling frequency of 24 kHz and sends the digital data to the PC in order to post-processing and analyze the signals acquired.

Front-End Characterization The assembled board was characterized in terms of gain and bandwidth measured to evaluate the real value obtained according to the design requirements imposed. Finally, a basic noise analysis was performed and quantified.

The measurement of signal bandwidth and gain obtained was carried out according different frequencies along the spectrum (in a range of 10 Hz to 100000 Hz) in order to evaluate the front-end performance and the obtained value of gain is 972 $\pm$ 102 in the signal bandwidth of interest between 1 to 10000 Hz. The cut-off at -3 db (high) is 13 kHz with an attenuation of 40 db/decade.

The noise analysis is quantified in order to evaluate the component of the noise added at the final signal acquired. The analysis of the noise was performed by acquiring the signal onto the PCB in the output pins. Measurements of circuit noise were performed connecting the inputs in shortcuts. The obtained noise value was evaluated in terms of V_{pp}=15 mV and V_{rms}= 4.6 mV for the entire PCB. The noise recorded in this condition produced a PSD constant over our frequencies of interest, with a total power of approximately $9.03 \cdot 10^{-10}$ V^2/Hz and can be used as a background noise level. While, at the first amplification stage, the noise analysis showed a value of V_{pp}=12.75 mV and V_{rms}= 3.7 mV. As we might have expected the noise component is preponderant in the first amplification stage due to the gain of 1000 for the amplification of the signal. Finally, the noise performance is quantified by connecting the printed MEA to the PCB without applying signals nor stimuli and the values obtained were V_{pp}=14.5 mV and V_{rms}= 6.7 mV.

5.6.4 Interface

A dedicated VI (Virtual Instrument) has been developed in LabVIEW to communicate, acquire, and store the measurement data. This program receives the data, composed of 16 signals recorded from the respective microelectrodes which are shown on the screen. The saved data will be elaborated and analyzed with a dedicated Matlab script and the relevant features of the acquisition extrapolated.

5.7 Biocompatibility evaluation of the MEA

In order to demonstrate the biocompatibility of the specific PEDOT:PSS sensing electrodes and the overall device, STO cell line were cultured on the printed MEA at 2 DIV (days *in vitro*). In particular, a culture chamber was realized with additive manufacturing technique in order to culture the biological cells and allow a sterilization and biocompatibility of the overall device.

5.7.1 Culture Chamber and MEA Adapter

Once the printed MEA was realized, the kapton substrate of the printed MEA was used as a bottom chamber where culture the fibroblast cells. The wall and the lid of the culture chamber were 3D-printed by stereolithography (SLA) (Form 2, Formlabs, United States)

using the biocompatible and autoclavable BioMed Clear Resin (Formlabs, United States) and glued to the printed MEA with polydimethylsiloxane (PDMS).

5.7.2 Biocompatibility test

STO line is a fibroblast cell line isolated from a mouse embryo. STO cells are used as feeder layers to maintain stem cells in the undifferentiated state. STO are also suitable transfection hosts. The cell suspension was diluted in DMEM 10 % FBS, plated on plastic dishes and incubated at 37°C in 5 % CO2. Medium was replaced every 2/3 days. At 70-80 % of confluence, the cell layer was dissociated with Trypsin-EDTA solution, seeded at a density of $9*10^4$ cells/chip on MEA in complete DMEM 10% FBS and incubated at 37°C in 5 % CO2.

After that, the printed MEA requires the sterilization of the components in order to avoid contamination during the cell culture. To guarantee a higher level of sterilization the following protocol was used in according with the assembly procedure:

- All the Biomed resin components were washed with 70 % ethanol three times.
- The Biomed resin and MEA components were exposed to UV for 2 hours.
- The culture chamber components were assembled on MEA with PDMS.
- The MEA reservoirs were filled up to the edge with 70 % ethanol for 24 hours.
- Ethanol was discarded and MEA was dried under a laminar hood and exposed to UV for 2 hours.

The following days cells were visualized with the Olympus IX51 microscope (Olympus Italia Srl, Milan, Italy) to monitor the vitality and growth of cells.

The results from the evaluation of cytocompatibility on the MEA samples showed an adequate adhesion of the fibroblast cell on the printed MEA as reported in the microscope images in 5.29. In particular, the cells did grow on the printed MEA indicating that the overall device are in fact biocompatible and suitable for cell culture. The microscope image showed the top view of the microelectrode array before the cell culture, after the culture of STO cell line at day 1 and at day 2, and it is possible to observe the STO cells that covered with a confluent monolayer. In particular, the cells are nicely spread and tightly adhering to the surface of the device. Furthermore, the polyimide(Kapton) and the multistructure layers can be clearly distinguished in the images. Results from

microscope images showed a good cell viability on the produced sensors. In particular, the fibroblast appeared to be adherent and evenly distributed on the surface of the printed MEA, suggesting a good cytocompatibility of printed inks and substrate.

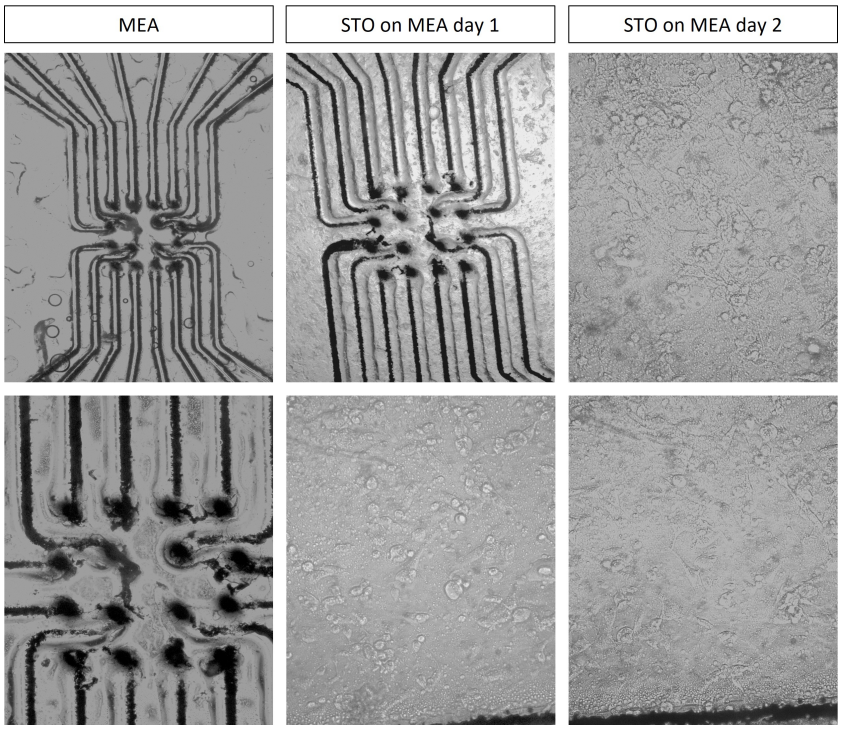

Figure 5.29 Photograph of the STO cell line at the following days, the cells were visualized with the Olympus IX51 microscope (Olympus Italia Srl, Milan, Italy) to monitor the vitality and growth of cells.

Chapter 6

General Conclusions and Future Outlooks

In summary, the present dissertation discussed two main applications in biotechnological research, in which the combination of advanced technology, biophysical stimulation, and printed electronics are exploited as suitable tools for obtaining relevant results in terms of cell culture improvements and quantitative feedback from cells, with low-costs and limiting the invasiveness for the cell culture.

This thesis dissertation is focused from one side on providing the initial insight into the development of an electrical field stimulation to improve differentiation and maturation of human induced pluripotent stem cells-derived dopaminergic neurons. The results obtained from this preliminary work suggest the need for a novel device able to overcome the critical aspects that have been brought to light by this initial work about the electrical stimulation of hIPSC. Consequently, the design and improvement of printed microelectrode array (MEA) by using Aerosol Jet Printing for *in vitro* neuronal culture for electrophysiological study and drug screening and, as the integration of the first study, as a biophysical stimuli device to promote differentiation and maturation of hIPSC.

The results obtained in the use of electrical stimulation to improve differentiation and maturation of human-induced pluripotent stem cells-derived dopaminergic neurons have shown promising findings. In this case, the aim was to verify that electrical stimulation was able to accelerate the maturation of hIPSC. The development of this technology makes it possible to develop low-cost, highly controllable and customizable protocols compared to standard protocols without biophysical stimuli. On the other hand, the results achieved with the electrical stimulation on hIPSC are a promising starting point that suggests the feasibility of the proposed approach since the developed

electrical stimulation device worked adequately and efficiently and the morphological characterization of the neuronal cells showed typical morphological features of mature neurons as preliminary evaluation about the electrical stimulation efficacy on the hIPSC maturation. Despite the relevant preliminary results obtained, some improvements are needed in order to overcome the critical aspects unearthed by the system used. Building on these initial insights, the printed MEA work was focused on the development of such bioelectronic device for improving the electrical stimulation system and providing real-time monitoring of the cell culture process by exploiting the printing techniques.

Aerosol Jet Printing was explored as a means to achieve a microelectrode array for electrical stimulation and action potential signal recording. The proposed preliminary prototypes were able to achieve the imposed requirements. In particular, this work outlines the development of a printed Micro Electrode Array (MEA) using Aerosol Jet Printing (AJP) as an additive manufacturing technology. The MEA results showed the realization of low cost, multilayer structure, and use of biocompatible inks to enhance sensor performance. The technique allows the customization of the electrode design to match specific neuronal network architectures, serving as an alternative to traditional microfabrication methods. The achieved MEAs result from an optimized design and material selection for biomedical applications. The optimization and customization of the MEA design aim to advance knowledge in neuronal tissue engineering and neuroscience through new printing techniques. Computational methods are employed to design the setup and electrical parameters to achieve the desired outcomes e.g. electrode dimension and position and optimal thickness of insulation layer in order to limit the crosstalk signals. The fabrication process involves the deposition of silver tracks, passivation and coating layer with the use of PEDOT:PSS-based ink for the biological interface and sensing electrode array. The printed devices are characterized in terms of geometry and electrical properties, with promising results regarding the repeatability of the printing process according to the three printed layers. Moreover encouraging results are obtained regarding the impedance electrode values obtained through electrical characterization. The impedance was lower with respect to the impedance reported in the literature and in commercial devices and in addition, the long-term stability test showed an electrode degradation consistent with neuronal application.

A preliminary realization of the analog front end (AFE) and the interface for data transmission and collection was developed to provide the system for the visualization and analysis of data recording by the printed microelectrode array. The main finding regards the validation of the sterilization and biocompatibility with the cell culture routine for the specific assessment of the adhesion and vitality of fibroblast on printed MEA. The

results obtained showed the biocompatibility of the printed MEA, and its capability to successfully establish a tight coupling with cells was proved.

While commercially available devices like commercial stimulation systems and MEAs are established and effective methodologies, the innovative combination of printed tailored and cytocompatible electrode/sensor may improve the culture process and the investigation of biological cells and their bioproducts. Indeed, the preliminary results obtained are an important starting point, due to the integration of sensing elements directly in the cell culture environment without affecting culture conditions and the design of dedicated electronics to record signals may represent a powerful strategy to carry out significant improvement in a monitor and control engineered interaction with cells in their own environment.

In light of the objectives of this study, which aimed at developing preliminary prototypes to assess their feasibility through characterization and *in vitro* testing to provide novel biotechnological applications, it is noteworthy that this research has yielded successfully several outcomes and findings as previously delineated. However, a few points still require deeper investigation, among them, other combinations of conductive inks e.g. carbon paste or other conductive polymers with different properties and substrates, to further explore and optimize the fabrication metrological characteristics (e.g. repeatability, stability, ...) of the printed MEAs. After that, a set of specific characterization tests can be performed in order to improve the electrochemical characterization of the printed electrodes e.g. cyclic voltammetry to evaluate the surface coating. Further optimization of printed MEA may target to increase sensitive area, electrode density, and number of parallel recording/stimulation channels. A larger sensitive array area will extend the observable region of a sample, allowing for simultaneous access to more neurons in cell cultures and to more distal brain areas in slices and this is easily achievable due to the printing techniques employed that promote the customization of the microelectrode array in terms of biologist requirements and material and design electrodes. Parallel and multiple printed MEAs can be combined in a multiwell-plate format, in order to perform parallel MEA measurement, for applications in drug development. Lastly, the microelectrode arrays can be integrated within a bioreactor device directly printing within the device along with other environmental sensors (e.g. temperature, pH, humidity, glucose and lactate) exploiting the printing techniques that could be used to provide complementary information about cell culture activity in order to realize an automated control and monitor system for *in vitro* cell culture to improve scalability and standardization of the cell culture adding information about the environmental condition both in clinical and research application.

Appendix A

Electronic Front End

In Figs. A.1a and A.1b the analog front end for the recording system of printed MEA described in 5 is shown.

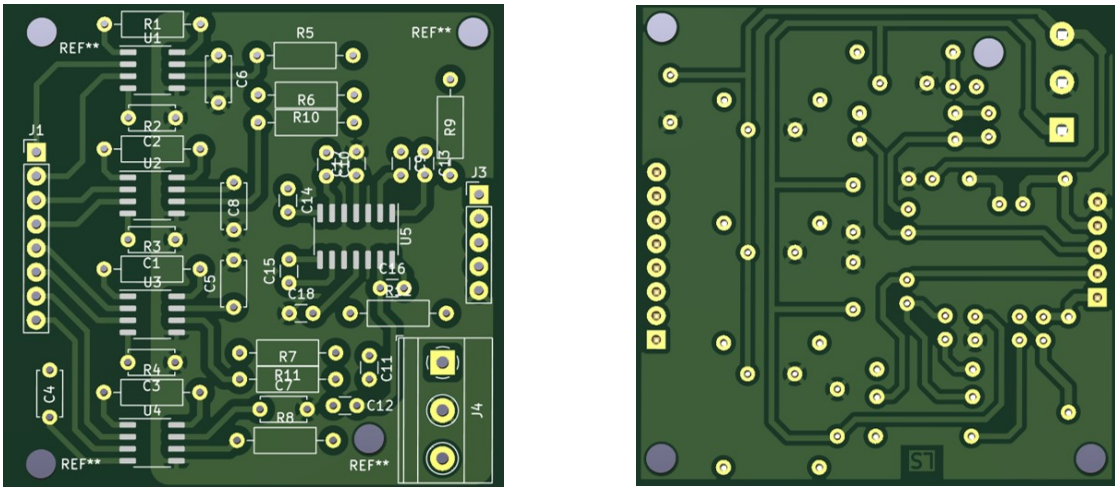

(a) (b)

Figure A.1 Layout with a) top view and b) bottom view for the board of the analog front end of the printed MEA recording system

The size of the single board (Fig. A.2) which includes four recording channels is (50 x 50) mm^2. In Table A.1 the components and the value of the capacitors and of the resistors used in the board are listed.

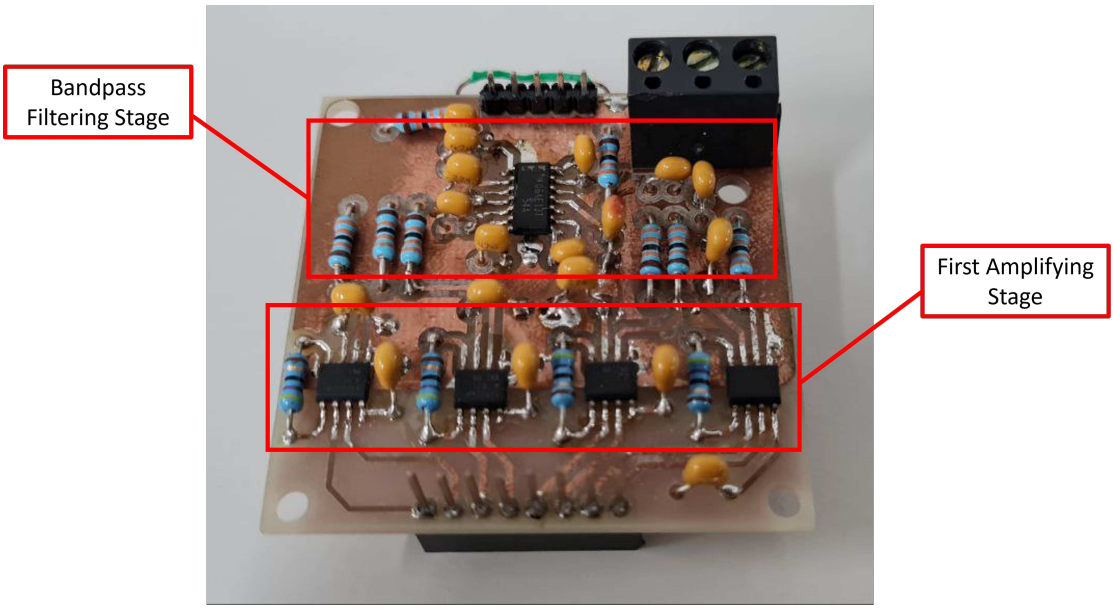

Figure A.2 Photo of the PCB assembled of the board of the analog front end of the printed MEA recording system

Item	Reference	Quantity	Part
1	C1, C2, C3, C4, C5, C6, C7, C8	8	220 nF
2	C9, C10, C11, C12	4	470 nF
3	C13, C14, C15, C16	4	47 pF
4	C17,C18	2	220 nF
5	J1	1	Conn_01x08_Pin
6	J2	1	Conn_01x05_Pin
7	J3	1	Conn_01x03_Pin
8	R1, R2, R3, R4	4	47 Ω
9	R5, R6, R7, R8, R9, R10, R11, R12	8	330 kΩ
10	U1, U2, U3, U4	4	INA128
11	U5	1	TLV2254IN

Table A.1 Bill of Material of the Analog Front End for MEA recording

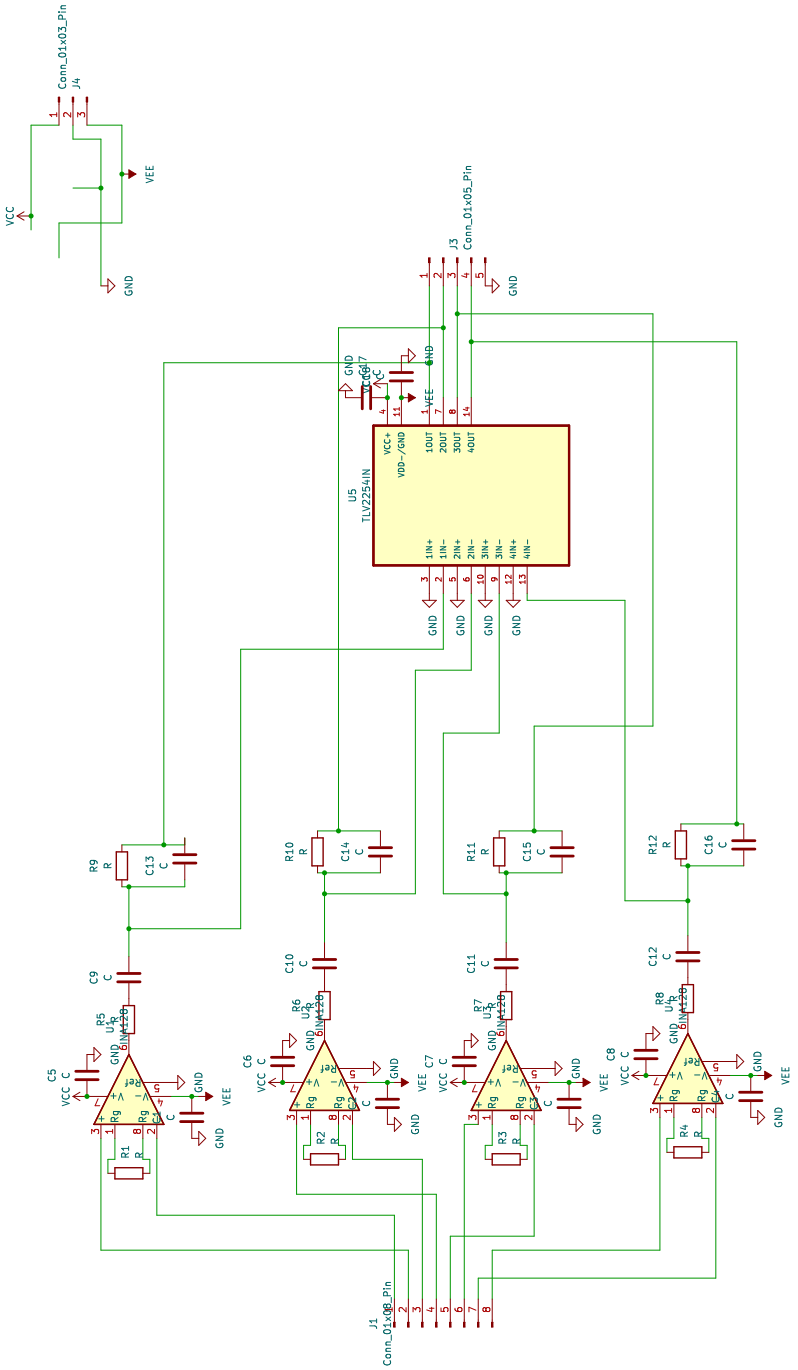

Figure A.3 Block diagram of Electronic Front End for printed MEA

Ringraziamenti

Grazie.

Bibliography

[1] Cecile Legallais Benoit Carpentier, Pierre Layrolle. Bioreactors for bone tissue engineering. *Int J Artif Organs*, 34 (3):259–270, 2011.

[2] Ivan Martin, David Wendt, and Michael Heberer. The role of bioreactors in tissue engineering. *Trends in Biotechnology*, 22(2):80–86, 2004.

[3] Robert Langer and Joseph Vacanti. Tissue Engineering. *Science*, 260:920–926, 1993.

[4] Jason M. Keller and Monica Frega. Past, Present, and Future of Neuronal Models In Vitro. *Advances in Neurobiology*, 22:3–17, 2019.

[5] John M Walker. *Cardiac Tissue Engineering Series Editor*, volume 2.

[6] Richard Balint and Sarah H Cartmell. Electrical Stimulation : A Novel Tool. 19(1):48–57, 2013.

[7] Gyuhyun Jin, Gi-hoon Yang, and Geunhyung Kim. Review Article Tissue engineering bioreactor systems for applying physical and electrical stimulations to cells. pages 1–14, 2014.

[8] Cen Chen, Xue Bai, Yahui Ding, and In-seop Lee. Electrical stimulation as a novel tool for regulating cell behavior in tissue engineering. pages 1–12, 2019.

[9] Greeshma Thrivikraman, Sunil Kumar Boda, and Bikramjit Basu. Unraveling the mechanistic effects of electric field stimulation towards directing stem cell fate and function: A tissue engineering perspective. *Biomaterials*, 150:60–86, 2018.

[10] Sara Abasi, John R. Aggas, Naren Venkatesh, Iris G. Vallavanatt, and Anthony Guiseppi-Elie. Design, fabrication and testing of an electrical cell stimulation and recording apparatus (ECSARA) for cells in electroculture. *Biosensors and Bioelectronics*, 147(October 2019):111793, 2020.

[11] Daniel R Merrill, Marom Bikson, and John G R Jefferys. Electrical stimulation of excitable tissue : design of efficacious and safe protocols. 141:171–198, 2005.

[12] Alexis M. Kuncel and Warren M. Grill. Selection of stimulus parameters for deep brain stimulation. *Clinical Neurophysiology*, 115(11):2431–2441, November 2004.

[13] Amorn Wongsarnpigoon, John P. Woock, and Warren M. Grill. Efficiency analysis of waveform shape for electrical excitation of nerve fibers. *IEEE Transactions on Neural Systems and Rehabilitation Engineering*, 18(3):319–328, June 2010.

[14] Stuart F Cogan. Neural Stimulation and Recording Electrodes. 2008.

[15] Shiyun Meng, Mahmoud Rouabhia, and Ze Zhang. Electrical stimulation and cellular behaviors in electric field in biomedical research. *Materials*, 15(1):165, December 2021.

[16] Sahba Mobini, Spanish National, Liudmila Leppik, and John H Barker. IN IT IS IO. (February), 2016.

[17] Saranya B. Rajendran, Kirsty Challen, Karen L. Wright, and John G. Hardy. Electrical stimulation to enhance wound healing. *Journal of Functional Biomaterials*, 12(2):40, June 2021.

[18] Saad Javeed, Amir H. Faraji, Christopher Dy, Wilson Z. Ray, and Matthew R. MacEwan. Application of electrical stimulation for peripheral nerve regeneration: Stimulation parameters and future horizons. *Interdisciplinary Neurosurgery*, 24:101117, June 2021.

[19] Liudmila Leppik, Karla Mychellyne Costa Oliveira, Mit Balvantray Bhavsar, and John Howard Barker. Electrical stimulation in bone tissue engineering treatments. *European Journal of Trauma and Emergency Surgery*, 46(2):231–244, February 2020.

[20] Nina Tandon, Christopher Cannizzaro, Pen-hsiu Grace Chao, Robert Maidhof, Anna Marsano, Hoi Ting, Heidi Au, Milica Radisic, and Gordana Vunjaknovakovic. Electrical stimulation systems for cardiac tissue engineering. 4(2):155–173, 2009.

[21] Wang Heng, Mit Bhavsar, Zhihua Han, and John H. Barker. Effects of electrical stimulation on stem cells. *Current Stem Cell Research &amp Therapy*, 15(5):441–448, July 2020.

[22] Christopher Bertucci, Ryan Koppes, Courtney Dumont, and Abigail Koppes. Neural responses to electrical stimulation in 2D and 3D in vitro environments. *Brain Research Bulletin*, 152(February):265–284, 2019.

[23] Pavel Damborský, Juraj Švitel, and Jaroslav Katrlík. Optical biosensors. *Essays in Biochemistry*, 60(1):91–100, June 2016.

[24] Veeradasan Perumal and Uda Hashim. Advances in biosensors: Principle, architecture and applications. *Journal of Applied Biomedicine*, 12(1):1–15, January 2014.

[25] Valery L Feigin, Theo Vos, Emma Nichols, Mayowa O Owolabi, William M Carroll, Martin Dichgans, Günther Deuschl, Priya Parmar, Michael Brainin, and Christopher Murray. The global burden of neurological disorders: translating evidence into policy. *The Lancet Neurology*, 19(3):255–265, March 2020.

[26] Jeroen Van Schependom and Miguel D'haeseleer. Advances in neurodegenerative diseases. *Journal of Clinical Medicine*, 12(5):1709, February 2023.

[27] Bin He. *Neural Engineering*. Springer Nature Switzerland AG 2013, 2020, third edit edition, 2020.

[28] Nicholas Graziane and Yan Dong. *Extracellular and Intracellular Recordings*, volume 187. 2022.

[29] Nicholas Graziane and Yan Dong. *Electrophysiological Analysis of Synaptic Transmission, Extracellular and intracellular recordings*. Springer Protocols, Neuromethods 112, 2016.

[30] Micha E. Spira and Aviad Hai. Multi-electrode array technologies for neuroscience and cardiology. *Nature Nanotechnology*, 8(2):83–94, 2013.

[31] Longqian Xu, Chenxuan Hu, Qi Huang, Kai Jin, Ping Zhao, Dongping Wang, Wei Hou, Lihua Dong, Siyi Hu, and Hanbin Ma. Trends and recent development of the microelectrode arrays (MEAs). *Biosensors and Bioelectronics*, 175(88):112854, 2021.

[32] Hideaki Yamamoto, Leroy Grob, Takuma Sumi, Kazuhiro Oiwa, Ayumi Hirano-iwata, and Bernhard Wolfrum. Ultrasoft Silicone Gel as a Biomimetic Passivation Layer in Inkjet-Printed 3D MEA Devices. 1900130:1–6, 2019.

[33] Silvia Ronchi, Michele Fiscella, Camilla Marchetti, Vijay Viswam, Jan Müller, Urs Frey, Andreas Hierlemann, Francesco Greco, Marcel Böttrich, Jarno M A Tanskanen, Jari A K Hyttinen, Aerosol Jet Printing, Mauro Serpelloni, Edoardo Cant, Michela Borghetti, Twinkle Pandhi, Eric Kreit, Roberto Aga, Kiyo Fujimoto, Mohammad Taghi Sharbati, Samane Khademi, A Nicole Chang, Feng Xiong, Jessica Koehne, Emily M Heckman, David Estrada, and Revathi Appali. Single-Cell Electrical Stimulation Using CMOS-Based High-Density Microelectrode Arrays. *Frontiers in Neuroscience*, 13(March):1–17, 2019.

[34] Yang Liu, Xiuting Li, Jie Chen, and Chonglin Yuan. Micro/Nano Electrode Array Sensors: Advances in Fabrication and Emerging Applications in Bioanalysis. *Frontiers in Chemistry*, 8(November):1–9, 2020.

[35] Vera Lucia Da Silveira Nantes Button. *Electrodes for Biopotential Recording and Tissue Stimulation*. 2015.

[36] Giovanni Melle, Giulia Bruno, Nicolò Maccaferri, Giuseppina Iachetta, Nicolò Colistra, Andrea Barbaglia, Michele Dipalo, and Francesco De Angelis. Intracellular Recording of Human Cardiac Action Potentials on Market-Available Multielectrode Array Platforms. *Frontiers in Bioengineering and Biotechnology*, 8(February):1–10, 2020.

[37] Geon Hwee Kim, Kanghyun Kim, Eunji Lee, Taechang An, Woo Seok Choi, Geunbae Lim, and Jung Hwal Shin. Recent progress on microelectrodes in neural interfaces. *Materials*, 11(10), 2018.

[38] Tamás Árpádffy-Lovas and Norbert Nagy. ActionPytential: An open source tool for analyzing and visualizing cardiac action potential data. *Heliyon*, 9(3):e14440, March 2023.

[39] Raha M. Dastgheyb, Seung-Wan Yoo, and Norman J. Haughey. MEAnalyzer – a spike train analysis tool for multi electrode arrays. *Neuroinformatics*, 18(1):163–179, July 2019.

[40] Daniel C. Bridges, Kenneth R. Tovar, Bian Wu, Paul K. Hansma, and Kenneth S. Kosik. MEA viewer: A high-performance interactive application for visualizing electrophysiological data. *PLOS ONE*, 13(2):e0192477, February 2018.

[41] Nicolò Giuseppe Di Novo, Edoardo Cantù, Sarah Tonello, Emilio Sardini, and Mauro Serpelloni. Support-Material-Free Microfluidics on an Electrochemical Sensors Platform by Aerosol Jet Printing. *Sensors, MDPI*, 2019.

[42] Sarah Tonello, Andrea Bianchetti, Simona Braga, Camillo Almici, Mirella Marini, Giovanna Piovani, Michele Guindani, Kamol Dey, Luciana Sartore, Federica Re, Domenico Russo, Edoardo Cantù, Nicola Francesco Lopomo, Mauro Serpelloni, and Emilio Sardini. Impedance-based monitoring of mesenchymal stromal cell three-dimensional proliferation using aerosol jet printed sensors: A tissue engineering application. *Materials*, 13(10), 2020.

[43] Mauro Serpelloni, Edoardo Cant, and Michela Borghetti. Printed Smart Devices on Cellulose-Based Materials by means of Aerosol-Jet Printing and Photonic Curing. 2020.

[44] Haipeng Yang, Md Taibur Rahman, Dan Du, Rahul Panat, , , and Lin Yuehe. 3-D Printed Adjustable Microelectrode Arrays for Electrochemical Sensing and Biosensing. *Physiology behavior*, 230(12):600–606, 2017.

[45] Nouran Adly, Sabrina Weidlich, Silke Seyock, Fabian Brings, Alexey Yakushenko, Andreas Offenhäusser, and Bernhard Wolfrum. Printed microelectrode arrays on soft materials: from PDMS to hydrogels. *npj Flexible Electronics*, 2(1):1–9, 2018.

[46] Affan K. Waafi, Nikolas Gaio, William F. Quiros-Solano, Paul Dijkstra, Pasqualina M. Sarro, and Ronald Dekker. Low-Impedance PEDOT:PSS MEA Integrated in a Stretchable Organ-on-Chip Device. *IEEE Sensors Journal*, 20(3):1150–1157, 2020.

[47] Allen J Bard and Larry R. Faulkner. *ELECTROCHEMICAL METHODS Fundamentals and Applications*, volume 677. 2001.

[48] Kazutoshi Takahashi and Shinya Yamanaka. Induction of pluripotent stem cells from mouse embryonic and adult fibroblast cultures by defined factors. *Cell*, 126(4):663–676, August 2006.

[49] Robert Lanza, Robert Langer, Joseph P. Vacanti, and Anthony Atala. *Principles of Tissue Engineering*. Fifth edit edition, 2020.

[50] Laura Ylä-outinen, Jarno M A Tanskanen, Fikret E Kapucu, Anu Hyysalo, Jari A K Hyttinen, and Susanna Narkilahti. *Advances in Human Stem Cell-Derived Neuronal Cell Culturing and Analysis*. 2019.

[51] Yishai Avior, Ido Sagi, and Nissim Benvenisty. Pluripotent stem cells in disease modelling and drug discovery. *Nature Reviews Molecular Cell Biology*, 17(3):170–182, January 2016.

[52] Sonja Kriks, Jae-Won Shim, Jinghua Piao, Yosif M. Ganat, Dustin R. Wakeman, Zhong Xie, Luis Carrillo-Reid, Gordon Auyeung, Chris Antonacci, Amanda Buch, Lichuan Yang, M. Flint Beal, D. James Surmeier, Jeffrey H. Kordower, Viviane Tabar, and Lorenz Studer. Dopamine neurons derived from human ES cells efficiently engraft in animal models of parkinson's disease. *Nature*, 480(7378):547–551, November 2011.

[53] Stefania Fedele, Ginetta Collo, Katharina Behr, Josef Bischofberger, Stephan Müller, Tilo Kunath, Klaus Christensen, Anna Lisa Gündner, Martin Graf, Ravi Jagasia, and Verdon Taylor. Expansion of human midbrain floor plate progenitors from induced pluripotent stem cells increases dopaminergic neuron differentiation potential. (May):1–11, 2017.

[54] Nina Tandon, Anna Marsano, Robert Maidhof, Leo Wan, Hyoungshin Park, and Gordana Vunjak-novakovic. Optimization of electrical stimulation parameters for cardiac tissue engineering. (January):115–125, 2011.

[55] Stefano Gabetti, Beatrice Masante, Andrea Cochis, Giovanni Putame, Alessandro Sanginario, Ileana Armando, Elisa Fiume, Alessandro Calogero Scalia, Farah Daou, Francesco Baino, Simona Salati, Umberto Morbiducci, Lia Rimondini, Cristina Bignardi, and Diana Massai. An automated 3D - printed perfusion bioreactor combinable with pulsed electromagnetic field stimulators for bone tissue investigations. *Scientific Reports*, pages 1–14, 2022.

[56] Hong Cheng, Yan Huang, Hangqi Yue, and Yubo Fan. Electrical stimulation promotes stem cell neural differentiation in tissue engineering. *Stem Cells International*, 2021:1–14, April 2021.

[57] Greeshma Thrivikraman, Sunil Kumar, and Bikramjit Basu. Biomaterials Unraveling the mechanistic effects of electric fi eld stimulation towards directing stem cell fate and function : A tissue engineering perspective. *Biomaterials*, 150:60–86, 2018.

[58] Amy K. Butler, Jami L. Dantzker, Ravi B. Shah, and Edward M. Callaway. Development of visual cortical axons: Layer-specific effects of extrinsic influences and activity blockade. *The Journal of Comparative Neurology*, 430(3):321–331, 2001.

[59] Susan M. Catalano and Carla J. Shatz. Activity-dependent cortical target selection by thalamic axons. *Science*, 281(5376):559–562, July 1998.

[60] Ming T. Tsuang, William S. Stone, and Stephen V. Faraone. Genes, environment and schizophrenia. *British Journal of Psychiatry*, 178(S40):s18–s24, April 2001.

[61] S. J. Pelletier and F. Cicchetti. Cellular and molecular mechanisms of action of transcranial direct current stimulation: Evidence from in vitro and in vivo models. *International Journal of Neuropsychopharmacology*, 18(2):pyu047–pyu047, October 2014.

[62] Elise Stewart, Nao R. Kobayashi, Michael J. Higgins, Anita F. Quigley, Sina Jamali, Simon E. Moulton, Robert M.I. Kapsa, Gordon G. Wallace, and Jeremy M. Crook. Electrical stimulation using conductive polymer polypyrrole promotes differentiation of human neural stem cells: A biocompatible platform for translational neural tissue engineering. *Tissue Engineering Part C: Methods*, 21(4):385–393, April 2015.

[63] L Cavalleri, E Merlo Pich, M J Millan, C Chiamulera, T Kunath, P F Spano, and G Collo. Ketamine enhances structural plasticity in mouse mesencephalic and human iPSC-derived dopaminergic neurons via AMPAR-driven BDNF and mTOR signaling. (August 2017):812–823, 2018.

[64] Ileana Armando, Michela Borghetti, Emilio Sardini, and Mauro Serpelloni. A Computational Model For The Design Optimization Of Multi-Electrode Arrays By Aerosol-Jet Printing. *Procedia CIRP*, 110(C):87–92, 2022.

[65] Ileana Armando, Michela Borghetti, Emilio Sardini, and Mauro Serpelloni. Preliminary study on printed microelectrode array by Aerosol Jet Printing technology. *2022 IEEE International Workshop on Metrology for Industry 4.0 and IoT, MetroInd 4.0 and IoT 2022 - Proceedings*, pages 261–266, 2022.

[66] Ileana Armando, Michela Borghetti, Emilio Sardini, and Mauro Serpelloni. A feasibility study of customized and fully aerosol-jet-printed micro-electrode arrays for in vitro application. *IEEE Sensors Journal*, pages 1–1, 2023.

[67] Anssi Pelkonen, Cristiana Pistono, Pamela Klecki, Mireia Gómez-Budia, Antonios Dougalis, Henna Konttinen, Iveta Stanová, Ilkka Fagerlund, Ville Leinonen, Paula Korhonen, and Tarja Malm. Functional characterization of human pluripotent stem cell-derived models of the brain with microelectrode arrays. *Cells*, 11(1), 2022.

[68] Avra Kundu, Crystal Nattoo, Sarah Fremgen, Sandra Springer, Tariq Ausaf, and Swaminathan Rajaraman. Optimization of makerspace microfabrication techniques and materials for the realization of planar, 3D printed microelectrode arrays in under four days. *RSC Advances*, 9(16):8949–8963, 2019.

[69] Leonardo D. Garma, Laura M. Ferrari, Paola Scognamiglio, Francesco Greco, and Francesca Santoro. Inkjet-printed PEDOT:PSS multi-electrode arrays for low-cost: In vitro electrophysiology. *Lab on a Chip*, 19(22):3776–3786, 2019.

[70] Jonathan Rivnay, Huiliang Wang, Lief Fenno, Karl Deisseroth, and George G. Malliaras. Next-generation probes, particles, and proteins for neural interfacing. *Science Advances*, 3(6), 2017.

[71] Jan Schnitker, Nouran Adly, Silke Seyock, Bernd Bachmann, Alexey Yakushenko, Bernhard Wolfrum, and Andreas Offenhäusser. Rapid Prototyping of Ultralow-Cost, Inkjet-Printed Carbon Microelectrodes for Flexible Bioelectronic Devices. *Advanced Biosystems*, 2(3):1–9, 2018.

[72] Matthias Schürmann, Norman Shepheard, Natalie Frese, Kevin Geishendorf, Holger Sudhoff, Armin Gölzhäuser, Ulrich Rückert, Christian Kaltschmidt, Barbara Kaltschmidt, and Andy Thomas. Technical feasibility study for production of

tailored multielectrode arrays and patterning of arranged neuronal networks. *PLoS ONE*, 13(2):1–20, 2018.

[73] Jiaying Ji, Xiang Ren, and Pinar Zorlutuna. Cardiac cell patterning on customized microelectrode arrays for electrophysiological recordings. *Micromachines*, 12(11), 2021.

[74] Nikolas Gaio, Berend van Meer, William Quirós Solano, Lambert Bergers, Anja van de Stolpe, Christine Mummery, Pasqualina M. Sarro, and Ronald Dekker. Cytostretch, an Organ-on-Chip platform. *Micromachines*, 7(7):1–14, 2016.

[75] Mafalda Ribeiro, Pamela Ali, Benjamin Metcalfe, Despina Moschou, and Paulo R.F. Rocha. Microfluidics integration into low-noise multi-electrode arrays. *Micromachines*, 12(6):1–9, 2021.

[76] Tao Han, Sudip Kundu, Anindya Nag, and Yongzhao Xu. 3D printed sensors for biomedical applications: A review. *Sensors (Switzerland)*, 19(7), 2019.

[77] Dinesh Maddipatla, Binu B. Narakathu, and Massood Atashbar. Recent Progress in Manufacturing Techniques of Printed and Flexible Sensors: A Review. *Biosensors*, 10(12), 2020.

[78] Andrew J. Capel, Matthew A.A. Smith, Silvia Taccola, Maria Pardo-Figuerez, Rowan P. Rimington, Mark P. Lewis, Steven D.R. Christie, Robert W. Kay, and Russell A. Harris. Digitally Driven Aerosol Jet Printing to Enable Customisable Neuronal Guidance. *Frontiers in Cell and Developmental Biology*, 9(August):1–16, 2021.

[79] Neville E. Sanjana and Sawyer B. Fuller. A fast flexible ink-jet printing method for patterning dissociated neurons in culture. *Journal of Neuroscience Methods*, 136(2):151–163, 2004.

[80] Rahul P. Panat Mohammad Sadeq Saleh, Sandra M. Ritchie, Mark A. Nicholas, Rriddhiman Bezbaruah, Jay W.W. Reddy, Maysamreza Chamanzar, Eric A. Yttri. The CMU Array: A 3D Nano-Printed, Fully Customizable Ultra-High-Density Microelectrode Array Platform. *bioRxiV*, pages 1–29, 2019.

[81] Socrates Dokos. *Modelling Organs, Tissues, Cells and Devices Using MATLAB and COMSOL Multiphysics*. 2017.

[82] Marcel Böttrich, Jarno M A Tanskanen, and Jari A K Hyttinen. Lead field theory provides a powerful tool for designing microelectrode array impedance measurements for biological cell detection and observation. *BioMedical Engineering OnLine*, pages 1–17, 2017.

[83] T. Taghian, D. A. Narmoneva, and A. B. Kogan. Modulation of cell function by electric field: A high-resolution analysis. *Journal of the Royal Society Interface*, 12(107):21–25, 2015.

[84] Bernd Bachmann, Nouran Y Adly, Jan Schnitker, Alexey Yakushenko, and Philipp Rinklin. All-inkjet-printed gold microelectrode arrays for extracellular recording of action potentials. *Flexible and Printed Electronics*, 2 035003, 2017.

[85] A.L. Hodgkin and A.F. Huxley. A quantitative description of membrane current and its application to conduction and and excitation in nerve. *J. Physiol. (I952) I I7, 500-544*, pages 500–544, 1952.

[86] Richard Feynman, Robert Leighton, and Matthew Sand. *The Feynman Lectures on Physics*. 1963.

[87] Revathi Appali. MODELING THE COUPLING OF ACTION POTENTIAL AND ELECTRODES. 1985.

[88] Yi Qiang, Wen Gu, Zehua Liu, Shanchuan Liang, Jae Hyeon Ryu, Kyung Jin Seo, and Wentai Liu. Crosstalk in polymer microelectrode arrays. 14(9):3240–3247, 2021.

[89] J R Naughton, J A Varela, T J Connolly, and S Shepard. Suppression of crosstalk in multielectrode arrays with local shielding. (August):1–11, 2022.

[90] Kisuk Yang, Seung Jung Yu, Jong Seung Lee, Hak Rae Lee, Gyeong Eon Chang, Jungmok Seo, Taeyoon Lee, Eunji Cheong, Sung Gap Im, and Seung Woo Cho. Electroconductive nanoscale topography for enhanced neuronal differentiation and electrophysiological maturation of human neural stem cells. *Nanoscale*, 9(47):18737–18752, 2017.

[91] C. Simitzi, A. Ranella, and E. Stratakis. Controlling the morphology and outgrowth of nerve and neuroglial cells: The effect of surface topography. *Acta Biomaterialia*, 51:21–52, 2017.

[92] Mattia Bramini, Anna Rocchi, Fabio Benfenati, and Fabrizia Cesca. Neuronal Cultures and Nanomaterials. *Advances in Neurobiology*, 22:51–79, 2019.

[93] Genesink. "Product Datasheet Smartink Genesink smart aerosol, 2019.

[94] Tomi Ryynänen and Pasi Kallio. Microelectrode Array Designing for Dummies : Contribution of the Tracks to the Impedance Behavior and the Noise Level. pages 2020–2023, 2020.

[95] Dimitrios A. Koutsouras, Paschalis Gkoupidenis, Clemens Stolz, Vivek Subramanian, George G. Malliaras, and David C. Martin. Impedance Spectroscopy of Spin-Cast and Electrochemically Deposited PEDOT:PSS Films on Microfabricated Electrodes with Various Areas. *ChemElectroChem*, 4(9):2321–2327, 2017.

[96] Christopher M.A. Brett. Electrochemical Impedance Spectroscopy in the Characterisation and Application of Modified Electrodes for Electrochemical Sensors and Biosensors. *Molecules*, 27(5), 2022.

[97] Alexander R. Harris, Paul J. Molino, Robert M.I. Kapsa, Graeme M. Clark, Antonio G. Paolini, and Gordon G. Wallace. Correlation of the impedance and effective electrode area of doped PEDOT modified electrodes for brain-machine interfaces. *Analyst*, 140(9):3164–3174, 2015.

[98] Norberto Pérez-prieto and Manuel Delgado-restituto. Recording Strategies for High Channel Count , Densely Spaced Microelectrode Arrays. 15(July):1–21, 2021.

[99] Giulia Regalia, Emilia Biffi, Giancarlo Ferrigno, and Alessandra Pedrocchi. A Low-Noise , Modular , and Versatile Analog Front-End Intended for Processing In Vitro Neuronal Signals Detected by Microelectrode Arrays. 2015, 2015.

[100] Marie Engelene J. Obien and Urs Frey. *Large-Scale, High-Resolution Microelectrode Arrays for Interrogation of Neurons and Networks*, volume 22. 2019.

[101] Robert Rieger and John T. Taylor. Design strategies for multi-channel low-noise recording systems. *Analog Integrated Circuits and Signal Processing*, 58(2):123–133, November 2008.

MODULO DI EMBARGO DELLA TESI
(da compilare solo se si richiede un periodo di segretazione della tesi)

Il/La sottoscritto/a…. Ileana Armando…… Nato/a il……27/02/1993…….
a (indicare anche l'eventuale paese estero) Cuneo……..
provincia di (ovvero sigla del paese estero) Cuneo…….
Dottorato di Ricerca in Technology for Health…….
……..……

DICHIARA

- che il contenuto della tesi **non può essere immediatamente consultabile per il seguente motivo**

alcuni dati presenti nella tesi non sono ancora stati pubblicati e saranno utilizzati per un futuro protocollo/brevetto

La motivazione deve essere dettagliata e controfirmata obbligatoriamente dal Primo Supervisore di tesi
(Brevetto, segreto industriale, motivi di priorità nella ricerca, motivi editoriali, altro)

- che il testo completo della tesi potrà essere reso consultabile dopo:

☐ 6 mesi dalla data di conseguimento titolo
☑ 12 mesi dalla data di conseguimento titolo

- che sarà comunque consultabile immediatamente l'abstract della tesi, che viene caricato in Esse3, profilo studente.

Luogo e Data
Brescia, 10 Novembre 2023

Firma del Dichiarante
Ileana Armando

Controfirma del Primo Supervisore di tesi
per la motivazione di embargo e il periodo.